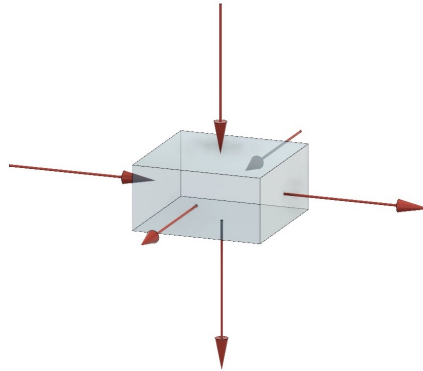




**TÉCNICO**  
LISBOA



## **Thermal Study of a Module for SWGO**

(Southern Hemisphere Wide field-of-view Gamma-ray Observatory)

**Ricardo Manuel dos Santos Lordelo**

Thesis to obtain the Master of Science Degree in

### **Mechanical Engineering**

Supervisors: Prof. Pedro Jorge Martins Coelho  
Prof. Luís Filipe Moreira Mendes

### **Examination Committee**

Chairperson: Prof. Carlos Frederico Neves Bettencourt da Silva  
Supervisor: Prof. Pedro Jorge Martins Coelho  
Member of the Committee: Prof. Miguel Abreu de Almeida Mendes

**November 2019**



To my Mother and to my Father.



## **Acknowledgments**

I would like to express my gratefulness to both my Supervisors, Prof. Pedro Jorge Martins Coelho and Prof. Luís Filipe Moreira Mendes. Their knowledge has been to me, of the greatest quality and helpfulness during this Thesis. I would like to thank them also for their patience with me, and for their support during this Thesis, without which its completion could have been jeopardised.

I would like to thank LIP for the opportunity given for producing this Thesis. I am specially grateful.

I would like to thank IST and all its people for enabling the existence of this higher education institution.

I would also like to thank every single reader of this Thesis for the time spent in doing so.

I would like to thank my family, and people that are or have been close to me and also the ones that will be.



## Resumo

Ao abrigo do Projecto SWGO (Southern Wide Field-of-view Gamma-ray Observatory), esta Tese, desenvolveu uma ferramenta de cálculo numérico para simular o comportamento térmico num Módulo de detecção de radiação Gamma. Este Módulo, é constituído por um Water Cherenkov Detector (WCD), que consiste num sensor de radiação imerso num reservatório de água, e opcionalmente um sensor Resistive Plate Chamber (RPC). O Observatório será instalado na região dos Andes, Hemisfério Sul, exposto às condições climatéricas locais onde a temperatura de inverno atinge os  $-10^{\circ}C$ .

Através das suas superfícies externas vão existir trocas de energia com o exterior. Os detalhes da evolução das temperaturas em zonas críticas do Módulo, e.g. na água, onde há a hipótese de congelamento, que é detrimental para os dados adquiridos pelo sensor, é estudada ao longo do ciclo climático anual. Assim, o código-fonte implementado usa o método dos Volumes Finitos escrito na linguagem de programação Python. Esta ferramenta, baseia-se nas características do Módulo, dimensões, materiais, propriedades da superfície, etc., e nas opções escolhidas, tipo de análise, condições iniciais, localização geográfica, etc., e no ficheiro de dados meteorológicos (típicos da região), que contem irradiação, temperatura do ar, velocidade do vento, etc., para calcular a solução de temperaturas do intervalo de tempo seguinte.

Os resultados obtidos para o Módulo proposto, dados climáticos extremos e refinamento da solução em função da disponibilidade computacional existente, mostram que a água não atinge os  $0^{\circ}C$ . No entanto, a ferramenta desenvolvida permite a obtenção de resultados com as características desejadas aquando requerido.

**Palavras-chave:** Módulo de detecção, Temperatura da Água, Irradiação, Dados Climáticos, Método dos Volumes Finitos





## Abstract

Under SWGO (Southern Wide Field-of-view Gamma-ray Observatory) Project, this Thesis, developed a numerical analysis tool to simulate the thermal behaviour of a Module for the detection of Gamma radiation. This Module includes a Water Cherenkov Detector (WDC), which comprises a radiation sensor immersed in a water reservoir, and possibly an additional Resistive Plate Chamber (RPC). The Module is to be installed in Andes mountains, Southern Hemisphere exposed to the weather where winter temperatures reach  $-10^{\circ}C$ .

The Module exchanges heat with its surroundings through its external surfaces. The temperature evolution in critical areas of the Module, e.g. water domain, where freezing may occur, which is detrimental to the acquired data, is studied throughout the yearly climatic cycle. Therefore, the implemented source code uses the Finite Volume Method written in the programming language Python. The created tool uses the Module's characteristics like dimensions, materials, surface properties, etc., and the chosen options like analysis type, initial conditions, geographical location, etc., and the meteorological data (representative of the region) which contains irradiation, air temperature, wind velocity, etc., to calculate the temperature solution at each time step.

Results obtained, for the proposed Module, with extreme climate data and the viable mesh refinement, show that the water does not reach  $0^{\circ}C$ . Nevertheless, the created tool allows the computation of results with any desired characteristics.

**Keywords:** Detection Module, Water temperature, Irradiation, Climate Data, Finite Volume Method



# Contents

Acknowledgments . . . . .	v
Resumo . . . . .	vii
Abstract . . . . .	ix
List of Tables . . . . .	xv
List of Figures . . . . .	xvii
Nomenclature . . . . .	xxi
Glossary . . . . .	xxiii
<b>1 Introduction</b>	<b>1</b>
1.1 Initial Considerations . . . . .	2
1.1.1 Meteorological Data . . . . .	3
1.1.2 Computational Cost . . . . .	4
1.2 Motivation . . . . .	4
1.3 Topic Overview . . . . .	5
1.4 Objectives . . . . .	5
1.5 Thesis Outline . . . . .	5
<b>2 Background</b>	<b>7</b>
2.1 Theoretical Overview . . . . .	7
2.2 Conduction . . . . .	7
2.3 Convection . . . . .	8
2.3.1 Forced Convection . . . . .	9
2.3.2 Free Convection . . . . .	11
2.3.3 Mixed Convection . . . . .	12
2.3.4 Dimensionless Groups . . . . .	12
2.4 Radiation . . . . .	14
2.5 Phase Change . . . . .	17
<b>3 Implementation</b>	<b>19</b>
3.1 Governing equations for fluid flow and heat transfer . . . . .	19
3.2 Finite Volume Method . . . . .	22
3.2.1 Boussinesq Approximation . . . . .	25

3.2.2	Staggered Grid . . . . .	26
3.2.3	Block Structured Grid . . . . .	27
3.3	Approximation Scheme . . . . .	28
3.4	Geometry . . . . .	30
3.4.1	Dimensions . . . . .	31
3.4.2	One-dimensional . . . . .	32
	Grid Assembly . . . . .	33
3.4.3	Two-dimensional . . . . .	35
	Grid Generation . . . . .	35
	Grid Assembly . . . . .	37
3.4.4	Three-dimensional . . . . .	38
	Grid Generation . . . . .	38
	Grid Assembly . . . . .	38
3.5	Boundary Conditions . . . . .	39
3.5.1	Convective Heat Flux . . . . .	39
	Logarithmic Wind Profile . . . . .	40
3.5.2	Radiative Heat Flux . . . . .	41
	Solar Radiation . . . . .	41
	Sky Radiation . . . . .	42
	Total Radiation . . . . .	42
3.6	Convection in Enclosures . . . . .	43
3.7	Water Phase Change . . . . .	44
3.8	Properties and Constants . . . . .	45
<b>4</b>	<b>Results</b>	<b>47</b>
4.1	Problem Description . . . . .	47
4.2	One-Dimensional Calculations . . . . .	48
4.3	Two-Dimensional Calculations . . . . .	53
	4.3.1 Results with Convection Correlation in the Water . . . . .	54
	4.3.2 Results with Convective Flow in the Water . . . . .	54
4.4	Three-Dimensional Calculations . . . . .	55
	4.4.1 Results with Convection Correlation in the Water . . . . .	55
	4.4.2 Results with Convective Flow in the Water . . . . .	56
<b>5</b>	<b>Discussion</b>	<b>57</b>
5.1	One Dimensional . . . . .	57
	5.1.1 Sources . . . . .	57
	5.1.2 Temperature . . . . .	59
	5.1.3 Thermal Resistance . . . . .	62
	5.1.4 Energy . . . . .	64

5.1.5	Rayleigh number . . . . .	67
5.2	Two Dimensional . . . . .	68
5.3	Three Dimensional . . . . .	70
<b>6</b>	<b>Conclusions</b>	<b>73</b>
6.1	General Conclusions . . . . .	73
6.2	Numerical Conclusions . . . . .	74
6.3	Achievements . . . . .	75
6.4	Future Work . . . . .	75
	<b>References</b>	<b>77</b>
<b>A</b>	<b>Source Code</b>	<b>78</b>
A.1	Code Structure . . . . .	78
A.2	GUI . . . . .	82
<b>B</b>	<b>Selected Subroutines</b>	<b>89</b>
B.1	Sources . . . . .	89
B.1.1	Convection . . . . .	89
B.1.2	Radiation . . . . .	91
B.2	Iteration Function . . . . .	92
B.3	Calculator . . . . .	93
<b>C</b>	<b>Convective Flow</b>	<b>95</b>
C.1	Two Dimensional . . . . .	95
C.2	Three Dimensional . . . . .	96
<b>D</b>	<b>Sparsity of Matrix</b>	<b>97</b>



# List of Tables

2.1	Dimensionless groups for heat transfer. . . . .	13
3.1	Governing Equations for fluid flow with heat transfer. . . . .	22
3.2	Correlations for Convection . . . . .	40
3.3	Properties of the used Materials in the Module. . . . .	46
4.1	Additional input parameters. . . . .	47
4.2	One-dimensional test instances. . . . .	49





# List of Figures

1.1	SWGO Module. . . . .	1
1.2	SWGO Array of Modules. . . . .	2
1.3	Climate Data. . . . .	3
2.1	Convection. . . . .	8
2.2	Free Vs. Forced Convection. . . . .	12
2.3	Spectrum of electromagnetic radiation. . . . .	14
2.4	Directional nature of incident radiation. . . . .	15
2.5	Radiation exchange in an isothermal enclosure. . . . .	16
2.6	Two Surface Enclosure. . . . .	17
2.7	Schematic of phase change in a semi-infinite domain. . . . .	18
3.1	Generic Control Volume. . . . .	22
3.2	Finite Volume Method. . . . .	24
3.3	Transient discretisation of FVM. . . . .	25
3.4	Pressure Field. . . . .	26
3.5	Staggered Grid. . . . .	27
3.6	Block Structured Grid. . . . .	27
3.7	Connection between Blocks. . . . .	28
3.8	Control Volume. . . . .	29
3.9	Water Volume. . . . .	31
3.10	Module Geometry with RPC and insulation. . . . .	31
3.11	Detail of Lead Plate, RPC and Water. . . . .	32
3.12	Detail of the RPC. . . . .	33
3.13	Depth of no temperature difference. . . . .	34
3.14	One-dimensional domain. . . . .	34
3.15	Two-dimensional Layout. . . . .	35
3.16	Two-dimensional Module sketch. . . . .	36
3.17	Two-dimensional Block Assembly with Mesh in each Block. . . . .	36
3.18	Three-dimensional Grid. . . . .	38
3.19	Properties of Water near freezing. . . . .	44

3.20 Water Density. . . . .	45
4.1 Climate Data Set. . . . .	48
4.2 One-dimensional Water Temperature, Cases 1 and 2. . . . .	49
4.3 One-dimensional Water and Air Temperature, and Heat flux through the top surface, Cases 1 and 2. . . . .	50
4.4 One-dimensional Water Temperature, Cases 1, 2, 3 and 4. . . . .	50
4.5 One-dimensional Convection in Water, Cases 1 and 3. . . . .	51
4.6 One-dimensional Convection in Water, detail, Cases 1 and 3. . . . .	52
4.7 One-dimensional Temperature of RPC, Cases 3 and 4. . . . .	52
4.8 One-dimensional Water Temperature, Cases 1, 2, 3, 4, 5, 6, 7 and 8. . . . .	53
4.9 Two-dimensional Water Temperature using convection correlation, Case 1. . . . .	54
4.10 Two-dimensional Water Temperature with convective flow, Case 1 through 8. . . . .	54
4.11 Three-dimensional, correlated convection, water temperature. . . . .	55
4.12 Three-dimensional, water temperature. . . . .	56
4.13 Three-dimensional, water temperature, cooling. . . . .	56
5.1 One-dimensional initial condition, Case 1. . . . .	58
5.2 One-dimensional initial condition influence of wind speed in convection, Case 1. . . . .	59
5.3 One-dimensional initial condition, Grashof number, Case 1. . . . .	60
5.4 One-dimensional initial condition, zero air velocity, Case 1. . . . .	60
5.5 One-dimensional initial condition, temperatures, Case 1. . . . .	61
5.6 One-dimensional initial condition, Water temperature, Case 1. . . . .	61
5.7 One-dimensional sun rise, temperatures, Case 1. . . . .	61
5.8 One-dimensional, Air temperature, Case 1. . . . .	62
5.9 One-dimensional, characteristic dimensions. . . . .	63
5.10 One-dimensional, Thermal Resistance for the Air enclosure. . . . .	64
5.11 One-dimensional, Energy change at each CV. . . . .	65
5.12 One-dimensional, Energy change in the first four CV's. . . . .	65
5.13 One-dimensional, Energy change in air and water. . . . .	66
5.14 One-dimensional, Energy change in air and water, detail. . . . .	66
5.15 One-dimensional, Energy change at each CV, detail. . . . .	66
5.16 One-dimensional, Heat Flux between CV's. . . . .	67
5.17 One-dimensional, Rayleigh number in Water domain. . . . .	67
5.18 One-dimensional, Rayleigh number in Water domain, one year. . . . .	68
5.19 Two-dimensional, Correlation Vs. Convection. . . . .	68
5.20 Two-dimensional, Convection heat flux in East and West walls. . . . .	69
5.21 Two-dimensional, Correlation Vs. Convection, detail. . . . .	70
5.22 Two-dimensional, Correlation Vs. Convection, Energy variation. . . . .	70
5.23 Three-dimensional, Correlation Vs. Convection. . . . .	71

5.24	Three-dimensional, Convection heat flux in North South East and West walls. . . . .	71
5.25	Three-dimensional, Correlation Vs. Convection, detail. . . . .	72
5.26	Three-dimensional, Correlation Vs. Convection, Energy variation. . . . .	72
6.1	Surface area to volume ratio for a cube. . . . .	73
A.1	Flowchart Pre Processor (1). . . . .	79
A.2	Flowchart Pre Processor (2). . . . .	80
A.3	Flowchart Processor (1). . . . .	80
A.4	Flowchart Processor (2). . . . .	81
A.5	Data File example. . . . .	82
A.6	First Window GUI. . . . .	83
A.7	Second Window GUI. . . . .	83
A.8	Third Window GUI. . . . .	84
A.9	Fourth Window GUI. . . . .	84
A.10	Fifth Window GUI. . . . .	85
A.11	Simple Plot GUI. . . . .	86
A.12	Sixth Window GUI. . . . .	86
A.13	Two-Dimensional plot of Convective Flow. . . . .	87
A.14	Three-Dimensional plot of Convective Flow. . . . .	87
B.1	Calculator Scheme. . . . .	93
C.1	Two Dimensional flow at 03:20 and at 07:00. . . . .	95
C.2	Two Dimensional flow at 12:00. . . . .	96
C.3	Three Dimensional flow at 00:40 and 07:10. . . . .	96
D.1	One and Two Dimensional matrix with correlation, Case 1. . . . .	97
D.2	Two-dimensional matrix, with flow, Case 1. . . . .	98
D.3	Three-dimensional matrix, with flow, Case 1. . . . .	98



# Nomenclature

## Greek symbols

$\alpha$	Thermal diffusivity. [ $m^2/s$ ]
$\beta$	Coefficient of thermal expansion. [ $1/K$ ]
$\delta$	Boundary layer thickness. [ $m$ ]
$\epsilon$	Emission coefficient.
$\lambda$	Wavelength. [ $m$ ]
$\nabla$	Operator.
$\nu$	Kinematic viscosity. [ $Pa\ s$ ]
$\phi$	Generic intensive property.
$\rho$	Density. [ $Kg/m^3$ ]
$\sigma$	Stefan Boltzman constant. $\sigma = 5.670 [W/m^2\ K^4]$
$\tau$	Shear stress. [ $Pa$ ]
$\Theta$	Divergence of velocity field.

## Roman symbols

$C$	Advective flux. [ $Kg/m^2\ s$ ]
$c$	Speed of light in vacuum. [ $m/s$ ]
$C_p$	Specific Heat. [ $J/Kg\ K$ ]
$D$	Diffusive flux. [ $\phi/m^2\ s$ ]
$E$	Emission.
$F$	View Factor.
$G$	Irradiation. [ $W/m^2$ ]
$g$	Acceleration of gravity. [ $m/s^2$ ]

$Gr$	Grashof number.
$h$	Coefficient of Convection. $[W/m^2 K]$
$I$	Spectral Intensity. $[frac{W sr m}]$
$J$	Radiosity. $[W/m^2]$
$k$	Thermal conductivity coefficient. $[W/m K]$
$L$	Lenght. $[m]$
$Nu$	Nusselt number.
$p$	Pressure. $[Pa]$
$Pr$	Prandtl number.
$q$	Heat flux. $[W]$
$R$	Gas constant. $R = 8.3145 [J/mol K]$
$Ra$	Rayleigh number.
$Re$	Reynolds number.
$T$	Temperature. $[K]$
$t$	Time. $[s]$
$\vec{v}$	Velocity vector. $[m/s]$
$u, v, w$	Velocity Cartesian components. $[m/s]$

### Subscripts

$\infty$	Free-stream condition.
$i, j, k$	Computational indexes.
$n$	Normal component.
$x, y, z$	Cartesian components.

# Glossary

- APEX** Atacama Pathfinder Experiment is a collaboration between Max Planck Institute fur Radioastronomie (MPIfR) , Onsala Space Observatory (OSO) and the European Southern Observatory (ESO) to construct and operate a modified ALMA prototype antenna as a single dish on the high altitude site of Llano Chajnantor.
- BSD** BSD licenses are a family of permissive free software licenses imposing minimal restrictions on the use and distribution of the covered software. The original license was named BSD since it was a Berkeley Software Distribution. Later version have kept the name.
- CDS** Central Differencing Scheme is a method for approximating the differential operator in a node in between the considered path in order to solve differential equations numerically. This method interpolates the value at the node by using both lateral values.
- CFD** Computational Fluid Dynamics is a branch of fluid mechanics that uses numerical methods and algorithms to solve problems that involve fluid flows.
- CV** Control Volume, is a unit of the subdivision of the domain into a finite number of Volumes. Each of these volumes is interpreted as having an homogeneous characteristic about its properties, which is to say, properties are constant within each Control Volume.

- FVM** Finite Volume Method, is a method used in computational fluid dynamics to obtain algebraic equation arising from the discretisation of the respective partial differential equations through their integral form.
- GMT** Greenwich Mean Time is the mean solar time at the Royal Observatory in Greenwich, London, reckoned from midnight. Other locations may set their mean solar time relative to GMT which translates to time difference in hours for each Country relative to GMT, east positive.
- GUI** Graphical User Interface is a form of user interface that allows users to interact with electronic devices through graphical icons and visual indicators.
- IST** Instituto Superior Técnico, is the largest school of Architecture, Engineering, Science and Technology in Portugal, involving a community of over 10,000 people.
- LIP** Laboratory of Instrumentation and Experimental Particle Physics, is the reference institution for experimental particle physics and associated technologies in Portugal.
- LS** Level-set methods (LSM) are a conceptual framework for using level sets as a tool for numerical analysis of surfaces and shapes. The advantage of the level-set model is that one can perform numerical computations involving curves and surfaces on a fixed Cartesian grid without having to parameterize these objects.
- NPT** Normal Temperature and Pressure refers to standard conditions for temperature and pressure. This standard uses a temperature of 20 °C and an absolute pressure of 1 atm.
- PDE** Partial differential equation is a multi variable differential equation that contains partial derivatives.



- RPC** Resistive Plate Chamber is a particle detector used for detecting high energy particles.
- SWGO** Southern Wide Field-of-view Gamma-ray Observatory is the ongoing International Project for R&D and installation a new Gamma-ray observatory in the Southern Hemisphere. The founding nine Countries of this Collaboration Project are, Argentina, Czech Republic, Germany, Italy, Mexico, Portugal, the United Kingdom and the United States of America. This new Observatory is intended to be installed the Andes at an altitude above 4,4 [km] to detect the highest energy gamma rays.
- TMY** Typical Meteorological Year is a collation of selected weather data for a specific location, listing values of solar radiation and meteorological elements for a one-year period.
- UDS** The Upwind Differencing Scheme is a method for approximating the differential operator in a node in between the considered path in order to solve differential equations numerically. This method interpolates the value at the node direction wise through its lateral value.
- VOF** In computational fluid dynamics, the volume of fluid (VOF) method is a free-surface modelling technique, i.e. a numerical technique for tracking and locating the free surface (or fluid–fluid interface). It belongs to the class of Eulerian methods which are characterized by a mesh that is either stationary or is moving in a certain prescribed manner to accommodate the evolving shape of the interface.
- WCD** Water Cherenkov Detector is a particle detector which uses the light production of a particle entering a medium when the speed of the particle is greater than the speed threshold for light in the medium, in this case, the medium is pure water, .



# Chapter 1

## Introduction

The Southern Wide Field-of-view Gamma-ray Observatory (SWGGO) is an ongoing Project for the installation of a new observatory for Gamma radiation coming from outer space in the Southern Hemisphere. The detection of Gamma radiation uses a Modular detection unit and several detection units placed in a field for flexibility of the observatory layout. A representation of the Module is shown in Figure 1.1

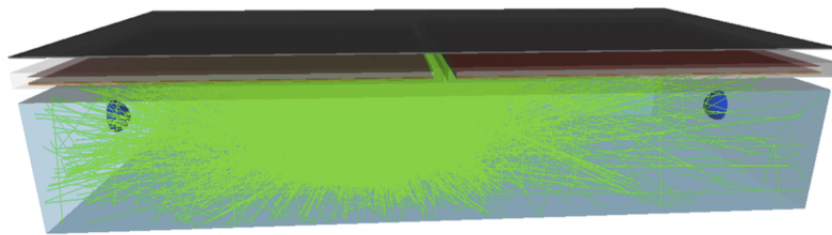


Figure 1.1: SWGGO Module.

Also, due to the particularities of Gamma ray detection there may be a central area with a higher Module density and an outskirts with less Modules per unit area. An example of the layout of the field is shown in Figure 1.2.

The Gamma-ray detection Module being studied is comprised primarily of a water reservoir. Immersed in the water is the sensor that detects Gamma radiation through the consequences of its existence in the water. This detector is referred to as Water Cherenkov Detector (WCD). Additionally there may be another type of detector placed on top of this water reservoir. This detector is referred to as Resistive Plate Chamber (RPC). It has the same horizontal dimensions. Since the existence of this detector is not yet assured, both scenarios are considered.

When the RPC is present, there is a Lead plate that is placed on top of the Module. Although this plate is separated from the RPC itself, it is viewed from now on as a part of the RPC.

As a variation to this base geometry, for comparison purposes, an insulating layer may also be added around the Module. This insulation is meant to alter the thermal behaviour of the Module throughout the year and be judged against its results.

The Module is placed outside and is exposed to the local atmospheric conditions. It exchanges heat

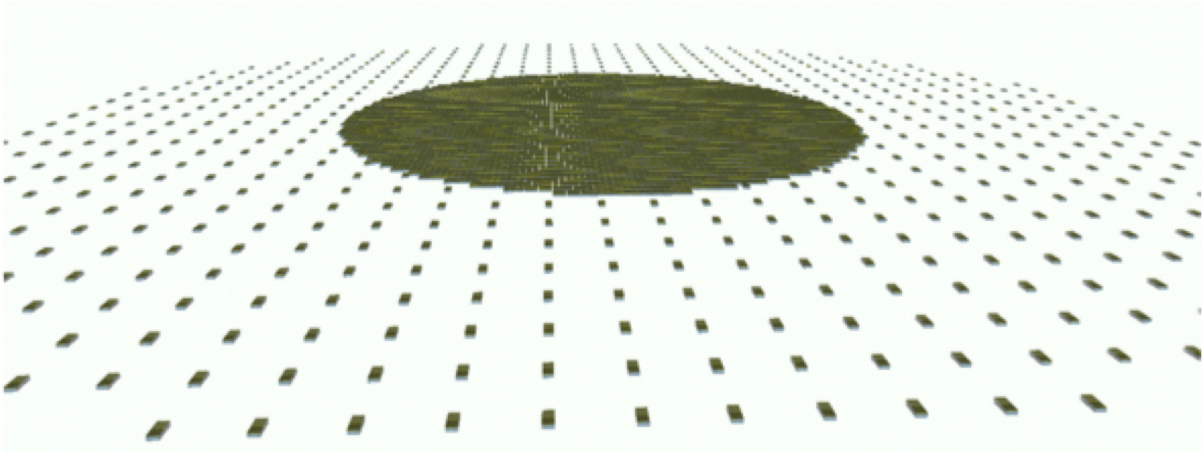


Figure 1.2: SWGO Array of Modules.

with its surroundings. The Module's exterior surfaces, if at a different temperature from the ambient air, impose a convection process that is a function of this temperature difference, of the air properties and of its velocity (wind). The generated heat flux has a direction opposite to the temperature gradient.

Also, the Sun Irradiates the Earth's outer atmosphere at about  $1353 [W/m^2]$  [1], this is called the extraterrestrial radiation, a part of which is absorbed, accounting for a temperature increase in the atmosphere, another part is scattered, a part of which is redirected to space, and the rest, eventually arrives at the Earth surface as Diffuse Solar Radiation. The Solar Radiation that arrives at the Earth surface without being absorbed or scattered, is called Direct Solar Radiation and has a directional nature. Finally, being immersed on the Earth atmosphere, there is a thermal radiation heat exchange between the Module and the atmosphere based on the temperature of the Module's surface and the temperature of the atmosphere .

In addition to these two phenomena, Convection and Radiation, there is also heat exchange through conduction with the ground, which works as a temperature buffer since at a certain depth there is no variation in temperature throughout the year.

The influence of these phenomena in the Module's temperatures is computed through a Finite Volume Method (FVM) analysis, implemented in the programming language Python. This source code builds the discretised geometry of the Module, and then, in a sequential way, time step after time step, applies the energy fluxes at the boundaries obtained through the energy sources mentioned above, and calculates the unknown properties (e.g. temperature) of the next time step within the Module's domain.

## 1.1 Initial Considerations

Some aspects should be mentioned in advance to set the context for the following Chapters and for the Thesis in general. These include the meteorological data, which is to be obtained externally and is of the uttermost importance and the computational cost.

### 1.1.1 Meteorological Data

The weather data is one of the most relevant inputs to this study. It is the “driver” of temperature change. Making it, from one perspective, the most important variable regarding what happens inside the Module temperature wise. Research made on this subject has accompanied this Thesis all round.

Considering that the solution is obtained through a sequential calculation process, implemented by a numerical model, the temperatures are calculated by a marching method, time step after time step. Hence, there needs to be a set of climate data that feeds its values as an input to this numerical model at each time step. An example of a data file is shown in Figure 1.3.

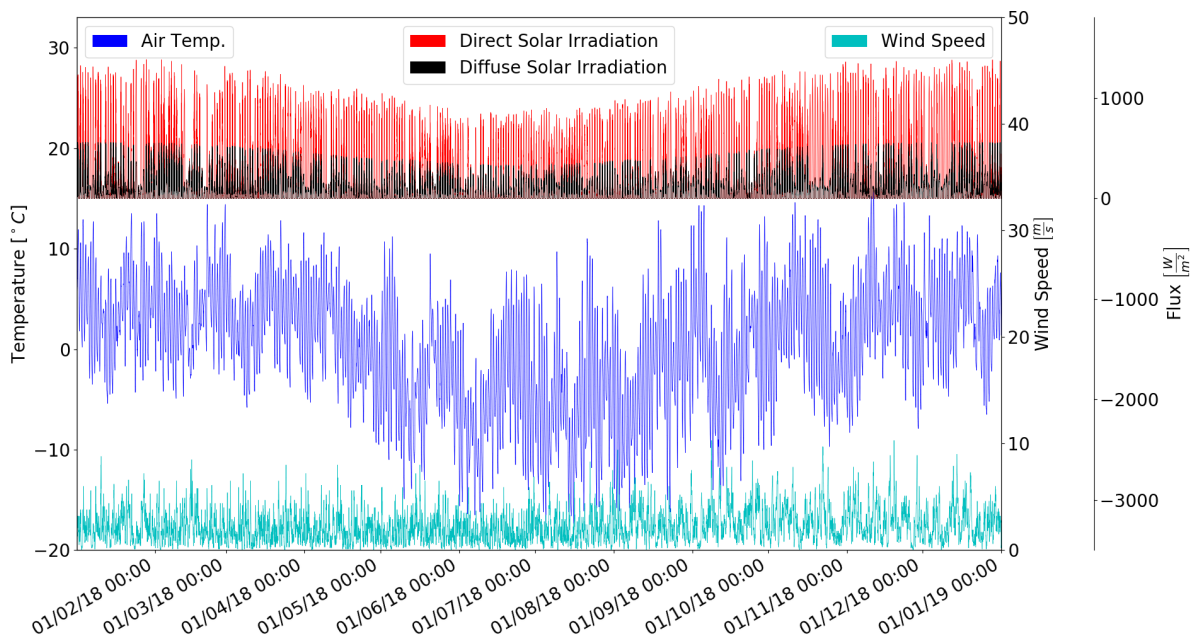


Figure 1.3: Climate Data.

Two aspects are relevant in this input, one is how long should the aforementioned time step last, and the other is for how long should all the time steps last (the total period covered by these sequential time steps).

The later one, the full duration of the analysis, is logically chosen in accordance to the time period where the climate is supposed to cycle its characteristics by repeating itself, so one year is the obvious choice as to go through all seasons which is directly related to one full rotation of the Earth around the sun which is nearly identical to any other.

The time step chosen is more of a design option regardless of the availability of data for a particular time step. It is possible to break down one time step into several smaller ones if a smaller time step is desired, or average several time steps of climate data for a longer numerical time step. Of course, during each time step there must not be any type of cycle in the temperature, unless the results are interpreted correspondingly, e.g. a time step of one day does not account for the day / night temperature cycle, but a time step of 12 h (solar day / solar night) could be regarded the highest permissible time step.

The chosen location for this Observatory is, to date, the Chilean Andes, more precisely, the Desert

of Atacama, one of the driest regions on Earth, at an altitude of 5000 [m]. Both these aspects, humidity and altitude, are favourable to the purpose of this observatory since the smaller the air mass on the top of the Module the less degradation there is to the incoming gamma radiation (although the subject of detection of gamma radiation is outside the scope of this Thesis). Nevertheless, while the location is ideal for the purpose when compared to other Earth locations, its characteristics from a meteorological standpoint are of concern if there is the need to keep the temperatures inside the Module, namely in the water, above freezing point and, if possible, around  $2 - 4^{\circ}C$ , provided the minimum and maximum temperatures at the site year round are respectively,  $\approx -15^{\circ}C$  and  $10^{\circ}C$ .

Climate data is available from entities that publish it from Weather Stations or satellite data. Some of these entities are commercial others not.

The coordinates of the location are set, approximately to,  $S 23^{\circ} W 68^{\circ}$ . At this site, there is a weather station, credited to the Atacama Pathfinder Experiment (APEX) that publishes the weather data at its [site](#). This weather station has several readings that concern the observation variables for their Telescope, including the ambient air temperature and the wind speed measurement. These readouts have a frequency of one minute which amounts to 525 600 time steps during the one year cycle. Unfortunately this weather station does not have Solar Radiation measurements, so the climate data has to be acquired somewhere else.

On the other hand, [Meteonorm](#) is a commercial Climate Data Provider that offers radiation data at the precise location where the Modules will be. Hence this data is assumed to better suit the needs of this analysis. Still, freely available data exists if desired.

### 1.1.2 Computational Cost

Regardless of the methods and discretisation used to calculate the temperatures in the Module during one year, there is always an associated computational effort that may render a solution unviable. As shall be seen later, if the most detailed solution is intended, the computational cost associated with its calculation quickly becomes too onerous for an ordinary Personal Computer. Throughout this Thesis this has been a concern with increasing magnitude specially towards the end, where a more complex and detailed solution was proposed.

## 1.2 Motivation

The main concern for the Project regarding this Thesis is related to the possible freezing of water in the Water Cherenkov Detector (WCD), although the Resistive Plate Chamber (RPC) detector is also sensitive to temperature in its data acquisition. The problem arises when there is a partial freezing of the water in the reservoir, in this situation the electromagnetic radiation emitted by the change in velocity of the photons produced by the incoming gamma rays is different in water and ice due to different properties of the water in its solid phase and in its liquid phase. Apparently this aspect is not problematic if there is a total freezing of the water, since the properties of the ice are homogeneous. Even so, the

details about detection of Gamma radiation are outside the scope of this Thesis.

Throughout the year, and given that the air temperature of the proposed location ranges between approximately  $-15^{\circ}\text{C}$  and  $10^{\circ}\text{C}$ , there may be a partial or total freezing of the water. Therefore, there is the necessity of gathering knowledge about whether the water does or does not freeze and all its associated aspects. For instance, if it freezes, for how long, what time of year is it most likely for it to happen (assuming it does), how much of the water freezes, when is it most likely to be all in liquid state, etc.. Also, is there any simple solution to control this aspect, for instance what would be the effect of adding a layer of some insulation material?

In other words, the purpose of the Southern Wide Field-of-view Gamma-ray Observatory (SWGGO) is compromised by the partial freezing of the water in the reservoir, with the worst case scenario being a constant layer of ice throughout the year.

### **1.3 Topic Overview**

There are other Observatories relying on water tanks to detect the Cherenkov Radiation, e.g. Pierre Auger Observatory and HAWC.

The problem that needs to be solved, is the temperature change in a body of water placed in the exterior, e.g. a water tank. A similar analysis happens, for example, in solar collector design, although this system is different in some aspects, the methods used are the same, both address the issue of thermal behaviour within an enclosed “box” exposed to atmospheric conditions throughout one year.

However, water freezing is not an issue in solar collectors. Still, some studies on solar collectors are relevant to this Thesis like the convection correlation for enclosures, [1, 2].

The subject of Heat Transfer in general is, of course, much broader, but the fundamentals regarding this study are within its domain.

### **1.4 Objectives**

The objective of this Thesis is to provide as accurately as possible the temperature field inside the Module at each point in its domain. Also, it should present the consequences of some differentiation factors like, e.g. an insulation layer over the Module or the height of the water reservoir.

The developed tool for computing the temperatures should have the flexibility to interpret a different climate data set or any of the main variables present in the domain like, e.g. the outer-surface characteristics like absorptivity and emissivity among others.

### **1.5 Thesis Outline**

Chapter 2 presents the fundamentals of Heat Transfer. The aforementioned Conduction, Convection and Radiation processes are described. For convection, since there are different types of convection, a generic formulation of the problem is firstly made followed by a specification for each of its cases.

This generic formulation is the foundation for the FVM numerical implementation. For radiation, the necessary background for this Thesis is presented.

Chapter 3 deals with how the results are obtained with the use of the FVM. The formulation of the governing equations that is used for fluid flow and heat transfer is presented. It starts by defining the mathematical model that is going to be implemented, then the details of how the FVM is implemented in this Thesis are explained along with the main options used in order to improve the accuracy of the results. Here, the method used to solve the PDE's is presented. Then, the dimensions of the Module are addressed and the geometry is defined for the one-dimensional, two-dimensional and three-dimensional cases. Then, the implementation of the boundary conditions is addressed. Finally, the properties of materials is briefly discussed.

Chapter 4 shows the available results and makes a brief interpretation of the results regarding the yearly behaviour of each case and why the behaviour is like so. The interpretation made in this Chapter regards the overall yearly temperature variation rather than a detail view into each time step which is passed on to the Chapter.

Chapter 5 provides an in depth view of what is happening during each time step regarding temperature change, boundary conditions, heat fluxes, energy variation, etc..

Chapter 6 states the achievements of this Thesis, where its hypothetical continuation would lead and the improvements to be made.



# Chapter 2

## Background

The Module, exposed to the atmospheric conditions is subject to heat exchange with its surroundings through Conduction, Convection and Radiation. These three phenomenon are addressed in this chapter. Only the aspects that are relevant to this Thesis are explained.

Also, the theory governing phase change is addressed regarding the freezing of the water.

### 2.1 Theoretical Overview

Heat transfer may be classified into three main groups, conduction, convection and radiation. In this study, all three are present.

Due to the nature of the geometry complexity, it is usually not possible to achieve an analytical solution. Therefore there is the need to approximate the solution by discretising the domain in question and solving each finite volume of this domain with the use of approximations to the PDE's. These approximations applied to all elements of the domain yield a solution to the problem. Historically these methods were used to make calculation by hand, but since the introduction of computers, the relevance of these methods grew.

There are different ways to go about these approximations to the PDE's, but from this Thesis stand-point FVM is used, hence this is the only method discussed here.

### 2.2 Conduction

Conduction is the process of heat transfer in which a higher temperature region transfers heat to an adjacent lower temperature region.

This type of heat transfer, if steady state is assumed, is governed by the Fourier's law, equation 2.1, which states that the thermal energy flux along a certain direction is proportional to the temperature gradient in that direction weighted by a constant  $k$  that is a property of the material subject to conduction.

$$q_x'' = -k \frac{\partial T}{\partial x} [W/m^2] \quad (2.1)$$

## 2.3 Convection

Convection may be viewed as conduction plus advection between two substances. The differentiating factor for convection, is that one of these substances is a solid and the other is a fluid with a relative motion caused either by density differences of the fluid near the solid wall or by a predefined velocity field in the fluid. Either way there must be a relative motion of this fluid or, there is only conduction between the solid and the fluid. One consequence of this behaviour is that a convection process always has a higher heat transfer rate at the surface than the equivalent conductive heat transfer (zero velocity in the fluid) since the motion of the fluid always increases the temperature gradient at the surface compared to a perfectly still fluid due to the mixing effect caused by velocity in a fluid near a wall. This temperature gradient at the surface, when normalised, is referred to as *Nusselt* number, which is a dimensionless parameter, and is equal to one, if the fluid is still, or higher if there is relative motion of the fluid.

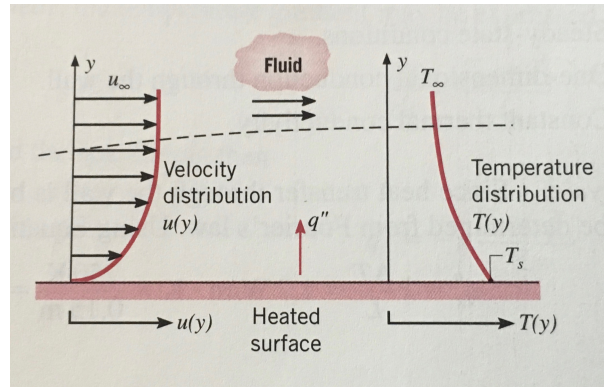


Figure 2.1: Convection, [1].

The underlying process of heat transfer is coupled with fluid flow [3, 1]. This aspect is represented in Figure 2.1. The rate of heat flux at the surface is given by equation 2.2 where  $h$  is the convective heat transfer coefficient  $[\frac{W}{m^2 \cdot K}]$ . Contrary to the coefficient of conduction which is a property of the solid material, the coefficient of convection depends on the type of flow and the properties of both substances, hence it is a function of several variables, not a property. Equation 2.2 is termed Newton's law of cooling.

$$q_x'' = h (T_{surface} - T_{fluid}) [W/m^2] \quad (2.2)$$

Since the fluid at the surface is stagnant, Figure 2.1, the heat flux in the adjoining layer of fluid to the wall occurs through the process of conduction, hence respecting the Fourier's law, equation 2.1 at any point in the surface, hence is a function of the temperature gradient at the surface. Additionally, the convection equation 2.2 must also be taken into consideration and must yield the same heat flux. Equation 2.3 derives the coefficient of convection in this manner.

$$h (T_s - T_\infty) = -k_f \left. \frac{\partial T}{\partial x} \right|_{y=0} \implies h = \frac{-k_f \left. \frac{\partial T}{\partial x} \right|_{y=0}}{T_s - T_\infty} \quad (2.3)$$

Convection may be caused only by the density difference caused by the temperature difference at the surface of the solid. In this case, the free stream velocity is zero. For this to happen, the fluid must

have a thermal expansion coefficient different from zero, which nearly all fluids do. Therefore, in this case, the sole “force” that drives the fluid flow is its buoyancy within itself. This type of convection is referred to as Free Convection.

If, on the other hand, there is an imposed relative motion of the fluid, and if the corresponding velocity is relatively higher than the velocity due to free convection, the effects of free convection may then be disregarded (the ratio between the momentum created by these two velocities is later acknowledged has Richardson number,  $Ri = (Grashof/Reynolds^2)$ ). In this case, the convective heat transfer accounts only for the free stream velocity of the fluid. This type of convection is referred to as Forced Convection.

Alternatively, if both effects are relevant, meaning that the corresponding velocities are of the same magnitude, then both effects must be taken into account, since they both contribute similarly to the heat transfer. This type is referred to as Mixed Convection.

Which ever the type of convection, if the flow is laminar, the underlying mechanisms governing heat transfer are the same. Both aspects of this phenomenon, fluid flow and heat transfer, are mathematically well defined, there is always the possibility of obtaining a numerical solution based on the laws that govern these processes. There are also correlations corresponding to each type of convection. These correlation have been proposed by several Authors, e.g. [2] based on experimental data. These correlate the relevant characteristics of the flow, such as temperature difference, fluid properties, dimensions, etc., to an average, or local, heat transfer coefficient. In this Thesis there is an extensive use of these correlations to calculate the heat transfer at the surfaces of the Module by applying the corresponding correlation to each situation.

### 2.3.1 Forced Convection

Taking a two-dimensional differential control volume (or area) situated in the flow, and applying the laws of conservation of mass, conservation of energy and conservation of momentum (Newton’s second law of motion), yields the set of equations 2.4a, 2.4b, 2.4c and 2.4d.

$$\frac{\partial u}{\partial x} + \frac{\partial v}{\partial y} = 0 \quad (2.4a)$$

$$\rho \left( u \frac{\partial u}{\partial x} + v \frac{\partial u}{\partial y} \right) = -\frac{\partial p}{\partial x} + \mu \left( \frac{\partial^2 u}{\partial x^2} + \frac{\partial^2 u}{\partial y^2} \right) + X \quad (2.4b)$$

$$\rho \left( u \frac{\partial v}{\partial x} + v \frac{\partial v}{\partial y} \right) = -\frac{\partial p}{\partial y} + \mu \left( \frac{\partial^2 v}{\partial x^2} + \frac{\partial^2 v}{\partial y^2} \right) + Y \quad (2.4c)$$

$$\rho C_p \left( u \frac{\partial T}{\partial x} + v \frac{\partial T}{\partial y} \right) = k \left( \frac{\partial^2 T}{\partial x^2} + \frac{\partial^2 T}{\partial y^2} \right) + \mu \Phi + \dot{q} \quad (2.4d)$$

$$\Phi = \left( \frac{\partial u}{\partial y} + \frac{\partial v}{\partial x} \right)^2 + 2 \left[ \left( \frac{\partial u}{\partial x} \right)^2 + \left( \frac{\partial v}{\partial y} \right)^2 \right] \quad (2.4e)$$

The terms  $X$  and  $Y$  represent sources of momentum in each direction and  $\dot{q}$  represents an energy source.

At the surface, there is a velocity boundary layer as well as a thermal boundary layer which may

be seen in Figure 2.1. Since the heat transfer between the solid and the fluid happens at the surface, the flow at this location is subject to boundary conditions. Several simplifications can be made due to the particularities of this region. These are shown in equation 2.5 and are straightforward, taking into account that the velocity at the surface is zero.

$$\text{Velocity boundary layer} = \begin{cases} u \gg v \\ \frac{\partial u}{\partial y} \gg \frac{\partial u}{\partial x}, \frac{\partial v}{\partial x}, \frac{\partial v}{\partial y} \end{cases}, \quad \text{Thermal boundary layer} = \begin{cases} \frac{\partial T}{\partial y} \gg \frac{\partial T}{\partial x} \end{cases} \quad (2.5)$$

The term,  $(\mu \Phi)$  in equation 2.4d is responsible for the conversion of kinetic energy into thermal energy through dissipation due to viscous stresses. So, from 2.5 the only relevant shear stresses in the boundary layer region are those related to the gradient of  $u$  in the  $y$  direction according to equation 2.6.

$$\tau_{xy} = \tau_{yx} = \mu \left( \frac{\partial u}{\partial y} \right) \quad (2.6)$$

These simplifications applied to equations 2.4a, 2.4b, 2.4c and 2.4d yield equations 2.7a, 2.7b and 2.7c

$$u \frac{\partial u}{\partial x} + v \frac{\partial u}{\partial y} = -\frac{1}{\rho} \frac{\partial p}{\partial x} + \nu \frac{\partial^2 u}{\partial y^2} + X \quad (2.7a)$$

$$\frac{\partial p}{\partial y} = Y \quad (2.7b)$$

$$u \frac{\partial T}{\partial x} + v \frac{\partial T}{\partial y} = \alpha \frac{\partial^2 T}{\partial y^2} + \frac{\nu}{c_p} \left( \frac{\partial u}{\partial y} \right)^2 \quad (2.7c)$$

If there is no internal energy generation, the terms  $X$  and  $Y$  are zero. Also, the aforementioned viscous dissipation term in equation 2.7c is considered to be negligible in comparison to the advection terms in the left hand side, which is also coherent with the low viscosities and low velocities of the fluids used in this study, namely, air and water.

If the previous equations are to be normalised, the variables involved need to be dimensionless, so choosing a characteristic length and velocity  $L$  and  $V$ , equations 2.8, and substituting, yields equation 2.9a and equation 2.9b for the velocity and for energy fields respectively.

$$x^* = \frac{x}{L}, \quad y^* = \frac{y}{L}, \quad u^* = \frac{u}{V}, \quad v^* = \frac{v}{V}, \quad T^* = \frac{T - T_s}{T_\infty - T_s} \quad (2.8)$$

$$\text{Velocity} \quad u^* \frac{\partial u^*}{\partial x^*} + v^* \frac{\partial u^*}{\partial y^*} = -\frac{\partial p^*}{\partial x^*} + \frac{\nu}{VL} \frac{\partial^2 u^*}{\partial y^{*2}}, \quad Re_L = \frac{VL}{\nu} \quad (2.9a)$$

$$\text{Thermal} \quad u^* \frac{\partial T^*}{\partial x^*} + v^* \frac{\partial T^*}{\partial y^*} = \frac{\alpha}{VL} \frac{\partial^2 T^*}{\partial y^{*2}}, \quad Pr = \frac{VL}{\alpha Re_L} \quad (2.9b)$$

The term  $\frac{\partial T^*}{\partial y^*}$  at the surface stands for the dimensionless temperature gradient at the surface, *Nusselt* number. Applying this dimensionless term to equation 2.3, yields the *Nusselt* number as a function of the related coefficients of heat transfer and geometry parameters, equation 2.10

$$\left. \frac{\partial T^*}{\partial y^*} \right|_{y^*=0} = \frac{T_\infty - T_s}{L} \left. \frac{\partial T}{\partial y} \right|_{y=0} \implies Nu \equiv \frac{hL}{k_f} = \left. \frac{\partial T^*}{\partial y^*} \right|_{y^*=0} \quad (2.10)$$

### 2.3.2 Free Convection

In free convection, there is no velocity in the free stream region and the motion of the fluid is driven by the density difference due to temperature difference. To this end, one way to deal with the body force caused by the buoyancy of a differential control volume, is to account for its own weight assuming an average density in the pressure term of equation 2.4b, and imposing a body force (term  $X$  in equation 2.4b) assuming the variable density due to temperature difference. The balance of these two terms yields the body force applied to the differential control volume regarding its buoyancy relative to the entire domain of the fluid.

$$u \frac{\partial u}{\partial x} + v \frac{\partial u}{\partial y} = -\frac{1}{\rho} \frac{\partial p}{\partial x} + \nu \frac{\partial^2 u}{\partial y^2} + g, \quad \left. \frac{\partial p}{\partial x} \right|_{x=\infty} = \rho_\infty g \quad (2.11a)$$

$$u \frac{\partial u}{\partial x} + v \frac{\partial u}{\partial y} = g \left( \frac{\Delta \rho}{\rho} \right) + \nu \frac{\partial^2 u}{\partial y^2} + \rho g \quad (2.11b)$$

Since this deduction assumes an incompressible fluid,  $\Delta \rho$  may be approximated by the volumetric thermal expansion coefficient  $\beta$  and temperature difference instead of density difference. Equation 2.12 shows an approximation to  $\Delta \rho$  based on the coefficient  $\beta$  assuming reference properties at free stream ( $\infty$ ). This is referred to as the Boussinesq approximation.

$$\beta = -\frac{1}{\rho} \left( \frac{\partial \rho}{\partial T} \right)_P \implies \beta \approx -\frac{1}{\rho} \frac{\rho_\infty - \rho}{T_\infty - T} \implies (\rho_\infty - \rho) = \rho \beta (T_\infty - T) \quad (2.12)$$

Acknowledging that the energy equation remains the same in free convection, the set of governing equations are

$$\frac{\partial u}{\partial x} + \frac{\partial v}{\partial y} = 0 \quad (2.13a)$$

$$u \frac{\partial u}{\partial x} + v \frac{\partial u}{\partial y} = \rho \beta (T_\infty - T) + \nu \frac{\partial^2 u}{\partial y^2} \quad (2.13b)$$

$$u \frac{\partial T}{\partial x} + v \frac{\partial T}{\partial y} = \alpha \frac{\partial^2 T}{\partial y^2} \quad (2.13c)$$

The same dimensionless criteria, equation 2.8, may be used with the only difference being that the characteristic velocity can not be the free stream velocity since its zero, hence should be an arbitrary representative velocity. The momentum equation and the energy equation yield equations 2.14a and 2.14b

$$u^* \frac{\partial u^*}{\partial x^*} + v^* \frac{\partial u^*}{\partial y^*} = \frac{g \beta (T_s - T_\infty) L}{u_0^2} T^* + \frac{1}{Re_L} \frac{\partial^2 u^*}{\partial y^{*2}} \quad (2.14a)$$

$$u^* \frac{\partial T^*}{\partial x^*} + v^* \frac{\partial T^*}{\partial y^*} = \frac{1}{Re_L Pr} \frac{\partial^2 T^*}{\partial y^{*2}} \quad (2.14b)$$

The first term on the right hand side of equation 2.14a is responsible for the buoyancy force on a differential control volume, hence it may be regarded as a quantifier for free convection. Since the quantity,  $u_0^2$  participates in this term, it is not a convenient term to define free convection with because there is no characteristic velocity in pure free convection. To handle this issue, this term is multiplied by  $Re_L^2 = (u_0 L/\nu)^2$  yielding what is referred to as *Grashof* number.

By looking at the right side of equation 2.14a, it can be reasoned that the relative magnitude of the *Grashof* number dictates how much momentum the temperature difference ( $T_s - T_\infty$ ) generates.

### 2.3.3 Mixed Convection

The quantity  $(Gr_L/Re_L^2)$  is used to weight the relative magnitude of free vs forced convection. If  $(Gr_L/Re_L^2) \approx 1$  both effects must be taken into consideration, if  $(Gr_L/Re_L^2) \ll 1$  free convection may be disregarded and if  $(Gr_L/Re_L^2) \gg 1$  forced convection may be disregarded.

Since there are no sharp values to define when convection is considered free or forced or mixed, Figure 2.2 provides a visualisation of these values. This figure shows the magnitude of the deviation from pure, free and forced convection for an horizontal flat plate.

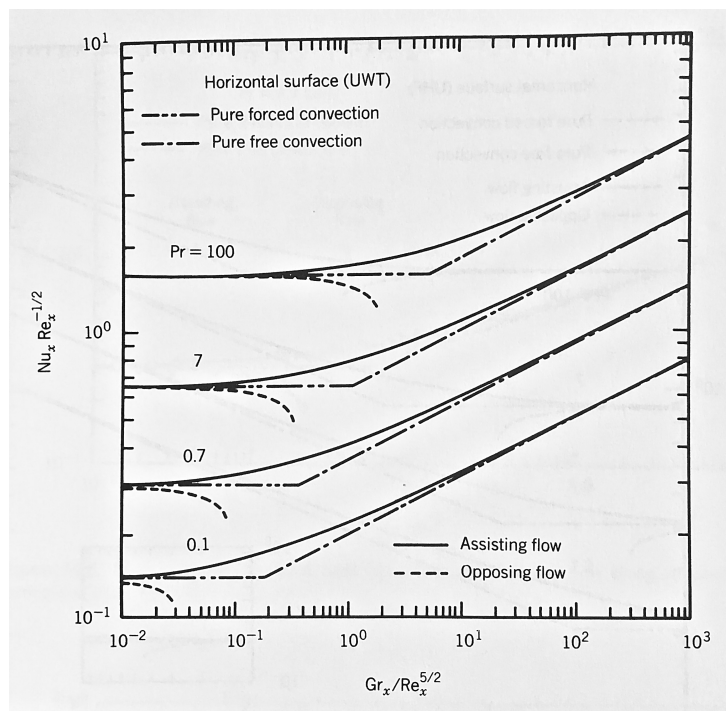


Figure 2.2: Free Vs. Forced Convection, [2].

### 2.3.4 Dimensionless Groups

In order to distinguish between each type of convection, free, forced and mixed, and within each type, a laminar or turbulent flow, there needs to be a well defined criterium to judge which is the case. This criterium is based on dimensionless groups that inform about the characteristics of the flow. Table 2.1 shows the most relevant of these groups for this study.

Symbol	Group	Definition	Interpretation
$Nu_L$	Nuselt number	$\frac{hL}{k_{fluid}}$	Temperature gradient at the surface.
$Pr$	Prandtl number	$\frac{c_p \mu}{k} = \frac{\nu}{\alpha}$	Ratio of Momentum and thermal diffusivities.
$Re_L$	Reynolds number	$\frac{U \cdot L}{\nu}$	Ratio of inertia and viscous forces.
$Gr_L$	Grashof number	$\frac{g\beta(T_s - T_\infty)L^3}{\nu^2}$	Ratio of buoyancy to viscous forces.
$Ra_L$	Rayleigh number	$Gr_L \cdot Pr$	Ratio of free Convective heat transfer and Transported heat.
$Ri_L$	Richardson number	$\frac{Gr_L}{Re^2}$	Relative strenght of natural to forced convection.

Table 2.1: Dimensionless groups for heat transfer.

The *Nusselt* number has been described earlier in Section 2.3 through equation 2.10, and represents the dimensionless temperature gradient at the surface.

The *Prandtl* number appeared in equation 2.9b and it relates the velocity field to the temperature field in the direction perpendicular to the wall. Apart from the *Prandtl* number, the governing equations for velocity and for energy, equations 2.9a and 2.9b, are almost alike for a zero pressure gradient in the flow direction. Therefore, apart from their boundary conditions and the *Prandtl* number, both velocity and temperature, behave in the same manner. Since the diffusive term, on the right side, is responsible for the thickness,  $\delta$ , of the boundary layer, the velocity boundary layer thickness may be related to the thermal boundary layer thickness by the *Prandtl* number, equation 2.15, where  $n = 1/3$  is used for most applications [1].

$$\frac{\delta_{vel}}{\delta_{ther}} = Pr^n \quad (2.15)$$

What has just been stated means that the *Prandtl* number is a measure of the ratio of diffusion of momentum and diffusion of thermal energy.

The *Reynolds* defines the point where the boundary layer undergoes transitions from laminar to turbulent. This transition occurs at a critical value of the *Reynolds* number. When the free stream arrives at the leading edge, Figure 2.1, the velocity profile is uniform. Since the velocity is zero at the surface and  $u_\infty$  at the free stream, the velocity profile evolves progressively and orderly from zero to  $0.99 u_\infty$  in the boundary layer. Disturbances to this organised flow originated from free stream or from surface roughness, may induce a turbulent flow, depending of wether these disturbances are amplified or dampened, which depends on the ratio of inertia to viscous forces which is the *Reynolds* number. A representative value of transition from laminar to turbulent flow in a flat plate is  $Re_x = 5 \cdot 10^5$ .

The details of the consequences of a turbulent flow, are vast. One of the most relevant is that the

higher mixing in the flow promotes an increase in the convective heat transfer due a higher temperature gradient at the surface.

The *Grashof* number, described in Section 2.3.2, taken from equation 2.14a and multiplied by  $Re_L^2$ , serves the purpose of deciding whether convection is to be interpreted as free convection, or forced or mixed. It indicates the ratio of buoyancy force to the viscous force acting on a differential control volume. There can be a resemblance between the *Reynolds* number and the *Grashof* number in the way that the first uses inertial forces and the second uses the buoyancy forces instead, to relate to viscous forces.

The *Rayleigh* number is simply the product of the *Grashof* number and *Prandtl* number.

The *Richardson* number relates the buoyancy forces to the shear forces. It is used to decide whether convection is to be interpreted as free convection, or forced or mixed using a reference velocity.

## 2.4 Radiation

Heat exchange through Radiation is a process that exchanges thermal energy through thermal radiation without the need of matter to conduct or transport this energy between two bodies or surfaces. In reality, radiation is a volumetric phenomenon, but throughout this study, a surface phenomenon is assumed (opaque materials in the thermal spectral region). The emission of radiation in general happens at the surface of a body in the first few layers of matter (approx.  $1 \mu m$ ). This emission may be viewed as the emission of photons or electromagnetic waves. Their frequency,  $\nu$  and wavelength,  $\lambda$  are related through the speed of light in the medium,  $c$ , through  $\lambda = c/\nu$ .

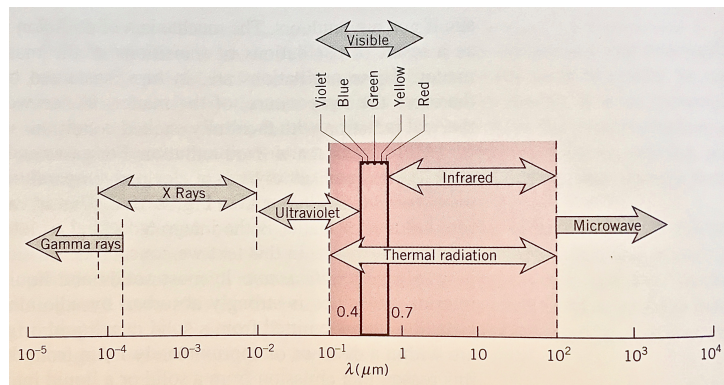


Figure 2.3: Spectrum of electromagnetic radiation, [1]

Thermal radiation has a well defined range in the full radiation spectrum. This range is approximately from  $0.1 \mu m$  to  $100 \mu m$  which includes part of Ultraviolet, visible and Infrared radiation, Figure 2.3.

A surface, exposed to Irradiation, at each wavelength, absorbs a portion of this energy either through a temperature increase or transmission of this energy, and reflects the remaining. Also, the surface emits thermal radiation according to its temperature and the characteristics of the surface.

The incident radiation or Irradiation,  $G_\lambda [W/m^2 \mu m]$  of a certain wavelength is the radiation that arrives at a surface from all directions, equation 2.16.



$$G_{\lambda}(\lambda) = \int_0^{2\pi} \int_0^{\pi/2} I_{\lambda,i}(\lambda, \theta, \phi) \cos \theta \sin \theta d\theta d\phi \quad (2.16)$$

In this equation, the term  $\sin \theta d\theta d\phi$  is the unit solid angle of the incoming radiation  $I_{\lambda,i}(\lambda, \theta, \phi)$  about a certain angle to the normal of the surface  $\cos \theta$ . The geometrical interpretation of these angles is represented in Figure 2.4.

The total irradiation is then the irradiation from all wavelengths  $G = \int_0^{\infty} G_{\lambda}(\lambda) d\lambda$

The term  $I_{\lambda,i}(\lambda, \theta, \phi)$  is referred to as the spectral intensity and is defined as the radiant energy of wavelength  $\lambda$ , propagating in  $(\theta, \phi)$  direction, per unit time, per unit area of the surface normal to this direction per unit solid angle about this direction per unit wavelength  $d\lambda$ . Therefore  $I_{\lambda,i}(\lambda, \theta, \phi)$  has units of  $[W/m^2 \text{ sr } \mu m]$ .

Integrating equation 2.16 over the whole hemisphere and assuming a diffuse irradiation, i.e. equal intensity from all directions, which implies  $I_{\lambda,i}(\lambda, \theta, \phi) = I_{\lambda,i}(\lambda)$ , yields the simple relation 2.17.

$$G = \pi I_i \quad (2.17)$$

What has been said for incident radiation, holds just the same for emission  $E$ . The spectral, spherical emissive power  $E_{\lambda, \text{emitted}} [W/m^2 \mu m]$  is the rate at which radiation of wavelength  $\lambda$  is emitted in all directions from a surface per unit surface area. So the corresponding equation is obtained just by substituting letter  $G$  by  $E$  and subscript  $i$  by  $e$  in equations 2.16 and 2.17.

Radiation exchange between two surfaces therefore depends on their view factor from one to the other. This can be verified by applying the aforementioned geometrical criteria to radiation exchange between two surfaces [1].

The term Black body, refers to a surface that absorbs all incident radiation regardless of wavelength and direction and emits, diffusely, the maximum possible amount of energy, at its temperature. Assuming this behaviour, the *Stefan – Boltzman* law, relates the total emissive power of a blackbody  $E_b$ , to its temperature through the spectral distribution of a blackbody's emission due to its temperature, referred to as *Planck's* distribution. The total emission of a black body is therefore  $E_b = \sigma T^4$  where  $\sigma$  is the *Stefan – Boltzman* constant and has a value of  $\sigma = 5,670 \cdot 10^{-8} [W/m^2 K^4]$ .

The parameter, total emissivity, is defined as the ratio of radiation emitted by the surface to the radiation emitted by a blackbody in all directions and all wavelengths.

$$\varepsilon(T) = \frac{\int_0^{\infty} \int_0^{2\pi} \int_0^{\pi/2} I_{\lambda,e}(\lambda, \theta, \phi, T) \cos \theta \sin \theta d\theta d\phi d\lambda}{\int_0^{\infty} \int_0^{2\pi} \int_0^{\pi/2} I_{\lambda,b}(\lambda, T) \cos \theta \sin \theta d\theta d\phi d\lambda} \quad (2.18)$$

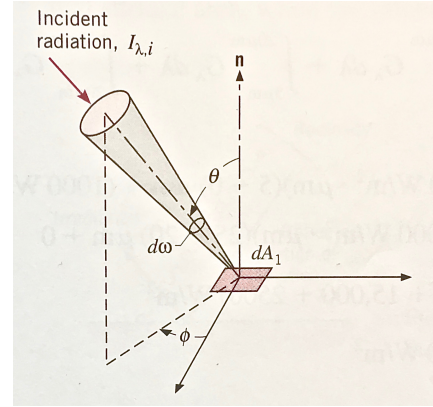


Figure 2.4: Directional nature of incident radiation, [1].

In shorthand notation becomes  $\varepsilon(T) = E(T)/E_b(T)$ .

The total absorptivity, is the part of the incoming radiation that is not reflected or transmitted but transformed into internal energy. The defining equation is just the same, only the spectral intensity is the irradiated one instead of the emitted one,  $I_{\lambda,i}(\lambda, \theta, \phi)$  which does not depend on the surface temperature. In shorthand notation is  $\alpha = G_{abs}/G$ .

Total reflectivity may have the same approach although there is a directional dependence that is not considered. Instead the average values of irradiation and reflected irradiation over the hemisphere are assumed [1]. It takes the same form as absorptivity, with  $I_{\lambda,r}(\lambda, \theta, \phi)$ . In shorthand notation,  $\rho = G_{ref}/G$ .

Considering an isothermal enclosure at temperature  $T_s$  shown in Figure 2.5 and assuming a steady-state thermal equilibrium, the surface emits diffusely according to its temperature  $T_s$  which is the behaviour of a blackbody cavity. Also, all bodies inside it are at temperature  $T_s$ . Hence, the irradiation experienced by a body in the cavity is diffuse and equal to  $G = E_b(T_s)$ . An energy balance to the surface of body  $A_1$ , yields the relation,  $\alpha_1 G A_1 - E_1(T_s) A_1 = 0$  and substituting  $G$  and  $E_1(T_s)$  yields equation 2.19

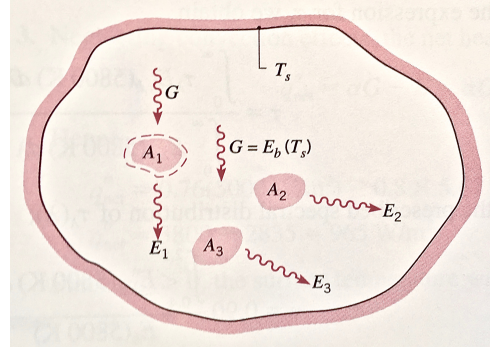


Figure 2.5: Radiation exchange in an isothermal enclosure, [1].

$$\alpha_1 E_b(T_s) A_1 = \varepsilon_1 E_b(T_s) A_1 \implies \varepsilon_1 = \alpha_1 \quad (2.19)$$

This is known as the *Kirshoff's law*. The same derivation just made could be made with emission and irradiance as a function of wavelength, then it would yield  $\varepsilon_{\lambda,1} = \alpha_{\lambda,1}$ , and also regarding direction which would yield  $\varepsilon_{\lambda,\theta,1} = \alpha_{\lambda,\theta,1}$ . In the first two cases restrictions to their validity apply. It can be shown that the restrictions to the validity of  $\varepsilon_{\lambda,1} = \alpha_{\lambda,1}$ , are that the enclosure is a diffuse emitter as well as the surface of body 1. The conditions for the validity of  $\varepsilon_1 = \alpha_1$  are that the enclosure has a blackbody behaviour, and the surface of body 1 is gray, which stands when emissivity and absorptivity are independent of wavelength.

Considering the net radiation exchange of a gray surface in an enclosure,  $q_s = A_s (J_s - G_s)$ , where  $J$  is the radiosity of the surface which is the emitted radiation plus the reflected irradiance,  $J_s \equiv E_s + \rho_s G_s$  and assuming an opaque, diffuse, gray surface,  $\rho_s = 1 - \alpha_s = 1 - \varepsilon_s$ , *Kirshoff's law*, and arranging these equations yields equation 2.20.

$$q_s = \frac{E_{b,i} - J_s}{(1 - \varepsilon_s)/(\varepsilon_s A_s)} \quad (2.20)$$

For a two surface enclosure, shown in Figure 2.6, the net rate of radiation transfer between the two,  $q_{12}$ , is, from the definition of view factor,  $q_{12} = A_1 F_{1,2} (J_1 - J_2)$ . Hence, the net rate of radiation transfer between the two surfaces yields equation 2.21. This result is used later to justify the radiation exchange between the surface of the Module and the sky.

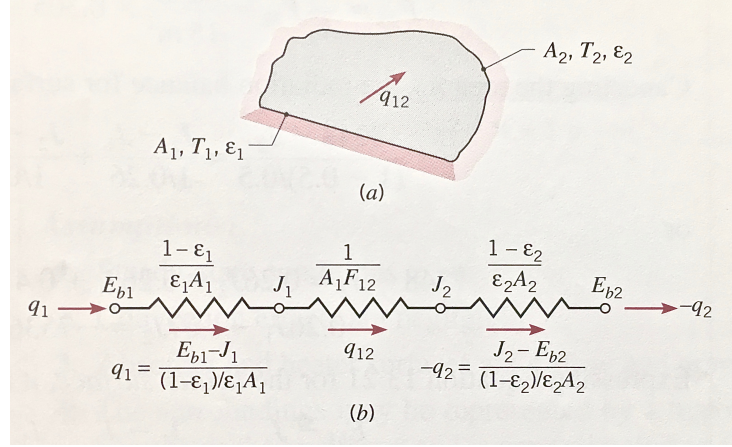


Figure 2.6: Two Surface Enclosure, [1]

$$q_{12} = \frac{\sigma (T_1^4 - T_2^4)}{\frac{1-\varepsilon_1}{\varepsilon_1 A_1} + \frac{1}{A_1 F_{12}} + \frac{1-\varepsilon_2}{\varepsilon_2 A_2}} \quad (2.21)$$

## 2.5 Phase Change

In this Thesis, phase change may occur in the water. This process happens between the solid and liquid phases of the water. The governing equations that describe phase change in a one dimensional domain in a semi-infinite solid with an initial temperature  $T_i$  above the phase change temperature and a wall temperature  $T_w$  below phase change are presented in equation 2.22a and equation 2.22b.

$$\rho_s c_{ps} \frac{\partial T_s}{\partial t} = k_s \frac{\partial^2 T_s}{\partial x^2} \quad (2.22a)$$

$$\rho_l c_{pl} \frac{\partial T_l}{\partial t} = k_l \frac{\partial^2 T_l}{\partial x^2} \quad (2.22b)$$

Equation 2.22b refers to the liquid side of the interface and equation 2.22a to the solid side. By imposing the boundary conditions stated in equations 2.23a and 2.23b yields equation 2.23c that defines the velocity of the advancing interface.

$$T_s(0, t) = T_w \quad (2.23a)$$

$$T_s(X, t) = T_m = T_l(X, t) \quad (2.23b)$$

$$-k_l \frac{\partial T_l}{\partial x} + k_s \frac{\partial T_s}{\partial x} = \rho L \frac{\partial X}{\partial t} \quad (2.23c)$$

In equation 2.23c, the term  $L$  denotes the Latent heat released due to solidification of the water. The term  $\partial X / \partial t$  represents the velocity of the advancing interface  $X(t)$ . Figure 2.7 shows a schematic of a one-dimensional case.

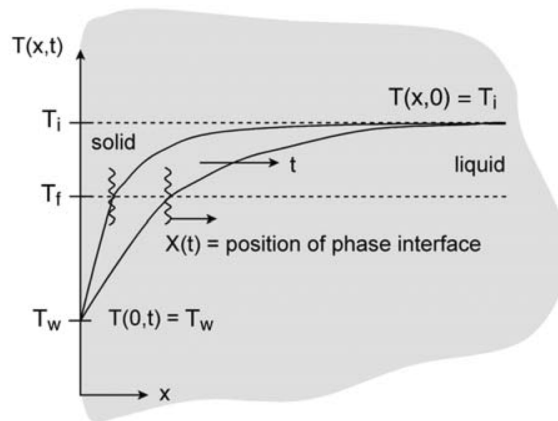


Figure 2.7: Schematic of phase change in a semi-infinite domain, [4].

# Chapter 3

## Implementation

Here, how the temperature profile in the Module during one year is obtained is presented.

The programming Language used is Python, a modern multi-paradigm, interpreted, high-level language. A library called Numpy is used for array manipulation, which is the bulk of the performed operations in each time step.

First the governing equations regarding heat transfer and fluid flow are addressed, then their solution using the FVM is discussed with its particularities regarding this implementation. Some of these particularities are considered separately for clarity. The detailed dimensions of the Module are presented and the building of the geometry is explained for all three cases, one, two and three-dimensional. The boundary conditions are addressed and each type is viewed separately. The implementation of phase change in the water domain is presented and finally the properties of materials used and other input data is presented.

### 3.1 Governing equations for fluid flow and heat transfer

The most generic equation used for conservation of a scalar property is the advection-diffusion equation 3.1.

$$\frac{\partial(\rho \phi)}{\partial t} + \text{div}(\rho \phi \vec{v}) = \text{div}(\Gamma \text{grad} \phi) + S_{\phi} \quad (3.1)$$

This equation originates from the advection equation and diffusion equation, which correspond to the second term on the left hand side and first term on the right hand side respectively. The term  $S_{\phi}$  represents internal source of  $\phi$ , the conserved property.

By inspection of this equation, if  $\phi = 1$ , mass conservation is imposed or continuity, if  $\phi = u, v, w$  [ $m/s$ ], the equation describes conservation of momentum in the respective direction and if  $\phi = h$  [ $J/Kg$ ] conservation of energy.

The first thing to be taken into account is the conservation of mass, equation 3.2.

$$\frac{\partial \rho}{\partial t} + \text{div}(\rho \vec{v}) = 0 \quad (3.2)$$

The second aspect regarding fluid flow is the conservation of momentum which states that the rate of change of momentum in a fluid particle equals the forces applied to this particle and is an interpretation of Newton's second law of motion.

The motion of a Newtonian fluid, is modelled by the Navier-Stokes equation. Its most generic form, for constant viscosity of the fluid, in vector notation, is equation 3.3.

$$\rho \frac{D\vec{v}}{Dt} = -\nabla p + \mu \nabla^2 \vec{v} + \frac{1}{3} \mu \nabla \Theta + S_M \quad , \quad \text{where } \Theta \equiv \frac{\partial u}{\partial x} + \frac{\partial v}{\partial y} + \frac{\partial w}{\partial z} \quad (3.3)$$

If the fluid is incompressible  $\Theta$  is naturally zero and the third term on the right hand side of equation 3.3 disappears. Additionally, the pressure term may be treated as a surface force and included in source term. Implementing equation 3.3 for one direction, e.g.  $x$ , yields equation 3.4.

$$\rho \frac{Du}{Dt} = -\frac{\partial p}{\partial x} + \mu \frac{\partial^2 u}{\partial x^2} + S_{Mx} \quad (3.4)$$

The total or substantive derivative appearing on the left hand side of equation 3.3 and equation 3.4 refers to the rate of change of property  $\phi$  of a fluid particle. For a stationary fluid element, this term includes the rate of change of  $\phi$  in the CV volume and also the flux of  $\phi$  through the CV faces as is seen next. Hence, expanding the total derivative of the left hand side of equation 3.3 in order to obtain the rate of change of property  $\phi$  with respect to time following a fluid particle yields equation 3.5.

$$\begin{aligned} \rho \frac{D\phi}{Dt} &= \rho \left( \frac{\partial \phi}{\partial t} + \frac{\partial \phi}{\partial x} \frac{dx}{dt} + \frac{\partial \phi}{\partial y} \frac{dy}{dt} + \frac{\partial \phi}{\partial z} \frac{dz}{dt} \right) \\ &= \rho \left( \frac{\partial \phi}{\partial t} + u \frac{\partial \phi}{\partial x} + v \frac{\partial \phi}{\partial y} + w \frac{\partial \phi}{\partial z} \right) \\ &= \rho \left( \frac{\partial \phi}{\partial t} + \vec{v} \text{grad} \phi \right) \end{aligned} \quad (3.5)$$

Now, taking the continuity equation 3.6a, for a fluid element of a generic property  $\phi$ , and calculating its derivative, yields equation 3.6b for an incompressible flow.

$$\frac{\partial(\rho \phi)}{\partial t} + \text{div}(\rho \phi \vec{v}) = 0 \quad (3.6a)$$

$$\begin{aligned} \frac{\partial(\rho \phi)}{\partial t} + \text{div}(\rho \phi \vec{v}) &= \rho \left( \frac{\partial \phi}{\partial t} + \vec{v} \text{grad} \phi \right) + \phi \left( \frac{\partial \rho}{\partial t} + \text{div}(\rho \vec{v}) \right) \\ &= \rho \left( \frac{\partial \phi}{\partial t} + \vec{v} \text{grad} \phi \right) \end{aligned} \quad (3.6b)$$

In equation 3.6b, the right hand side term of the above equality,  $\phi (\partial \rho / \partial t + \text{div}(\rho \vec{v}))$ , is zero due to mass conservation regardless of the incompressibility. Hence, by looking at both equations 3.5 and 3.6b, it can be seen that the total derivative of a generic intensive property  $\phi$  following a fluid particle with respect to time is equal to the rate of change of property  $\phi$  in a stationary fluid element plus the flux of property  $\phi$  through the same fluid element, equation 3.7.

$$\rho \frac{D\phi}{Dt} = \frac{\partial(\rho\phi)}{\partial t} + \text{div}(\rho\phi\vec{v}) \quad (3.7)$$

Now, the Navier-Stokes equation in all three directions, may be rewritten in the following form, equations 3.8a, 3.8b and 3.8c, by virtue of equation 3.7.

$$\frac{\partial(\rho u)}{\partial t} + \text{div}(\rho u\vec{v}) = -\frac{\partial p}{\partial x} + \text{div}(\mu \text{grad} u) + S_{Mx} \quad (3.8a)$$

$$\frac{\partial(\rho v)}{\partial t} + \text{div}(\rho v\vec{v}) = -\frac{\partial p}{\partial y} + \text{div}(\mu \text{grad} v) + S_{My} \quad (3.8b)$$

$$\frac{\partial(\rho w)}{\partial t} + \text{div}(\rho w\vec{v}) = -\frac{\partial p}{\partial z} + \text{div}(\mu \text{grad} w) + S_{Mz} \quad (3.8c)$$

Finally, the energy must also be conserved. According to the first law of thermodynamics, no energy is lost, hence, the rate of change of the property energy of a fluid particle is equal to the rate of heat addition to the fluid particle plus the rate of work done on the particle of fluid. The first type of energy, the type that is of concern to this study, refers to the internal energy that is accounted by heat. The second type, the rate of work done on the particle, is related to kinetic energy meaning that is associated with velocity and does not translate to heat.

For brevity sake, although a part of the work done on the fluid particle, is converted to heat through viscous dissipation of shear stresses in the fluid, these sources of heat are neglected in this study due to the low velocities and low viscosities. Therefore, regarding energy, only heat flux due to temperature difference is acknowledged.

So, considering the energy property as the enthalpy  $h$  [ $J/Kg$ ] and applying it to the advection-diffusion equation 3.1 yields equation 3.9

$$\begin{aligned} \frac{\partial(\rho h)}{\partial t} + \text{div}(\rho h\vec{v}) &= \text{div}(\Gamma \text{grad} h) + S_h \\ &= \text{div}(k \text{grad} T) + S_T \end{aligned} \quad (3.9)$$

Since for an incompressible fluid  $dh = i = C_p dT$ , within each time step, equation 3.9 may be rewritten using only temperatures  $T$  which is of much convenience when implementing the conservation of energy. This is accomplished simply by dividing all terms by  $C_p$  which is assumed to be constant within each time step. Equation 3.9 is then rewritten in the form of equation 3.10

$$\frac{\partial(\rho T)}{\partial t} + \text{div}(\rho T\vec{v}) = \text{div}(k/c_p \text{grad} T) + S_T \quad (3.10)$$

The set of governing equations to be solved is presented in Table 3.1.

Conservation	Governing Equation	Equation
Continuity	$\frac{\partial \rho}{\partial t} + \text{div}(\rho \vec{v}) = 0$	3.2
Momentum $x$	$\frac{\partial(\rho u)}{\partial t} + \text{div}(\rho u \vec{v}) = -\frac{\partial p}{\partial x} + \text{div}(\mu \text{grad } u) + S_{Mx}$	3.8a
Momentum $y$	$\frac{\partial(\rho v)}{\partial t} + \text{div}(\rho v \vec{v}) = -\frac{\partial p}{\partial y} + \text{div}(\mu \text{grad } v) + S_{My}$	3.8b
Momentum $z$	$\frac{\partial(\rho w)}{\partial t} + \text{div}(\rho w \vec{v}) = -\frac{\partial p}{\partial z} + \text{div}(\mu \text{grad } w) + S_{Mz}$	3.8c
Energy	$\frac{\partial(\rho T)}{\partial t} + \text{div}(\rho T \vec{v}) = \text{div}(k/c_p \text{grad } T) + S_T$	3.10

Table 3.1: Governing Equations for fluid flow with heat transfer.

## 3.2 Finite Volume Method

The Finite Volume Method (FVM) is a method for solving partial differential equations (PDE) by approximating them by algebraic equations. In this method, the values of the unknown variable are calculated at discrete Volumes in a meshed geometry. The volume integrals of the PDE are converted to surface integrals using the Gauss's divergence theorem, making this method intrinsically conservative as long as the areas from each face of a CV correspond to the same area of the adjacent CV, Figure 3.1.

The FVM discretizes the conservation laws of a scalar intensive property  $\phi$  for a Control Volume (CV). This CV has constant properties within itself and the rate of change of whatever the property, happens at its faces.

Starting with the most generic advection diffusion equation 3.1 and integrating over an entire CV, yields the conservation of a property in the CV's volume, equation 3.11a. Then, applying the Gauss Divergence Theorem, provides the same information, but now, what happens in the CV is related to what happens at its surfaces, equation 3.11b.

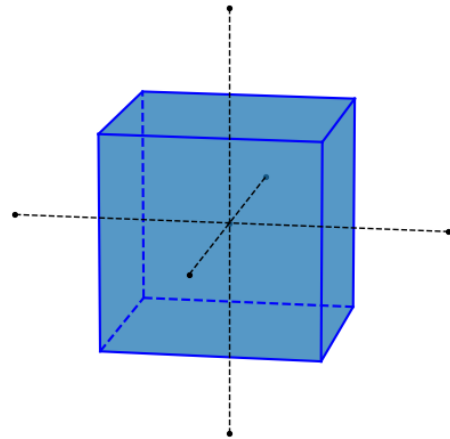


Figure 3.1: Generic Control Volume.

$$\int_V \frac{\partial(\rho \phi)}{\partial t} dV + \int_V \text{div}(\rho \phi \vec{v}) dV = \int_V \text{div}(\Gamma \text{grad } \phi) dV + \int_V S_\phi dV \quad (3.11a)$$

$$\frac{\partial}{\partial t} \left( \int_V \rho \phi dV \right) + \int_A \vec{n}(\rho \phi \vec{v}) dA = \int_A \vec{n}(\Gamma \text{grad } \phi) dA + \int_V S_\phi dV \quad (3.11b)$$



Finally, integrating over a time interval  $\Delta t$  and passing the second term on the left side to the right side of equation 3.11b in order to separate the volumetric rate of change and the surface's fluxes over the same time interval  $\Delta t$ , yields equation 3.12.

$$\int_{\Delta t} \frac{\partial}{\partial t} \left( \int_V \rho \phi dV \right) dt = \int_{\Delta t} \int_A -\vec{n} (\rho \phi \vec{v}) dA dt + \int_{\Delta t} \int_A \vec{n} (\Gamma \text{grad } \phi) dA dt + \int_{\Delta t} \int_V S_\phi dV dt \quad (3.12)$$

By inspecting equation 3.12, it can be acknowledged that the internal rate of change of a property  $\phi$  in the CV during a time interval  $\Delta t$  (term on the left side) equals the flow of this property through the CV faces due to bulk motion of the transporting medium (first term on the right side), plus the diffusive flux of this property through the CV faces (second term on the right side) and finally plus the respective sinks or sources of this property within the CV (third term on the right side).

A simplification of the above equation is shown next by considering only one direction, e.g.  $x$ . The term on the left side of equation 3.12 is approximated following a first order backward differencing scheme. This is shown on equation 3.13a. The first term on the right hand side, the advection term, is simply the difference in fluxes of property  $\phi$  at both sides of the one-dimensional CV during time interval  $\Delta t$ . These fluxes are shown in equation 3.13b (note that, the subscript  $e$  and  $w$  are cardinal directions meaning east and west respectively). The second term on the right hand side of equation 3.12, the diffusivity term, represents the difference in gradient of property  $\phi$  at both sides of the CV as stated in equation 3.13c. The last term is left out for simplicity, it represents the sources inside the CV.

$$\int_{\Delta t} \frac{\partial}{\partial t} \left( \int_V \rho \phi dV \right) dt = \rho (\phi_V^{t+\Delta t} - \phi_V^t) \Delta V \quad (3.13a)$$

$$\int_{\Delta t} \int_A -\vec{n} (\rho \phi \vec{v}) dA dt = -[(\rho u \phi A)_e + (\rho u \phi A)_w] \Delta t \quad (3.13b)$$

$$\int_{\Delta t} \int_A \vec{n} (\Gamma \text{grad } \phi) dA dt = \left[ \left( \Gamma A \frac{\partial \phi}{\partial x} \right)_e - \left( \Gamma A \frac{\partial \phi}{\partial x} \right)_w \right] \Delta t \quad (3.13c)$$

In the last equation 3.13c, the gradient of property  $\phi$  is approximated by a central differencing scheme applied to each face of the CV using the two adjoining CV's to the respective face, hence, by denoting subscripts  $E$  and  $W$  as the CV's to the east and to the west respectively, equation 3.13c reduces to equation 3.14.

$$\int_{\Delta t} \int_A \vec{n} (\Gamma \text{grad } \phi) dA dt = \left[ (\Gamma A)_e \frac{\phi_E - \phi_{CV}}{\delta x_{ECV}} - (\Gamma A)_w \frac{\phi_{CV} - \phi_W}{\delta x_{CVW}} \right] \Delta t \quad (3.14)$$

In equation 3.13b, the values of  $\phi$  are also relative to the CV's faces and not the CV itself, hence, in order to make the  $\phi$  values from equation 3.13b about the CV values, an average over both participating CV's is taken. The linear approximation to these CV face values assumes not only orthogonal volumes, but also equally spaced volumes. Therefore  $\phi$  values at each CV face are approximated by,  $\phi_e = (\phi_P + \phi_E)/2$  and  $\phi_w = (\phi_W + \phi_P)/2$ . Substituting the newly formulated terms in equation 3.13b yields equation 3.15.

$$\int_{\Delta t} \int_A -\vec{n}(\rho\phi\vec{v}) dA dt = - \left[ \left( \frac{\rho u A}{2} \right)_e (\phi_E + \phi_{CV}) + \left( \frac{\rho u A}{2} \right)_w (\phi_{CV} + \phi_W) \right] \Delta t \quad (3.15)$$

Finally, by acknowledging that the areas, as well as  $\delta x$  are all equal in this scenario (orthogonal CV's, equally spaced CV's) and assuming no sources, substituting in equation 3.12, equations 3.13a, 3.14 and 3.15, yields equation 3.16.

$$\begin{aligned} \frac{\rho(\phi_{CV}^{t+\Delta t} - \phi_{CV}^t) \Delta x}{\Delta t} &= C_w(\phi_E - \phi_{CV}) - C_e(\phi_{CV} - \phi_W) - D_w(\phi_{CV} - \phi_W) + D_e(\phi_E - \phi_{CV}) \\ &= \phi_W(C_w + D_w) - \phi_{CV}(-C_w + C_e + D_w + D_e) + \phi_E(-C_e + D_e) \\ &\approx \theta \left[ \phi_W(C_w + D_w) - \phi_{CV}(-C_w + C_e + D_w + D_e) + \phi_E(-C_e + D_e) \right]^{t+\Delta t} + \\ &\quad (1 - \theta) \left[ \phi_W(C_w + D_w) - \phi_{CV}(-C_w + C_e + D_w + D_e) + \phi_E(-C_e + D_e) \right]^t \\ &\quad \text{with, } C = \frac{\rho u}{2}, \quad D = \frac{\Gamma}{\delta x}, \quad 0 \leq \theta \leq 1 \end{aligned} \quad (3.16)$$

Figure 3.2 shows the behaviour described by equation 3.16 for a three-dimensional CV over a time interval  $\Delta t$ .

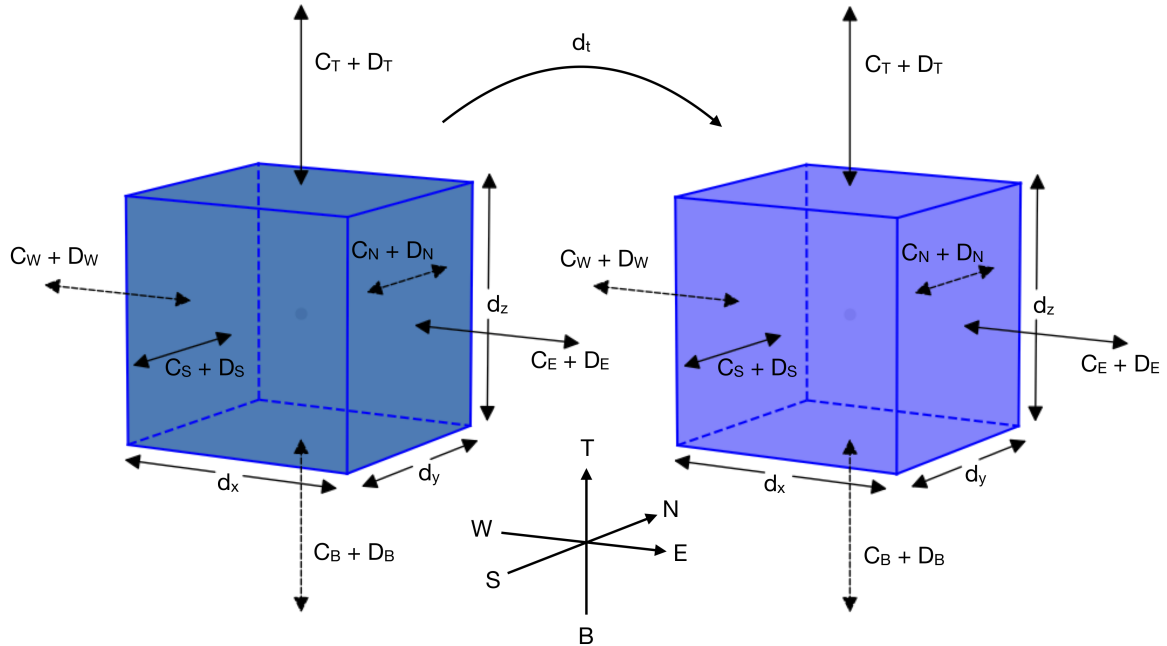


Figure 3.2: Finite Volume Method.

The left hand side of equation 3.16, representing the change of property  $\phi$  during the time step  $\Delta t$ , may be evaluated using the fluxes through the CV faces drawn from property  $\phi$  at time  $t$  where the properties are known, or at time  $t + \Delta t$  where the properties are unknown, or, with a weighted average

of both. This is implemented through the variable  $\theta$  in equation 3.16.

When  $\theta = 0$  the solution to the property  $\phi$  of the next time step is dependent only on the result of the previous time step, meaning that the solution over time may be obtained by successive calculations of the next time step. This method is referred to as the explicit scheme and is based on the backward differencing scheme. This method has a relevant restriction that limits the permissible time step to a maximum value. This value is well defined as a function of the properties and spacing of the grid, which is not shown here, but it may be interpreted has the diffusive and advective flux must not be such that within one time step, the property  $\phi$  entering one face of the CV reaches the opposing face, which would have to be accounted at the other CV, and is not due to the backward approximation of fluxes at the faces.

When  $\theta > 0$ , the property  $\phi$  at the next time step, which is unknown, is included in the calculation of the next time step. The equations for solving property  $\phi$  at each CV therefore depend on every other CV and as a result need to be solved together. If  $\theta = 0.5$  this method is referred to as Crank-Nicolson and the fluxes are based on an average of both times  $t$  and  $t + \Delta t$  which is in essence a central differencing scheme with respect to time and is therefore second-order accurate. For  $\theta \geq 0.5$  there is no longer a time restriction and the method is said to be unconditionally stable.

For  $\theta = 1$  the property  $\phi$  at the previous time step is no longer used (except in the volumetric rate of change), and the method is referred to as fully implicit scheme and is also unconditionally stable. This method is the advised one for general purpose transient calculations for its robustness and stability [5].

The influence of  $\theta$  on the solution of property  $\phi$  may be interpreted according to Figure 3.3

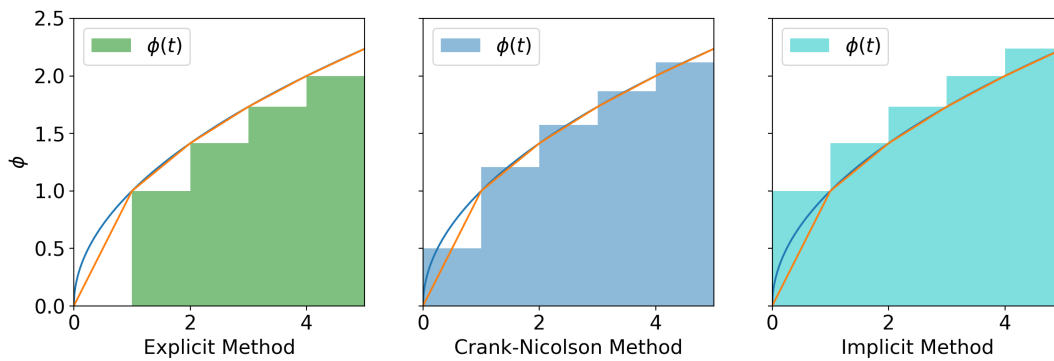


Figure 3.3: Transient discretisation of FVM.

### 3.2.1 Boussinesq Approximation

The flow occurring in the water domain, is driven by buoyancy forces due to a local density gradient arising from local temperature difference. This type of flow is the subject of natural convection in heat transfer, which was discussed in Section 2.3.2.

Since  $\rho$  is constant in the system of equations to be solved, equation 2.11a and equation 2.11b, the body force needs to be transformed into a function of temperature for it to be coupled to the existing unknowns, namely to the energy equation. To this end, the coefficient of volumetric expansion  $\beta [1/\kappa]$  is

used. Equation 3.17 shows this equality.

$$(\rho - \rho_0) g_i = -\rho_0 g_i \beta (T - T_0) \quad (3.17)$$

Therefore in flows driven by buoyancy forces, all equations governing the flow, including the energy equation are strongly coupled. This fact, then makes for a solver where the equations are better solved simultaneously, instead of iterating over each equation separately. This way of approaching the solution of the governing equations is referred to as coupled solver in detriment of a segregated solver.

### 3.2.2 Staggered Grid

The governing equation for the calculation of the temperature field are displayed in Table 3.1. The unknown variables to be solved are temperature, velocity in the three directions if the analysis is three-dimensional, and pressure in each CV. These properties are set at the CV centroid or center, which represents an average of the field of the respective property over the CV.

For the case of the velocity field, it is preferable to place the velocities at the CV faces instead of the CV center. This location is better, for the velocity field, because velocity is a consequence of pressure difference or body force, which exists between two adjoining CV's. If the velocities were to be placed at the CV center like the other properties, the body force acting on the CV would have to be interpolated since pressure is defined only at the CV center.

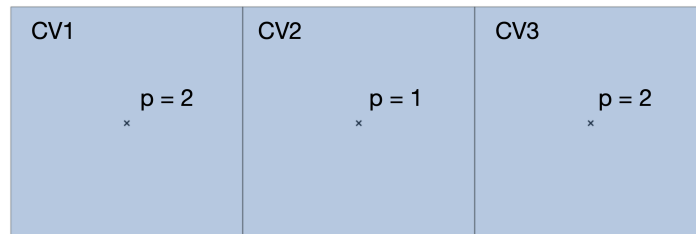


Figure 3.4: Pressure Field.

This interpolation may lead to an issue where the body force, caused by pressure difference, acting on a CV cancels out at both sides of the CV, although there is a pressure gradient between this CV and the adjacent ones. As can be seen in Figure 3.4, the pressure gradient at CV2 is zero since the interpolated pressure at both of its faces is equal even though the pressure field is not uniform.

This, of course, only happens if the pressure is not a monotonic function throughout the CV's, which implies a coarse grid. Nevertheless, the staggered arrangement for the velocity field yields a more realistic solution by avoiding the false situation described above.

To achieve this configuration, a dedicated grid for the velocity field as to be implemented. This additional grid is laid out of phase with the original one. Figure 3.5 shows this arrangement for a one dimensional case.

When the velocity field is placed at the center of the CV's like the other properties, the arrangement is called colocated, if it is placed as described above, is referred to as staggered.

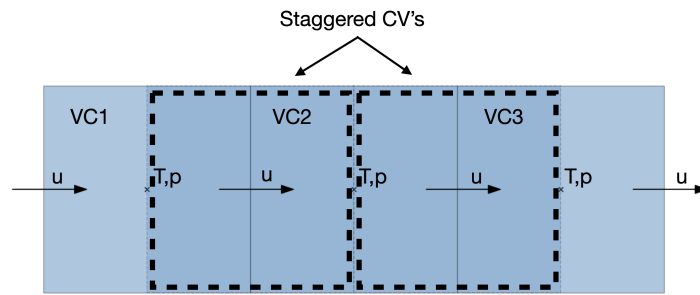


Figure 3.5: Staggered Grid.

In a staggered grid the properties that dictates the change in velocity do not need to be interpolated. In the colocated arrangement they do. Moreover, the velocities needed to calculate the scalar quantities also do not need to be interpolated. The disadvantage of this method is that there needs to be an implementation of the staggered grid for each direction.

### 3.2.3 Block Structured Grid

The approach to the domain discretisation in this Thesis is to subdivide it into blocks so that the mesh refinement at each block is independent. This allows the mesh to be refined only where a more detailed solution is desired, hence minimizing the computational cost of the solution.

The blocks are defined initially in the mesh generation routine of the code which creates a matrix for each block. This matrix carries the distances between CV's, properties of the material, etc.. Then, for each block an extra layer of CV's is added to the periphery of the block or matrix (both have the same shape). Figure 3.7 shows this arrangement in a  $3 \times 3$  two-dimensional grid.

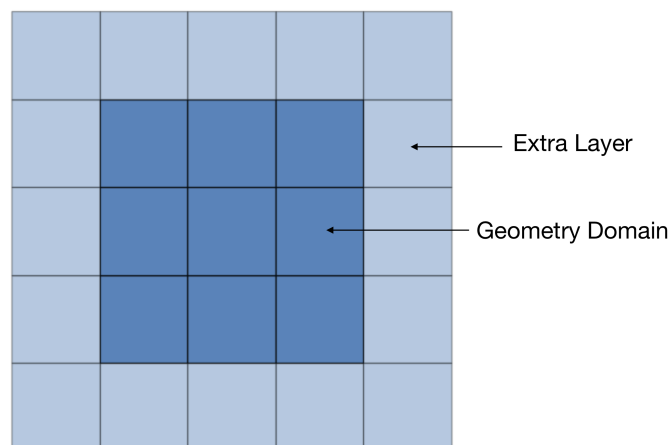


Figure 3.6: Block Structured Grid.

Each block, whether belonging to a fluid part or to a solid part, also has its own boundary conditions regarding its four or six adjacent blocks if two or three dimensional. Of course, if the block shares its boundaries with the exterior of the domain, the side of the block facing the exterior has no adjacent block

and the corresponding heat fluxes must be imposed at this surface.

The connection between each two adjoining blocks must be fully conservative regarding their properties. This connection is made when the full matrix containing all the blocks of the geometry is assembled. In this matrix each unknown variable of each CV of each block as its own line in the matrix, therefore, it is only a matter of ensuring the concerned properties (temperature, distances, etc.) of each CV in the extra layer are set equal to the corresponding CV in the adjacent block, hence replicating the outer CV's of the geometry domain (not the extra CV) in the adjoining blocks.

Figure 3.7 presents an example of a connection between two blocks in one direction only.

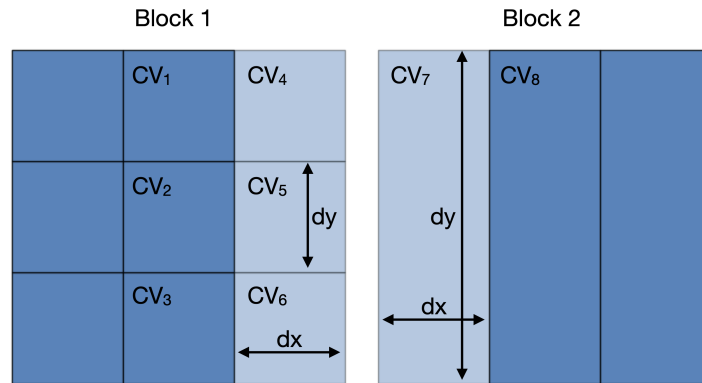


Figure 3.7: Connection between Blocks.

In this generic example, Block 1 has three CV's that need to be connected to one CV of Block 2. Hence, the temperature of  $CV_4$ ,  $CV_5$  and  $CV_6$  are set equal to the temperature of  $CV_8$ , and the temperature of  $CV_7$  is set equal to the average of the temperatures of  $CV_1$ ,  $CV_2$  and  $CV_3$ . Another aspect of this connection is that in this case  $dx$  is the same in both Blocks, but if it were not, the extra layer of Block 1 would have the  $dx$  of Block 2. This aspect is built into the subroutine responsible for implementing the extra layer of CV's in each block in the mesh creation. Moreover, the material of the extra layer of Block 1 is set in this same subroutine to the material of Block 2.

### 3.3 Approximation Scheme

The approach made in Section 3.2, is inherently a Central Differencing Scheme (CDS). This type of interpolation was assumed in order to show case how the FVM goes about implementing its surface and volume integrals.

The integrand of the volume integral of the property  $\phi$ , refers to the average property about the CV volume. The integrand of the surface integral, refers to the convective or diffusive flux, corresponding to equations 3.13b or 3.13c respectively, which is the average about the CV face of the flux  $\phi$ . Therefore the property  $\phi$  needs to be somehow approximated at the surfaces of the CV where it is not defined. This approximation is what the differencing scheme stands for.

By inspection of Figure 3.8, point  $P$  is the centroid of the CV, point  $E$  is the centroid of the CV to the right and  $e$  is the centroid of the face in between CV's  $P$  and  $E$ . The letters,  $N$ ,  $S$ ,  $E$ ,  $W$ , are referring

cardinal directions.

The scheme used in this Thesis is the Hybrid scheme which is based on the CDS and Upwind Differencing Scheme (UDS).

In the CDS the approximation is made by a linear interpolation between the two equally spaced adjacent nodes or CV's, equation 3.18.

$$\phi_e = \frac{\phi_P + \phi_E}{2} \quad , \quad \phi_w = \frac{\phi_W + \phi_P}{2} \quad (3.18)$$

This scheme of approximation may produce oscillatory solutions. This behaviour appears when the relative magnitude of the advection to diffusion is high. This measure is referred to as the *Peclet* number, or  $Pe$ , and is a dimensionless number, equation 3.19.

$$Pe = \frac{C}{D} = \frac{\rho u}{\Gamma/\delta x} \quad (3.19)$$

A high  $Pe$  number favours the oscillatory behaviour which translates to the conditions upstream dictating the conditions downstream. This is a consequence of the influence of the advective flux being greater than that of the diffusive flux, therefore the properties at  $CV_P$ , assuming a flow from west to east, are the most relevant to the properties at  $CV_E$ , and the diffusive flux plays a minor role in the properties of  $CV_E$ .

The problem with CDS and a high *Peclet* number is that in the case of a steep gradient of  $\phi$  at a boundary CV face, the average value of  $\phi$  at this CV is not able to reflect such gradient at this face since  $\phi$  represents an average value over the entire CV and is fixed at the CV center. Consequently, in order to respect continuity, the value of  $\phi$  at this CV is exaggerated so that the diffusive flux at the CV faces balances the advective flux into the CV. This erroneous behaviour is then propagated by oscillations so to respect continuity at each CV.

The Upwind Differencing Scheme (UDS), as the name suggests, approximates the fluxes at the CV faces  $e$  and  $w$  with the backward or forward difference approximation depending on the flow direction. Equation 3.20 shows this approximation.

$$\phi_w = \begin{cases} \phi_W \quad , & \text{if flow from west to east} \\ \phi_P \quad , & \text{if flow from east to west} \end{cases} \quad (3.20)$$

If the flow is from west to east, the flux at face  $w$ ,  $(\rho \phi u)_w$ , uses the value  $\phi_W$  instead of  $(\phi_w + \phi_P)/2$ , therefore assuming the upstream value of property  $\phi$ .

Since it is a first order accurate scheme, it never oscillates, because the used values of  $\phi$  at the

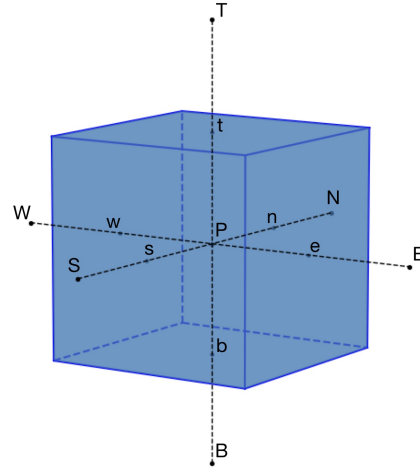


Figure 3.8: Control Volume.

face of the CV are values at one of the adjoining CV's and not a relative value between two CV's. The oscillatory behaviour of CDS is a consequence of the values of  $\phi$  at the faces being drawn from an average between the two adjoining CV's, allowing the values of  $\phi$  at the CV's to vary as long as continuity is respected.

The characteristic of taking flow direction into account in the discretisation scheme makes for the property of Transportiveness to be embedded in the scheme.

The fact that  $\phi$  is not an interpolated value, imposes that all values of  $\phi$  result from one or more reference values, consequently, in the absence of internal sources, the values of  $\phi$  are always within the maximum and minimum reference values, which makes overshoots non existing. This characteristic is referred to as Boundedness.

On the downside, in the presence of step gradients, this scheme produces smeared results. It can not represent sharp changes in property  $\phi$  accurately, unless there is such a grid refinement that the changes in  $\phi$  are not sharp any longer.

The Hybrid differencing scheme draws its name from using both the CDS and the UDS depending on the flow conditions. The criteria for using one or the other is the *Peclet* number. For small *Peclet* numbers,  $|Pe| < 2$ , CDS is used, for  $|Pe| \geq 2$  UDS. So, basically, for each CV face, this scheme calculates the corresponding *Peclet* number and depending on its value uses CDS or UDS.

This scheme, makes one more assumption in order to simplify it further. That is, when  $|Pe| \geq 2$ , which corresponds to advection playing the main role in the transfer of the property being calculated, the diffusive term is dropped since it plays a minor role.

### 3.4 Geometry

With an orthogonal geometry, cartesian coordinates are the obvious choice and are adopted here.

If one-dimensional, the grid generation is straightforward and yields temperatures in one direction only, which is the vertical direction. The respective boundary conditions are applied at the top and bottom. If the case is two or three-dimensional the lateral parts of the Module have to be added as well as their respective boundary conditions.

Although it would be possible to implement one single block for the whole Module comprehending all its parts with the desired grid refinement, for flexibility purposes, each part of the Module is implemented separately in the geometry allowing each part to be treated independently. As stated in Chapter 1 the main goal of this study is to know the temperatures in certain regions of the Module, which entails the knowledge of the temperatures in the Module all round. Therefore there are regions of the Module where a higher resolution of the solution may be advantageous, e.g. the water.

Computational cost is related to the level of grid refinement since the number of necessary calculations is proportional to the number of CV's. The implementation of separate parts with separate grid blocks indeed allows for a greater flexibility. Nevertheless, every time, there is a coarser grid next to a more refined grid, there is also the consequent reduction in accuracy. Hence this flexibility must be used with care and reason. The computational cost is the limiting factor and the use of coarse grids in some



regions is exclusively due to this limitation.

### 3.4.1 Dimensions

The dimensions of the Module are fixed throughout this Thesis. These may be changed if desired since they are an input parameter.

The water volume has a horizontal surface area of  $1 \times 1$  [m] and a height of 0.5 [m]. Later, a 1 [m] sided cube is also considered. The rest of the geometry (parts of the Module) are added to these base dimensions of the water itself. Figure 3.9 shows only the water volume.

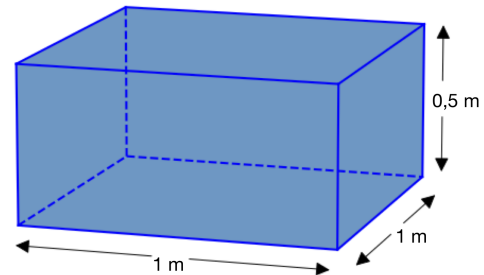


Figure 3.9: Water Volume.

Figure 3.10 shows the Module with all its possible constituents, RPC and insulation. The water is contained by a reservoir. Inside this reservoir there is an air gap between the water surface and the upper surface of the reservoir. Above the cover of the reservoir, there is another air gap, then the RPC, then another air gap, a lead plate and finally an insulation layer. In its simplest form, there would only be the water, the air gap above it and the reservoir without the upper protrusion to hold the RPC and lead plate.

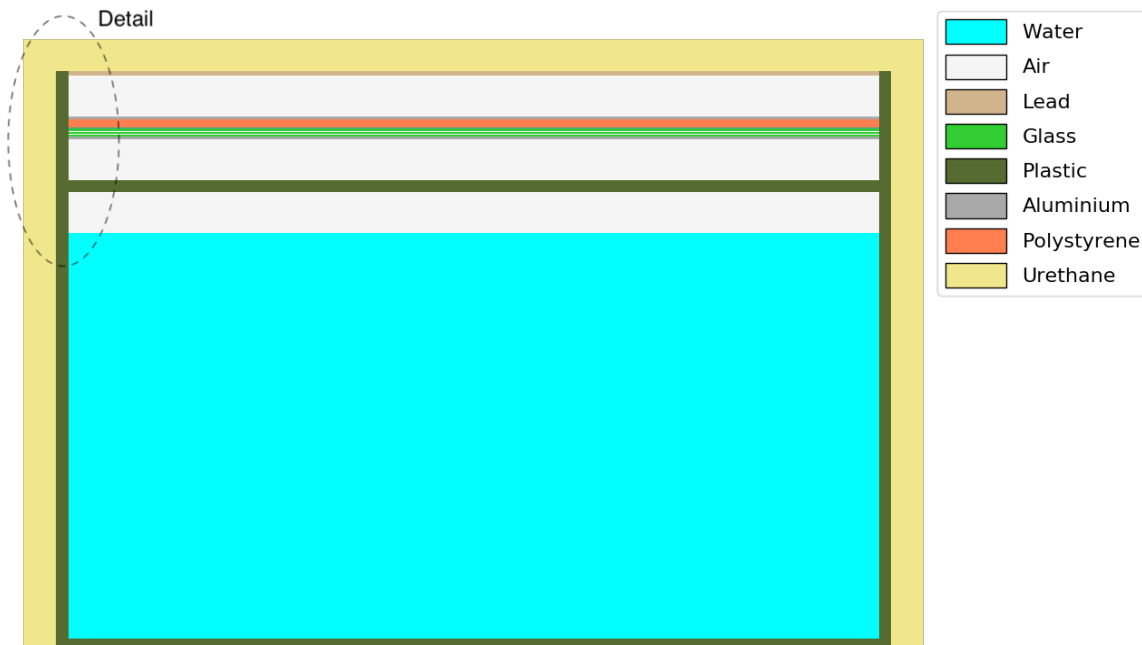


Figure 3.10: Module Geometry with RPC and insulation.

Dimension wise, and adding to the water volume, the thickness of the walls of the reservoir itself is 1.5 [cm] and the thickness of the insulation is 4 [cm]. These values are rough estimations of the

foreseeable ones since these are not defined yet. The height of the air gaps is assumed to be 5 [cm]. The thickness of the Lead Plate is 5.6 [mm] and the overall thickness of the RPC is 2.8 [cm]. Figure 3.11 shows a closeup of the upper constituents of the Module, corresponding to the area marked with a dashed line in Figure 3.10.

As can be seen in Figure 3.11, the RPC, is implemented as several layers stacked on top of each other. Each layer represents each of the main constituents of the RPC. The actual RPC, is made of several more minor parts like spacers and sidewalls that are not taken into account here. Although they are minor parts in relation to the implemented ones, they all contribute to the temperature response of the RPC. This contribution is considered to be negligible and is disregarded here. With that in mind, it is noted here that throughout this Thesis, the RPC sensor is interpreted according to the shown geometry, or, as said above, as a stack of layers of different materials. Of course, there could be a thorough implementation of all parts of the RPC sensor since this sensor is well defined and detailed drawings are available, but the consequent computational cost of the solution would increase significantly and the impact on the temperature distribution in the water, which is the main focus of the present work, is considered to be negligible.

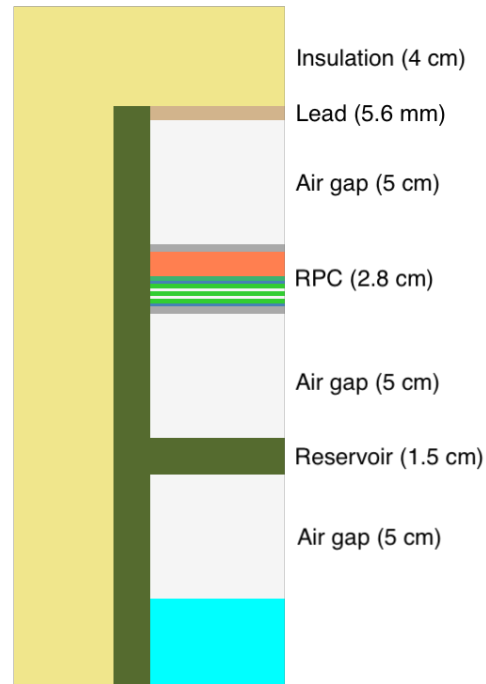


Figure 3.11: Detail of Lead Plate, RPC and Water.

The parts that make up the implemented RPC along with their vertical dimensions is shown in Figure 3.12 which is a close up of the RPC of Figure 3.11.

### 3.4.2 One-dimensional

The Module's domain has a parallelepiped shape, hence, in the one-dimensional case, the geometry consists of orthogonal CV's stacked on top of each other.

If only the WCD is to be considered, this geometry comprises the bottom of the reservoir, the water, an air gap between the surface of the water and the top of the reservoir and the top of the reservoir itself. The dimensions of this geometry are described in the previous Section. If the RPC is present, the corresponding layers exist on top of the reservoir. These may be seen in Figure 3.12. Each of these components may have any desired level of grid refinement in the vertical direction.

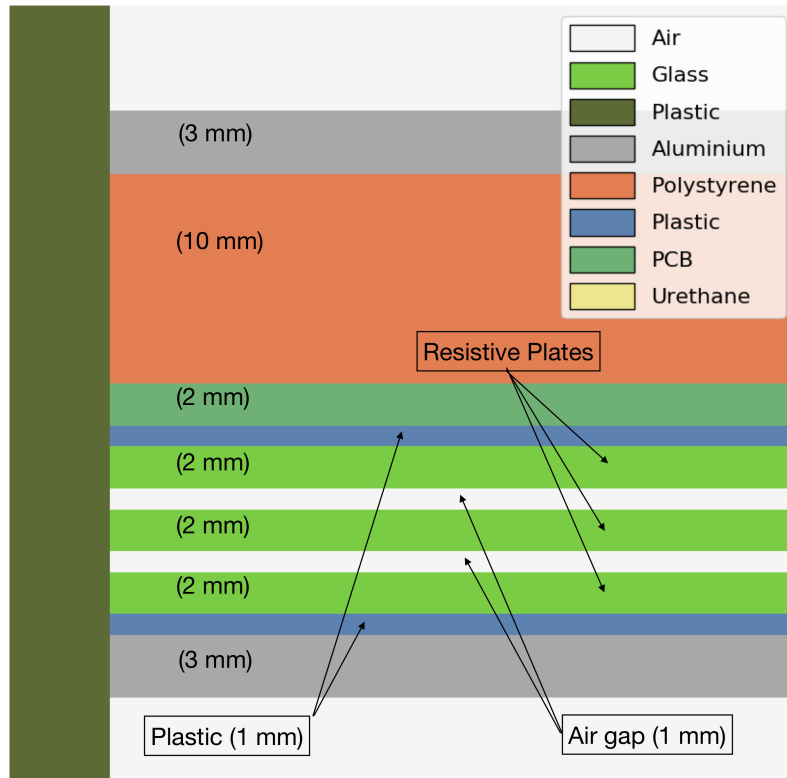


Figure 3.12: Detail of RPC.

### Grid Assembly

In a one-dimensional analysis, two boundary conditions must be set, one in the upper surface of the Module, and the other in its lower surface. The boundary condition in the upper surface is obtained by applying a convective heat exchange and thermal radiation exchange according to the climatic data set and temperature of the Module's surface as shall be seen later. At the lower surface of the Module, given the Module is standing on the ground, there is a conductive heat exchange to the ground which is not known. Hence a boundary condition at this location is not possible. In order to apply a known boundary condition at the lower surface of the whole geometry, the domain of the Module is extended to the underground. At a certain depth, temperatures may be assumed to be constant, hence an adiabatic condition may be imposed. The implemented depth is 10 [m]. This depth is conservative according to an analytical solution that roughly approximates the Module condition. The solution for a semi infinite solid with constant surface temperature is given by equation 3.21, [6].

$$\frac{T(x,t) - T_s}{T_i - T_s} = \text{erf} \left( \frac{x}{2\sqrt{\alpha t}} \right) \quad (3.21)$$

The graph of the depth at which there is no temperature difference from the initial temperature of the ground to the elapsed time, based on equation 3.21 is shown in Figure 3.13.

This graph uses the properties of sand taken from [1]. Since the site where the Module is to be located is a desert the assumption of a sandy ground is reasonable. The properties of sand are  $k = 0.27 [W/mK]$ ,  $\rho = 1515 [kg/m^3]$  and  $c = 800 [J/kg]$ , with  $\alpha = k/\rho c$ . This graph is obtained by setting  $(T(x,t) - T_s)/(T_i - T_s) = 0.9999$  which is interpreted as the depth at which there is no temperature difference. By inspection of this graph, it can be seen that for a depth of  $10 [m]$ , it takes about 6 months for a change in the dimensionless temperature to exist.

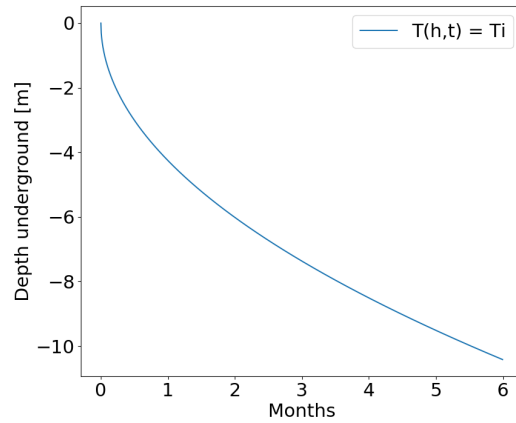
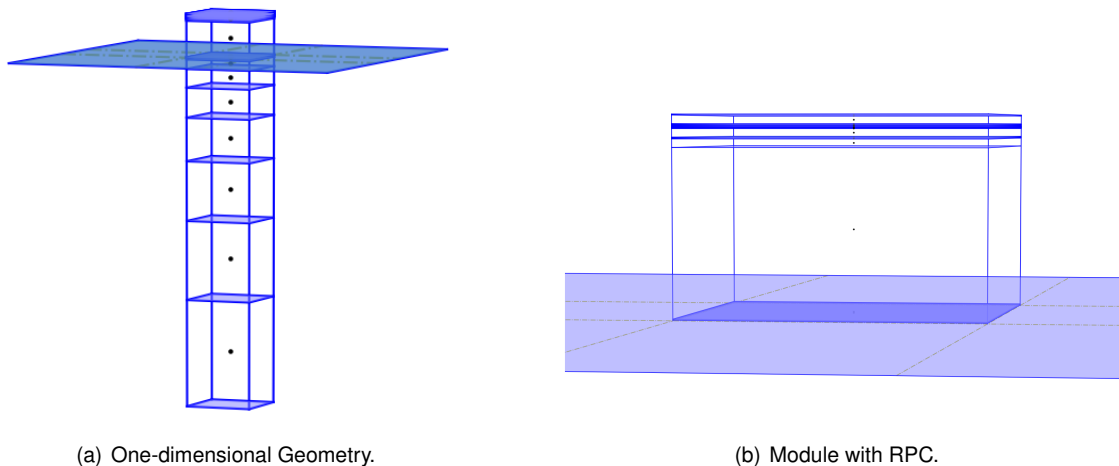


Figure 3.13: Depth of no temperature difference.

Considering the heat flux cycle through the ground to be 6 month in one direction and and 6 months in the other direction, it is assumed that the temperature  $10 [m]$  deep remains constant throughout the year. Since the underground domain is not part of the Module itself, but a “connection” of the bottom of the Module to a depth of ground that may be considered adiabatic, its grid may be treated in a different way as long as the desired effect of the adiabatic condition is reached. Hence, the temperature solution of the deepest part of the ground domain has a limited influence on the part near the surface. Only the part near the surface of this domain is relevant because of its transient interaction with the bottom of the Module. Therefore, this grid is implemented with a progressively increasing height of the next CV in the underground direction, with the height increasing according to a geometrical progression, so the biggest CV is the deepest one. Hence, minimizing the total number of CV’s in the domain, which brings down the computational cost, whilst retaining the adiabatic condition at  $10 [m]$  deep. This implementation is shown in Figure 3.14 left side. The Module’s domain only, without the underground, and with RPC, is shown in Figure 3.14 right side. In both these Figures, the wider flat part represents the surface of the ground.



(a) One-dimensional Geometry.

(b) Module with RPC.

Figure 3.14: One-dimensional domain.

### 3.4.3 Two-dimensional

In the two-dimensional case, the lateral components must be added to the geometry. These are the lateral reservoir wall and possibly a lateral layer of insulation.

The two-dimensional approach can only be applied if there is symmetry in one direction. In the case of the Module, the closest configuration that would comply with this symmetry condition would be to place several Modules in a row with adjoining faces and making this row as long as possible. This configuration is indeed one of the proposed ones in the central part of the Observatory as may be seen in Figure 1.2. In this central region, there is the intention of placing the Modules as close together as possible, hence increasing the concentration of readouts in the centre. Due to access reasons to the Modules by a person, there must be a “corredor” between each row of Modules. This layout is shown in Figure 3.15.

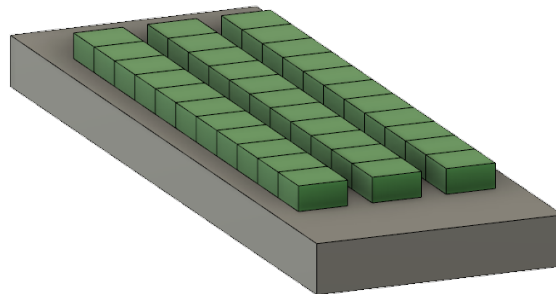


Figure 3.15: Two-dimensional Layout.

Under the above conditions, symmetry is a reasonable approximation to some extent. The fact that there are, in the row direction, different materials, namely, water and the walls of the reservoir, is not exactly symmetric from a numerical solution standpoint. But at least, inside each Module in between two other equal Modules, and so on, there is symmetry at the central plane of the Module perpendicular to the row direction. In this plane, the convective flow may be considered to have a velocity field that is constrained to this plane, and the temperatures at both sides of this plane may be considered symmetric. The two-dimensional condition would be fully satisfied if the reservoir was infinitely long in one direction. With that in mind, since the velocities due to convection are small, the magnitude of shear stresses at the walls are also small, hence, it is considered here that in the direction of the row there is symmetry. And for this central area of the Observatory, a two-dimensional approach is considered to be reasonable and is used in order to obtain a temperature profile in the Module.

#### Grid Generation

The geometry to be discretised is represented in Figure 3.16. The dimensions in this figure are not proportional to the real ones (Section 3.4.1) in order to make the visualisation of the process by which the geometry is discretised, clearer. In this drawing, the water itself as  $10 [cm]$  on the horizontal and vertical directions, the reservoir walls are  $1 [cm]$  thick, the insulation is  $3 [cm]$  thick and the air gap between the

water surface and the upper part of the reservoir is 5 [cm]. The model shown does not have RPC, but has insulation.

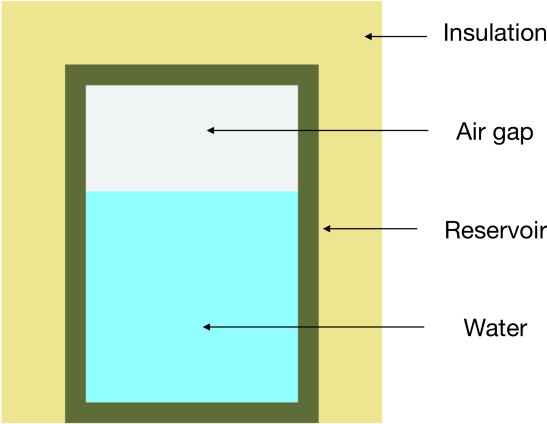


Figure 3.16: Two-dimensional Module sketch.

The grid generation in the two-dimensional case provides the base for the three-dimensional case. As stated in Section 3.4 the grid is built with the use of individual blocks for each part of the Module. Each block has a uniform orthogonal grid and is made of a single material. Then, the connection between each block is made upon assembling the coefficient matrix for the entire geometry. Figure 3.17 shows an exploded view of the several blocks that constitute the Module shown in Figure 3.16.

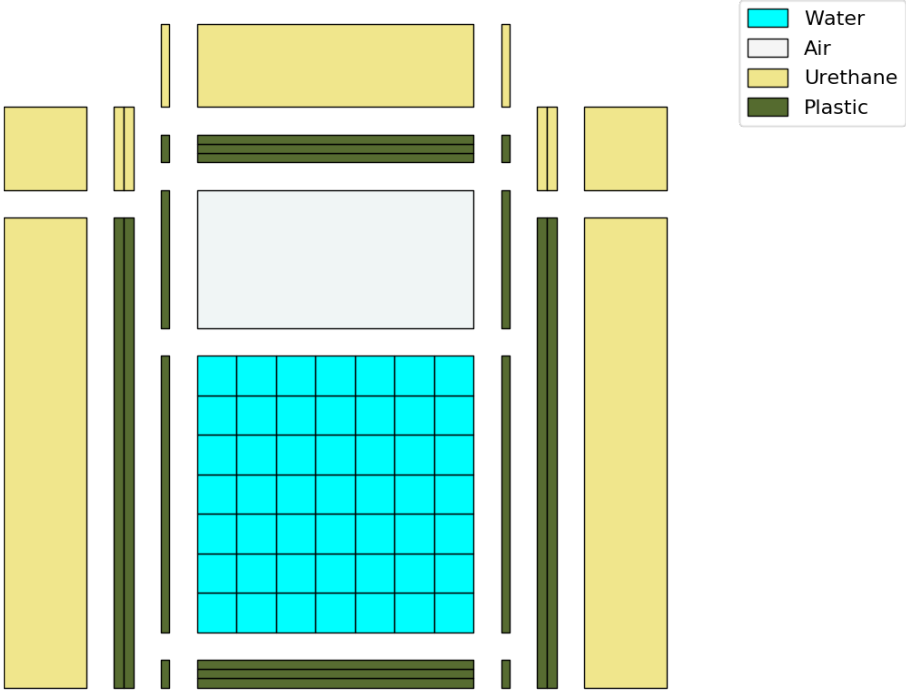


Figure 3.17: Two-dimensional Block Assembly with Mesh in each Block.

Each separate part in this Figure represents a block. Each block may have one or more CV's. The

water domain for example is treated with convective flow and has a mesh refinement of  $7 \times 7$  in this example and its represented by the blue part. This is a single block with 49 CV's.

The wall of the reservoir, the dark green part, is comprised of several blocks. For example the blocks underneath the water or above the air, which are similar, possess a grid refinement of three CV's each. Regarding the blocks corresponding to the vertical faces of the reservoir walls there is a different layout. As can be seen, taking for example the right reservoir wall of Figure 3.17, five distinct blocks are seen. The rightmost block is a two CV block and the other four are all one CV blocks. The necessity for these four one CV blocks arises from the fact that each side of each block may only be connected to a block or blocks of a single material. Therefore, there must be one block connecting the material of the reservoir wall (plastic) to the material of the water domain (water) and another to the air, another to the upper part of the reservoir and another to the lower part of the reservoir (these last two are the smaller ones). Then, because now these blocks have the same material, one single block running their total height may be placed next to them. Of course the four, one CV blocks just mentioned, could also be prolonged through the entire thickness of the wall, but that would increase the number of CV's without a reasonable justification for doing so because the exterior faces of the Module have a heat flux obtained through correlations, hence there is no point in refining the mesh in these faces since the heat flux is constant throughout its area, hence one single CV (in the vertical direction) is the logical choice. However there could be a marginal gains in accuracy in allowing the temperatures in the walls to have different values in the vertical direction, but the limitation created by the use of correlations complicates this argument. The weighted average of the temperatures of each outer surface is used in the correlation.

Of course, different implementations of the geometry can be made by changing the mesh creation routine. In this Thesis the shown one is used.

## **Grid Assembly**

In a succinct way, the assembly process of the blocks in a uniform grid is explained next.

First, each block is created previous to its assembly. The properties of the block, material, dimensions and refinement of the grid are set within each block. Hence, several blocks are created. Then, knowing the spacial location of each block, the process starts, from left to right, by carrying out the vertical connection of the lower block to the block just above it, and then, again, the vertical connection from these two already connected blocks to the next one above, until the first row is completed. Then, the second column of blocks is dealt with in exactly the same way, and now, the horizontal connection between these two columns (that are already connected vertically) is made. Then the third column is connected vertically and then horizontally to the previously, already connected, two first columns. And so on and so forth until all the geometry is addressed.

In the end of this process, the coefficient matrix to be calculated, has all the information about the connection between adjoining CV's of different blocks. Its sparsity may be viewed in Appendix D

### 3.4.4 Three-dimensional

The three-dimensional case is similar to the two-dimensional one, in the sense that geometry wise, it may be viewed as several different layers of a two-dimensional case stacked in the third direction.

#### Grid Generation

The grid generation in the three-dimensional case is equivalent to the two-dimensional case. An example of this assembly for a three-dimensional case, using the dimensions shown in Figure 3.17 but extrapolated to a three-dimensional case, and without the insulation for clarity sake is shown in Figure 3.18.

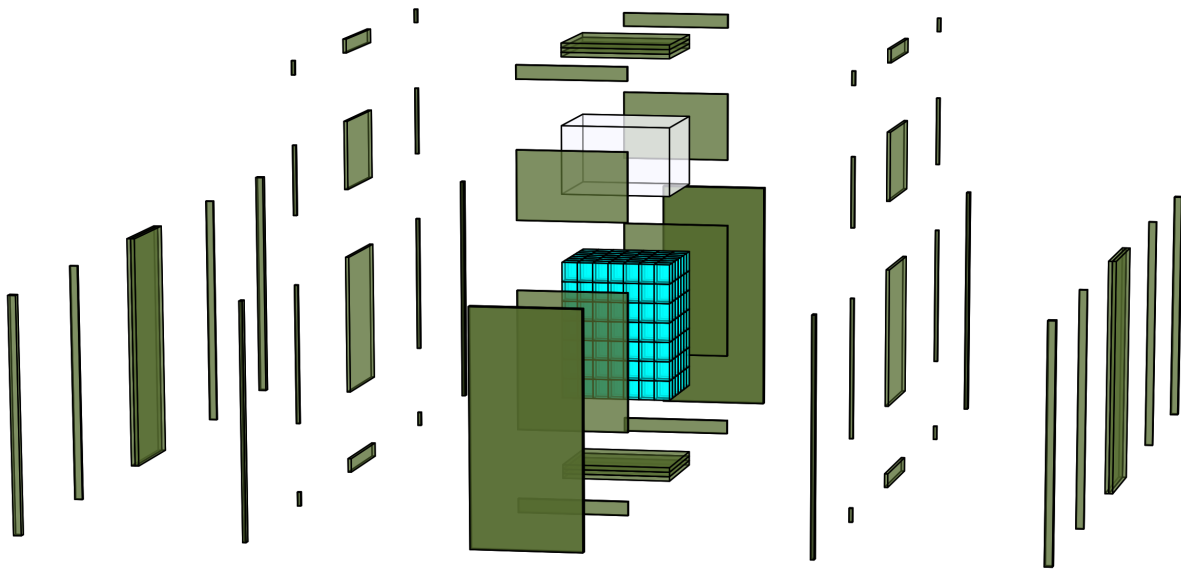


Figure 3.18: Three-dimensional Grid.

#### Grid Assembly

Regarding grid assembly, the three-dimensional case, may also be seen as an extension of the two-dimensional case. This means that the grid is constructed using several two-dimensional layers stacked together in the third direction. Therefore, following the same process described for the two-dimensional case, Section 3.4.3, after the first layer of blocks has been connected within itself, exactly the same process is made to the second layer. After this second layer is completed, the two resulting layers are linked together in the corresponding, new, third dimension. Then the same process is applied to the third layer, and this third layer is connected to previous already connected layers, and so on and so forth until all the domain has been linked. The sparsity of the resulting matrix to be calculated may be viewed in Appendix D.



## 3.5 Boundary Conditions

The boundary conditions apply at all the exterior faces of the domain being calculated. It should not be forgotten that this domain includes about 10[m] underground.

For the one-dimensional case the boundary conditions apply at the top and the bottom of the geometry. For the two-dimensional and three-dimensional cases, the lateral boundary conditions are added to the upper and lower ones, with the three-dimensional case having two more sides than the two-dimensional.

In the underground domain there is an adiabatic condition at the walls whether they are the lateral or the lower surface. The rest of the Module is subject to meteorological conditions. This includes the lateral walls above ground, and the upper surface of the Module. Here, there is an imposed heat flux, as a function of the Module temperature and exterior conditions.

### 3.5.1 Convective Heat Flux

The Module is subject to convection on its boundaries due to the temperature difference with the atmosphere it is immersed in. The properties of the air, temperature and velocity, are known beforehand from the climate data set, and the temperature of the surfaces of the Module, which is, at each time step, the solution from the previous time step, is also known. Therefore, a numerical calculation of the convective flow and corresponding heat transfer is possible. This type of analysis would not only be expensive in terms of computational power required, but also, its implementation would be time consuming. Hence, for the purpose of this Thesis, regarding the convection at the boundaries of the Module, a correlation based approach is used throughout. Nevertheless, the implementation of a convective flux in the Module's boundaries, could, in the future, be a matter to pursue.

Correlations for an horizontal surface, which corresponds to the top surface of the Module, and for the vertical surfaces with cross flow, meaning horizontal flow, which corresponds to the lateral surfaces of the Module are needed.

For each surface of the Module there may be several distinct types of flow depending on the air velocity and temperature difference between the surface and the air. The definition of what correlations are to be applied in each case, is well defined as to their range of applicability through the dimensionless groups mentioned in Table 2.1.

As stated in Section 2.3, according to  $(Gr_L/Re_L^2)$ , convection may be free, forced or mixed. In each of these types of convection there may be a turbulent or a laminar flow. These are judged against other dimensionless groups depending on the type of convection. The dimensionless groups rule all these characteristics by defining a sharp interface in between them.

In the actual case of the Module, the applied correlations are organised in Table 3.2. The description is self explanatory.

Since all the variables needed to calculate the *Nusselt* number are known, at each time step, the heat flux through the surfaces of the Module may be computed with the use of the definition of the *Nusselt* number, equation 2.3 and equation 2.2. Consequently, the heat flux through each surface is

Convection		
Free	Horizontal Plate	Hot surface $\overline{Nu}_L = 0.54 \cdot Ra_L^{1/4}$ [1] $(10^4 \leq Ra_L \leq 10^7)$
		$\overline{Nu}_L = 0.15 \cdot Ra_L^{1/3}$ [1] $(10^7 \leq Ra_L \leq 10^{11})$
	Cold Surface $\overline{Nu}_L = 0.27 \cdot Ra_L^{1/4}$ [1] $(10^5 \leq Ra_L \leq 10^{10})$	
	Vertical Plate	$\overline{Nu}_L = \left\{ 0.825 + \frac{0.387 Ra_L^{1/6}}{[1 + (0.492/Pr)^{9/16}]^{8/27}} \right\}^2$ [1] $(Ra_L > 10^9)$
$\overline{Nu}_L = 0.68 + \frac{0.67 Ra_L^{1/4}}{[1 + (0.492/Pr)^{9/16}]^{4/9}}$ [1] $(Ra_L < 10^9)$		
Forced	Horizontal Plate	$\overline{Nu}_L = 0.664 Re_L^{1/2} Pr^{1/3}$ [1] $(Re_L < 5 \cdot 10^5)$
		$\overline{Nu}_L = (0.037 Re_L^{4/5} - 871) Pr^{1/3}$ [1] $(5 \cdot 10^5 < Re_L < 10^8)$
Mixed	Horizontal Plate*	$\overline{Nu}_L^n = \overline{Nu}_{for}^n \pm \overline{Nu}_{nat}^n$ [2] $(10^3 < Re_L < 10^5)$
	Vertical Plate	$\overline{Nu}_L = \sqrt{Re_L} \left\{ 1 + \left[ 0.752 \frac{L}{H} \frac{Gr_H}{Re_L^{5/2}} \right]^{1/5} \right\}^{3.2}$ [2] $(Re_L > 10^5)$

\*Generic correlation for Mixed Convection. The functions and constants to be used according to each case are available in the respective Tables in [2].

Table 3.2: Correlations for Convection

calculated at each time step and used to calculate the temperatures at the next time step.

It may be mentioned that since the solution to each time step involves an iterative process, in case the convergence criteria is not met at the first iteration, in the following ones there could be another computation of convection based on the average values of the last time step and the previous solution, hence making a second order approximation to the respective boundary conditions. This approach was not adopted because its gains are marginal, but is a straightforward implementation.

### Logarithmic Wind Profile

The logarithmic wind profile is a relationship that describes the vertical wind velocity profile within the lowest portions of the planetary boundary layer. This model is limited to approximately the first 100 [m] of the atmosphere. The relation shown in equation 3.22 is a simplification of the most generic one in this model, which accounts for the conditions of stability of the atmosphere. This stability parameter refers to the tendency for mixing of the atmosphere, which is also a measure of the atmospheric turbulence. It mostly depends on wind and solar radiation, e.g. a situation where, during the day time, the air is hotter near the surface than at higher altitudes due to radiation heat gains at the surface that warms the air making it lighter than the air above it hence promoting its mixing. This stability parameter is set to zero, hence a stable atmosphere is assumed. The generic equation then reduces to equation 3.22

$$u_z = \frac{u_*}{k} \ln \left( \frac{z-d}{z_0} \right) \quad (3.22)$$

In this equation,  $k$  represents the Von Kármán constant,  $\approx 0.41$ ,  $d$  is the height above ground at which velocity is still zero, which depends on surface obstacles and it can be approximated as  $2/3$  to  $3/4$

of the average height of the obstacles and  $z_0$  accounts for the surface roughness. The parameter  $u_*$  is the friction velocity which is a measure of the shear stress related to flow velocity.

The air velocity is assumed to be measured in a meteorological station where the anemometer is located 6 [m] high, the air velocity at the Module's height is lower since it is 1 [m] tall or 0.5 [m] tall. To compute an approximate velocity at the Module's height, the friction velocity is obtained by using the known velocity at 6 [m] high and this same friction velocity is used to obtain the velocity at the Module's height. The parameter  $z_0$  is set to 0.005 which corresponds to a flat terrain like a desert and  $d$  is set to  $2/3$  of the Module's height.

Once the actual velocity at the Module's height is obtained, heat flux may be calculated through the respective correlation.

### 3.5.2 Radiative Heat Flux

This heat flux, as discussed in Section 2.4 and also in Chapter 1, has two components, the sun's radiation, or Irradiation, which accounts for the Solar radiation arriving at the Module's surface whether directly or indirectly, and the atmospheric radiation, which is a radiative heat exchange between the atmosphere and the Module.

First the solar radiation is dealt with, than the exchange with the atmosphere and finally the total radiative flux.

#### Solar Radiation

The direct solar radiation, has a directional characteristic and incides on Earth's surface with a certain angle relative to the Earth's surface normal, meaning its angle is zero when the visible Sun's disc is perpendicular to the surface. This angle is referred to as the *Zenith* angle,  $\theta_z$ . Diffuse solar radiation is considered equal from all directions although its intensity gradually decreases from the *Zenith* angle [1].

The Module has an horizontal surface and four vertical surfaces. The angle of incidence of the Sun on any surface is the angle between  $\theta_z$  and the normal to this surface. This angle is a function of several geometric variables. This angle may be found through equation 3.23 for any point in space and time in the surface of the Earth and any inclination relative to the horizontal and any cardinal orientation of this surface [7].

$$\begin{aligned} \cos \theta = & \text{sen } \delta \text{ sen } \phi \cos \beta - \text{sen } \delta \cos \phi \text{ sen } \beta \cos \gamma + \cos \delta \cos \phi \cos \beta \cos \omega \\ & + \cos \delta \text{ sen } \phi \text{ sen } \beta \cos \gamma \cos \omega + \cos \delta \text{ sen } \beta \text{ sen } \gamma \text{ sen } \omega \end{aligned} \quad (3.23)$$

Where,  $\phi$  represents the Latitude,  $\delta$  represents the declination of the Sun at solar noon,  $\beta$  is the inclination relative to the horizontal,  $\gamma$  is the cardinal orientation of the surface in question,  $\omega$  is the solar hour angle,  $15^\circ$  per hour and finally  $\theta$  is the aforementioned angle between the normal to the surface, and the *Zenith* angle  $\theta_z$ . The respective conventions for each of these quantities is defined in [7].

## Sky Radiation

The radiation exchange between the sky and the Module is due to a temperature difference between the Module and its surrounding atmosphere. "Although the spectral distribution of atmospheric emission does not correspond to that of a blackbody, its contribution to radiation of the Earth's surface can be estimated using equation,  $E_b = \sigma T^4$ " [1]. This equation is stated in Section 2.4.

Assuming the Module and the sky as a two surface enclosure of diffuse gray surfaces, according to the discussed in the final part of Chapter 2.4, equation 2.21 may be applied. Acknowledging that the area of the sky is much greater than that of the Module,  $A_{Mod}/A_{sky} \approx 0$ , and that the view factor of the Module to the sky is unity,  $F_{12} = 1$ , equation 2.21 yields equation 3.24

$$q'' = \varepsilon_1 \sigma (T_{sky}^4 - T_{obj}^4) \quad (3.24)$$

This result is achieved based on the assumptions above, but it could also be achieved by acknowledging that in Figure 2.6 the right hand resistance  $(1 - \varepsilon_2)/(\varepsilon_2 A_2)$  may be set to zero by the assumption of the sky as a blackbody.

The temperature of the sky is, therefore needed, and it is approximated by correlations [8], [9]. There are many propositions for correlating the sky temperature. One of these correlations is given by Swinbank (1963) [7], and relates the sky temperature to the air temperature with the simple relation,  $T_{sky} = 0.0552 T_{air}^4$ . These temperatures must be in *Kelvin*.

## Total Radiation

According to a model by Liu and Jordan (1963) [7], the total solar irradiation on a tilted surface, is made up of three components: beam radiation or direct solar radiation, diffuse solar radiation and solar radiation diffusely reflected from the ground. These quantities are expressed in equation 3.25

$$G_T = G_{dir} \left( \frac{\cos \theta}{\cos \theta_z} \right) + G_{dif} \left( \frac{1 + \cos \beta}{2} \right) + (G_{dir} + G_{dif}) \rho \left( \frac{1 - \cos \beta}{2} \right) \quad (3.25)$$

The first term on the right hand side is responsible for the beam radiation,  $G_{dir}$  is the beam radiation on a horizontal surface and,  $(\cos \theta / \cos \theta_z)$  is the corresponding beam radiation on the tilted surface, with a tilt angle of  $\beta$  and an orientation of  $\gamma$ . The second term, is the influence of the diffuse part of the solar radiation, where,  $\frac{(1 + \cos \beta)}{2}$  is the view factor of the tilted surface to the sky. The last term, is due to the reflection of the total solar radiation, direct and diffuse, on the ground. The view factor of the tilted surface to the ground is unity minus the view factor from the sky,  $1 - \frac{1 + \cos \beta}{2} = \frac{1 - \cos \beta}{2}$ , which is a reasonable approximation for a plateau, which holds for the observatory site, and a reflectance of the ground of  $\rho$ , which in this study is assumed to be  $\rho = 0.4$ , which is the sand reflectance from [1].

Hence, the total thermal radiation arriving at the Module's surfaces is simply the sum of the solar radiation explained above, and the radiative heat exchange with the atmosphere. The last one is obtained through equation 3.24.

Knowing the value of the total thermal radiation arriving at the Module's surfaces and multiplying it

by the parameter absorbance,  $\alpha$  of the surface, yields the flux at each surface. Hence, for the solar direct radiation,  $G_{dir}$ , the parameter  $\alpha$  is corrected according to equation 3.26 from [7] which accounts for angle  $\theta$  of incidence.

$$\frac{\alpha}{\alpha_n} = 1 - 1.5879 \cdot 10^{-3} \theta + 2.7314 \cdot 10^{-4} \theta^2 - 2.3026 \cdot 10^{-5} \theta^3 + 9.0244 \cdot 10^{-7} \theta^4 - 1.8 \cdot 10^{-8} \theta^5 + 1.7734 \cdot 10^{-10} \theta^6 - 6.9937 \cdot 10^{-13} \theta^7 \quad (3.26)$$

Note that only the direct irradiation is influenced by this correction in a direct way since the diffuse part, whether solar or exchanged has not a directional nature and is not affected in this implementation.

### 3.6 Convection in Enclosures

Inside the Module there are fluids which naturally are subject to convection under the appropriate conditions. As can be seen in Figure 3.10, there are several enclosures, or cavities, of air and one of water. Heat transfer in these enclosures may be calculated through the convective flow, or through correlations. Due to the computational cost of a numerically calculated convective flow, heat exchange in the air cavities is always obtained through correlations and only in the water domain the option is offered.

The used correlation is valid for an existing temperature difference in opposing walls in the vertical direction, and adiabatic walls in the other directions. This approach is in full agreement with the one-dimensional case, but for the two-dimensional and three-dimensional case, is not. In these cases, the side walls are at a different temperature than that of the water, hence the adiabatic condition is not met. Also, in these cases there may be a preferential direction for convection according to the Rayleigh number in each direction. Here, only the vertical direction is considered.

By disregarding the adiabatic constraint of the lateral walls, heat is exchanged with these walls, through conduction.

For a convective flow due to temperature difference to exist in the side walls, there needs only to be a  $\beta \neq 0$  and a temperature difference. Hence, the approximation being made of conduction in the lateral walls is intrinsically an underestimate of the actual heat flux.

For the water, a numerical implementation of the convective flow was made through the governing equations stated in Table 3.1. Even with a coarse grid, the qualitative aspects of convection still hold, e.g. lower density water floats and there is a flow according to the buoyant effects, and also the convective heat flux is now a non issue because it is built into the governing equations.

Equation 3.27 is the used convection correlation for cavities with a vertical temperature difference.

$$\overline{Nu}_L = 1 + 1.44 \left[ 1 - \frac{1708}{Ra_L \cos \tau} \right]^+ + \left[ \left( \frac{Ra_L \cos \tau}{5830} \right)^{1/3} - 1 \right]^+, \quad \text{with, } [x]^+ = (x \text{ if } x > 0, \text{ else, } 0) \quad (3.27)$$

The correlation yields a *Nusselt* number that is then transformed into a convection coefficient  $h$ . This

coefficient may then be applied to equation 2.2 and yield the heat flux through the surface.

The governing equations to be solved for FVM require a diffusion coefficient that is the thermal conductivity of the material in question. In the case of correlated convection the diffusion coefficient must be translated to an equivalent conductivity coefficient in order to be implemented. The way to accomplish this is by equating the heat flux through a CV using equation 2.2 and equation 2.1. The result is shown for a one-dimensional case in equation 3.28, where  $e,w$  represent east and west faces of the CV.

$$q = A h \Delta T_{e,w} = A k_{eq} \frac{\Delta T_{e,w}}{\Delta x_{CV}} \implies k_{eq} = h \Delta x_{CV} \quad (3.28)$$

Then, when the coefficient matrix is being constructed, there is a conditional statement checking if  $k_{eq}$  is higher than  $k_{fluid}$ , and if so,  $k_{eq}$  is used instead of  $k_{fluid}$  (if there is no convection the calculated  $k_{eq}$  is set to zero).

### 3.7 Water Phase Change

The phase change of a pure substance, like water, occurs at a sharp interface and at a single discrete temperature. The governing equations were presented in section 2.5. The methodology for their implementation in FVM varies. The most regarded methods are based in the Volume of Fluid (VOF) method that describes the proportion of each phase in each CV, and the Level Set (LS) method which describes the shape of the solid liquid interface, [10, 11]. These methods may account for mass conservation or expansion of the water during phase change.

In this Thesis a simpler approach is implemented. The properties of water near freezing gradually change to the properties of the solid phase. This variation in properties happens from  $0^\circ C$  to  $-0.3^\circ C$  in order to approximate the process of phase change in the water. Figure 3.19 shows the properties of density and kinematic viscosity of water in this region.

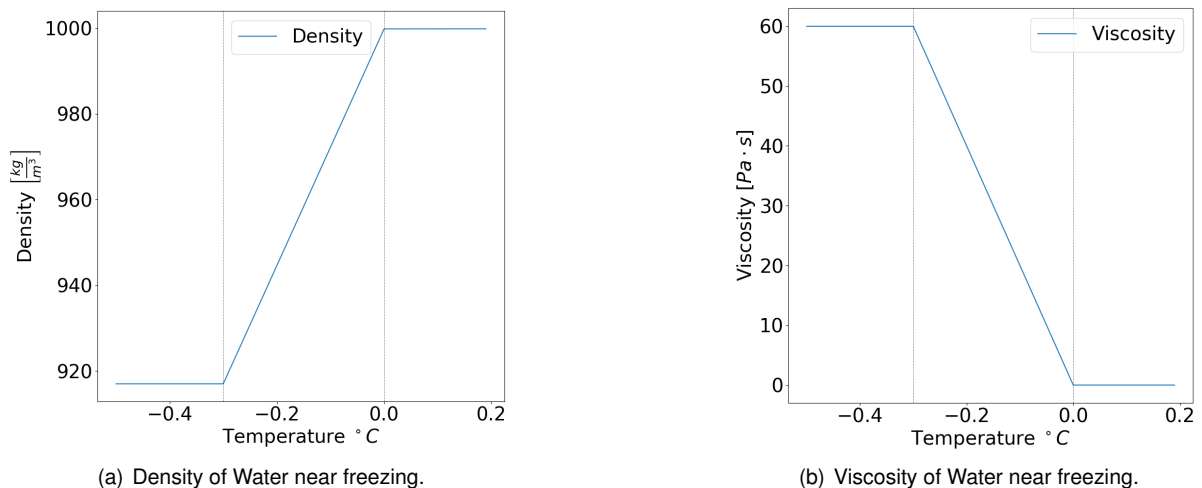


Figure 3.19: Properties of Water near freezing.

The Latent heat of solidification of water is  $334 \left[ \frac{KJ}{kg} \right]$ . This energy release is accounted for during this temperature interval by adding a corresponding term in the energy equation 3.10. During this temperature interval, the energy equation for the water becomes,

$$\frac{\partial(\rho T)}{\partial t} + \left( \frac{L}{\Delta T_{s-l} c_p} \right) \frac{\partial(\rho T)}{\partial t} + div(\rho T \vec{v}) = div(k/c_p grad T) + S_T \quad (3.29)$$

The properties  $c_p$  and  $k$ , specific heat and conductivity, also gradually change in this temperature region between both distinct values of the liquid and solid phase.

### 3.8 Properties and Constants

The properties of the materials needed for this analysis are density  $[kg/m^3]$ , thermal conductivity  $[W/m \cdot K]$ , specific heat  $[J/kg \cdot K]$ , dynamic viscosity  $[N \cdot s/m^2]$  and gravitational acceleration  $[m/s^2]$ . The used gravitational acceleration is set to  $g = 9.791$  accounting for the  $\approx 5000[m]$  of altitude. This correction treats the earth as a perfect homogenous sphere, equation 3.30.

$$g_h = g_0 (R_m/R_m + h)^2 \quad (3.30)$$

First it is assumed that these properties for the solid materials are not variable with temperature. If the material is a fluid, these properties may change with temperature. For example the air density is variable according to its temperature. Although all these properties are considered constant within each time step, they are updated at each time step. Nevertheless the differences in doing so are small if the temperature range in question is not great. The air correlates its density through the ideal gas law, shown in equation 3.31.

$$\rho = \frac{p}{R_{specific} T} \quad (3.31)$$

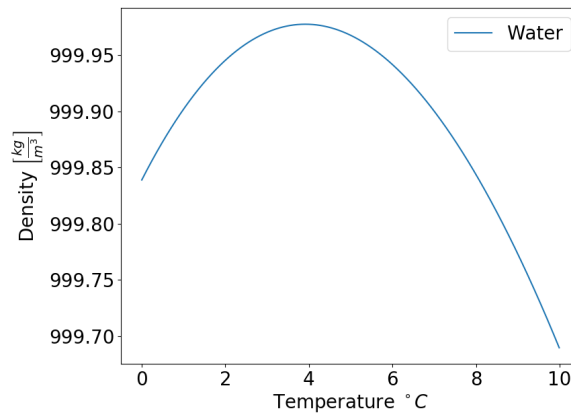


Figure 3.20: Water Density.

The water has a particular behaviour regarding its density to temperature relation. One is that density decreases upon cooling below a certain temperature at a certain pressure. For a pressure of  $1[atm]$  the

point of zero coefficient of volumetric expansion is about  $4^{\circ}C$ . The used data for water density is taken from [12]. This data is represented in Figure 3.20. Its thermal expansion coefficient is negative below  $4^{\circ}C$  which is an unusual behaviour. The other aspect is that upon freezing, it lowers its density which is contrary to most other materials that contract when going from a liquid phase to a solid phase.

For the other materials used in the Module, their thermal properties are shown in Table 3.3.

Material	Density [ $kg/m^3$ ]	Conductivity [ $W/m \cdot K$ ]	Specific Heat [ $J/kg \cdot K$ ]	Viscosity [ $N \cdot s/m^2$ ]
Water	Variable	Variable	Variable	Variable
Air	Variable	0.0263	1006	Variable
Sand	1515	0.27	800	n/a
Lead	11340	35.3	129	n/a
Glass	2500	1.4	750	n/a
Plastic	1300	1.4	1465	n/a
Aluminium	2770	177	875	n/a
Polystyrene	16	0.04	1210	n/a
Acrylic	1300	1.4	1465	n/a
PCB / FR4	1850	0.32	396	n/a
Polyurethane	70	0.026	1045	n/a

Table 3.3: Properties of the used Materials in the Module, [1].



# Chapter 4

## Results

The results focus on differentiating factors that may influence the temperature solution. Hence several test cases will be compared against each other so that conclusions to the response of this differentiating factors may be drawn.

The two-dimensional case presents yearly results obtained with the use of correlations for the convective heat transfer in the water. Also, results with convective flow in the water are presented although incomplete due to the lack of computational performance.

Three dimensional results with convective flow in the water are shown mainly to acknowledge their availability.

### 4.1 Problem Description

As mentioned in Section 1.1.1 the climate data uses information of nearby meteorological stations for interpolating air temperature and wind speed at the location of the Observatory and for direct solar radiation and diffuse solar radiation also uses satellite data. The data used is plotted in Figure 4.1.

This data has a discretisation of one minute time step. All the following test cases are according to this data, hence, the tested cases may be compared against each other. Nevertheless, if desired, a different data file may be fed to the source code.

Other input variables that are not given in the climate data file and also need to be defined as input and are presented in Table 4.1

Latitude	Longitude	GMT	Orientation
$22^{\circ} 56' 53.6'' S$	$68^{\circ} 12' 43.4'' W$	-4	$0^{\circ} S$
Absorptance	Emissivity	Ground reflectivity	Initial Temperature
0.9	0.4	0.4	$2 [^{\circ} C]$

Table 4.1: Additional input parameters.

The position variables of the Module, defined through a longitude and latitude, the local Greenwich

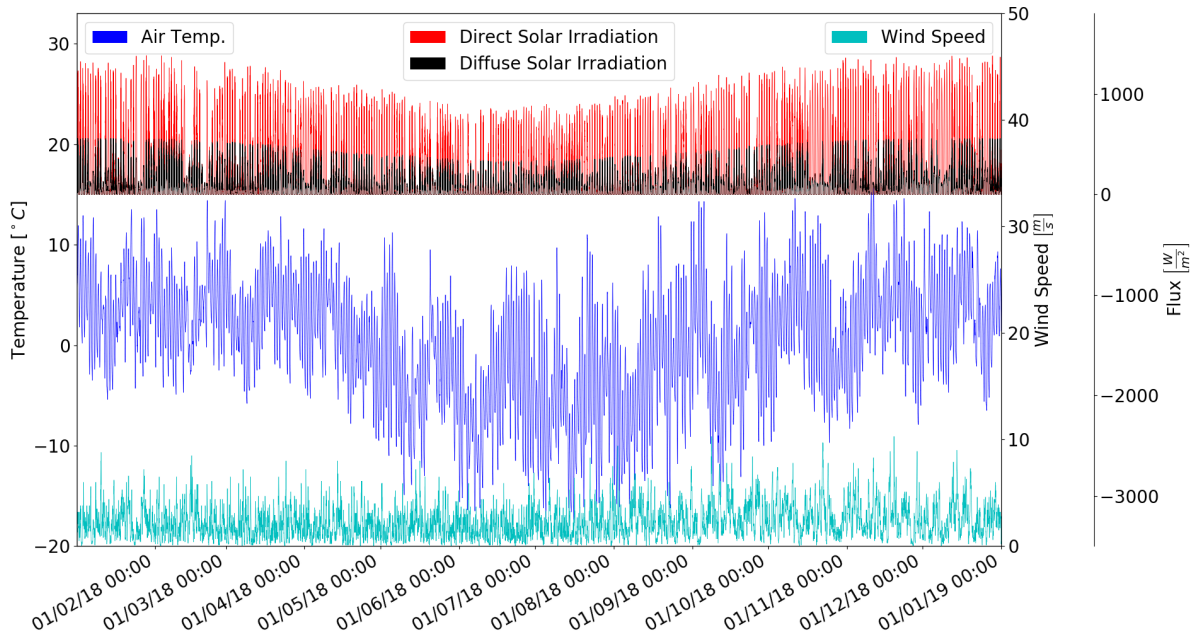


Figure 4.1: Climate Data Set.

Mean Time (GMT) and the Module's orientation, allow for the calculation of the solar angle  $\theta$  at the location in question at the local time at each surface. This is the angle between the direct solar irradiation in the data file and the surface as explained in Subsection 3.5.2. The values of absorptance and emittance used correspond to a selective black paint where its properties are engineered to absorb as much heat as possible and emit the less possible.

The initial temperature is assumed, in this case, to be constant throughout the entire domain, Module and ground. The temperature of the underground is a relevant parameter. Since this variable is not known, at least to date, one option is to set this temperature parameter to the average of the yearly air temperatures. As shall be seen later, since the Module is standing directly in contact with the ground, this temperature works as a buffer to any variation in the temperature of the water from the underground temperature.

Because all the aforementioned parameters are input variables, they may be altered freely. For example, if there is the intension of obtaining a solution for a particularly cold year, a corresponding climate data set should be used, or if different surface properties are to be tested, the corresponding parameters can be changed.

## 4.2 One-Dimensional Calculations

For the one-dimensional case, the computational cost of the solution for a one year period with one minute time step is manageable. Even so, each solution takes about one day to complete in the personal computer used in this Thesis (Processor - 2,3 GHz Intel Core i7, Memory - 4 GB 1600 MHz DDR3). The convective heat transfer is calculated only through correlations. As already stated in Section 3.4 the one-

dimensional approximation neglects the lateral heat sources which causes limitations to the reliability of the results.

The interpretation of these results is not straightforward. This case may be visualised as a Module where the horizontal dimensions are infinite and the upper heat flux would be applied at its infinite area.

The general variations that will be shown have already been set previously in Section 3.4.1, except for the insulation which has a thickness of 5 [cm] instead of the 4 [cm] used in the aforementioned Section. The different situations considered for analysis are stated in Table 4.2. The horizontal dimensions of the water volume are fixed to a 1 [m] sided square. Only its height varies between 0.5 and 1 meters, approximately 500 and 1000 litres respectively. Also the existence of the RPC and the existence of the insulation layer varies.

Case	Height of Water	RPC	insulation
1	1 [m]		
2	0.5 [m]		
3	1 [m]	✓	
4	0.5 [m]	✓	
5	1 [m]		✓
6	0.5 [m]		✓
7	1 [m]	✓	✓
8	0.5 [m]	✓	✓

Since the water is a part of the domain in all situations and the most important output of the results, Figure 4.2 shows the obtained average temperature of the water during one year for cases 1 and 2. Case 1, with 1000 litres, has a higher “thermal bulk” or heat capacity, ( $\rho C_p dV$ ), hence the evolution of its temperature is slower as can be seen in Figure 4.2. Also, the temperature does not drop from about 3 or 4 degrees.

Table 4.2: One-dimensional test instances.

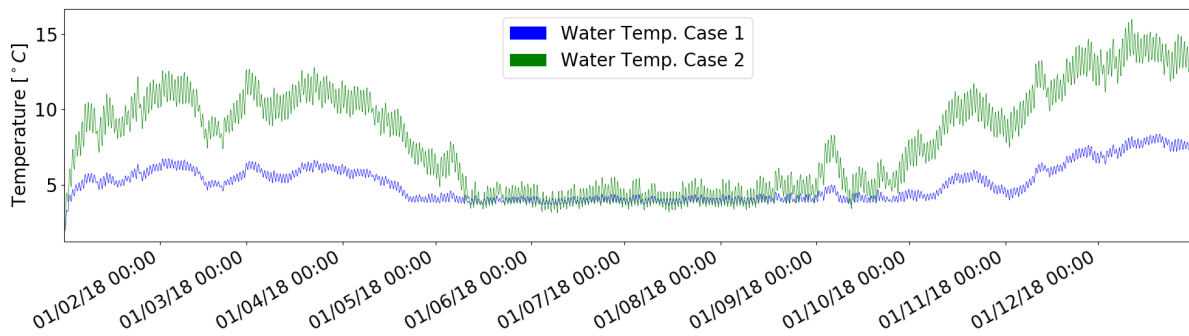


Figure 4.2: One-dimensional Water Temperature, Cases 1 and 2.

For this behaviour in the water temperature to happen, the Module’s heat flux during that region in time must average close to zero. On the other hand, the ambient air temperatures during this region in time are at their lower range which is significantly lower than the 3 – 4°C of the water during this period. Chilean Winter is from June to August. Figure 4.3 shows the same information of the Figure 4.2 together with the ambient air temperature and a daily average of the heat flux on the Module’s upper surface (variations due to the day time / night time of the flux would be hard to visualise for their disperse appearance when plotted with a one minute interval over one year). The heat flux of case 1 is offset by 15 [W/m<sup>2</sup>] for visualisation purposes.

As can be seen, when the heat flux is predominately positive corresponding to an increase in energy

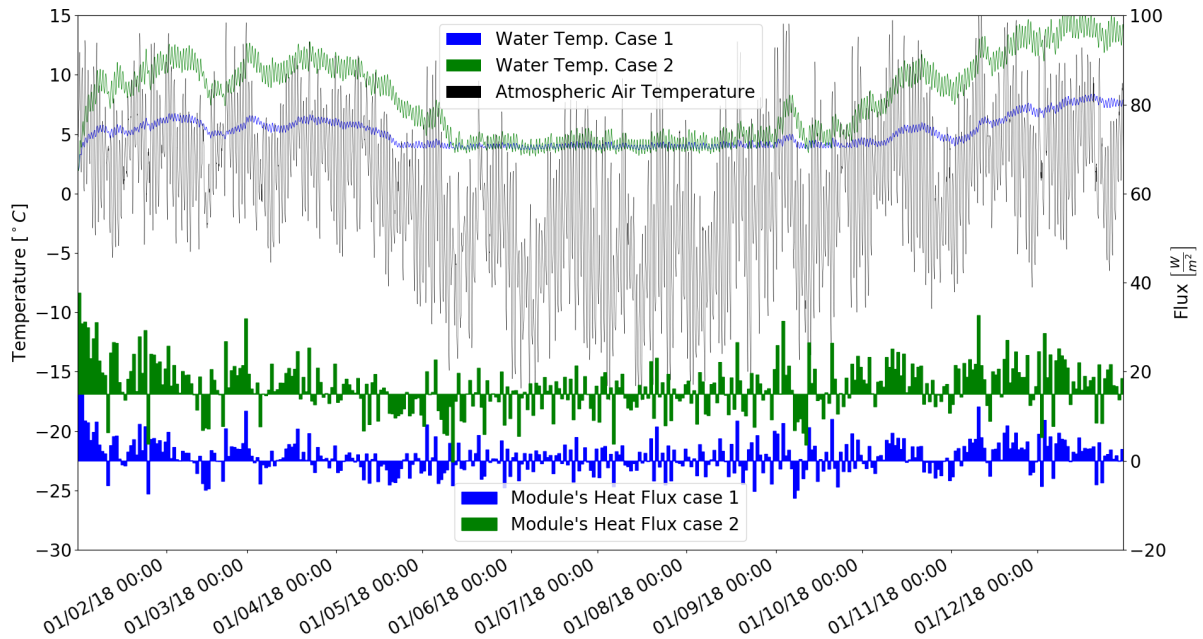


Figure 4.3: One-dimensional Water and Air Temperature, and Heat flux through the top surface, Cases 1 and 2.

in the Module there is an increase in the water temperature and vice versa. Around the winter months, the atmospheric air temperature is lower, but the heat flux through the Module does not follow the corresponding behaviour of lowering the energy in the Module, keeping an average value close to zero, hence the water temperature does not drop.

Cases 3 and 4 are presented in Figure 4.4. These two cases are shown together with the first two for comparison purposes. First, comparing cases 3 and 4 it can be observed that case 3 (1000[l]) with a higher heat capacity alters its temperature slower than case 4, changing its relative position (hotter / colder) in relation to case 4 when the concavity changes over a long enough time period.

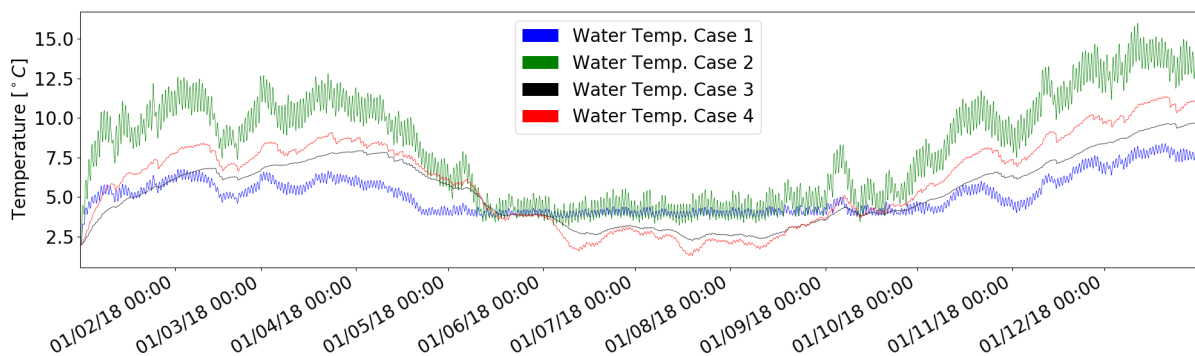


Figure 4.4: One-dimensional Water Temperature, Cases 1, 2, 3 and 4.

The second aspect that needs to be mentioned is that the temperatures of the water during the winter no longer stay at ( $4^{\circ}C$ ). Instead, when the RPC is present, the average water temperature falls below  $\approx 4^{\circ}C$ .

Figure 4.5 shows the convection coefficient in the water in both cases together with its temperature. The convection from case 3 is represented by its symmetric for visualisation purposes. The temperature scale is positioned so that the temperature of zero coefficient of thermal expansion ( $\approx 4^{\circ}\text{C}$ ) is approximately at the same level of the zero coefficient of convection also for visualisation purposes.

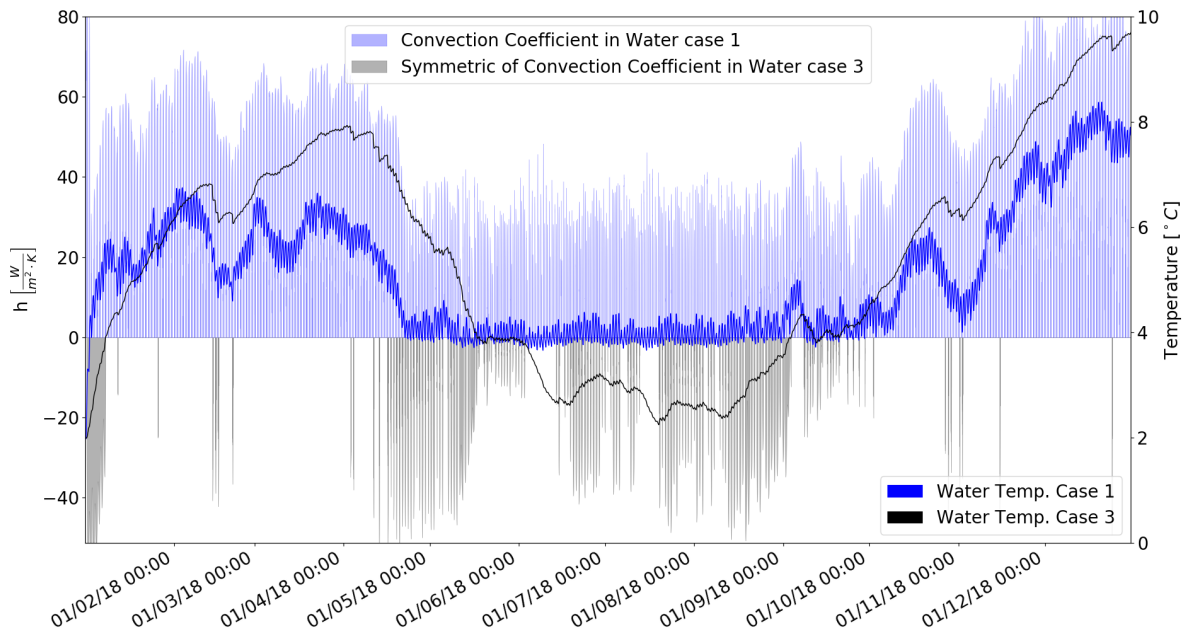


Figure 4.5: One-dimensional Convection in Water, Cases 1 and 3.

Looking at the winter months, case 3 has less convection during this period than case 1 because the air cavity above the water is at a lower temperature than that of the bottom of the reservoir for longer periods making for a conduction situation in the water in these periods. As stated in Section 2.3, the resistance to heat flow when a fluid is subject to conduction is higher than when the fluid is subject to convection. Hence, the heat exchange with the water is higher below  $4^{\circ}\text{C}$  if the top surface of the water is hotter than the lower surface and is lower if the top surface is colder than the lower surface. On the other hand, if the temperature of the water is above  $4^{\circ}\text{C}$  the heat exchange is higher when the top surface of the water is at a lower temperature than the bottom surface. This is the reason for the water not to drop below  $4^{\circ}\text{C}$  in case 1. In case 1 the day time period is sufficient to heat the air cavity above the water to a temperature where the water exchanges heat through convection increasing its temperature with less resistance and during the night reducing with a higher resistance due to conduction after  $\beta$  changes its sign. This is so because case 1 has no RPC which has the consequence of the air in the cavity above the water having only the reservoir upper wall separating it from the exterior which allows for a higher temperature range in the air cavity above the water in the day / night cycle than for case 3 with RPC where there are several layers of material above the air cavity that moderate the day / night temperature cycle and consequently the temperature in the air cavity above the water for case 3 is an “average” temperature that in this case is almost constantly below the water temperature due to the low ambient air temperatures making for a less frequent convection condition in the water during the

winter months which allows the water to lower its temperature below  $\approx 4^{\circ}C$ . Even so, it can be seen in Figure 4.5 that when there is convection (during winter months), the temperature of the water rises sharply when compared to its decrease through conduction. A detailed view of Figure 4.5 is shown in Figure 4.6 where this behaviour may be seen for a shorter period of one month.

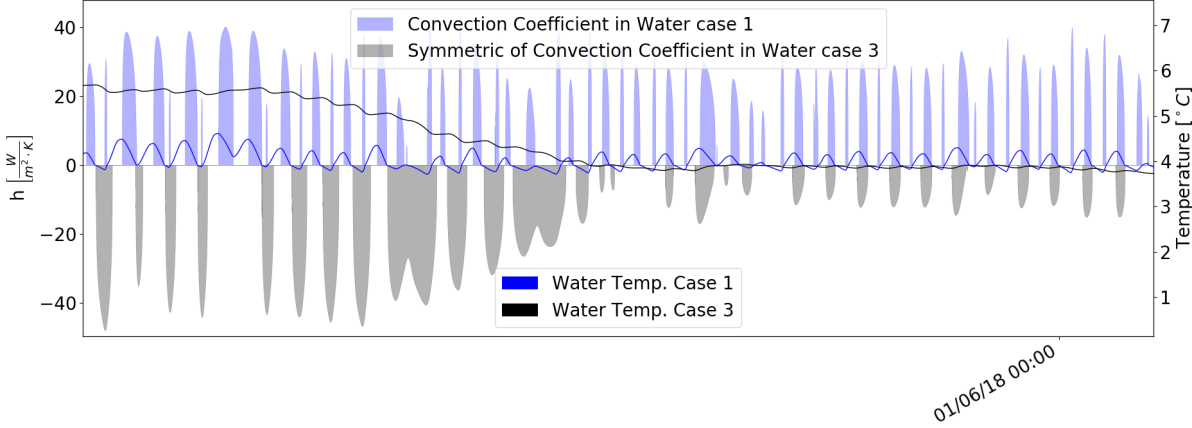


Figure 4.6: One-dimensional Convection in Water, detail, Cases 1 and 3.

Regarding the temperatures of the RPC, case 3 and case 4 are similar. Figure 4.7 shows the temperature of case 3 and the temperature difference between case 3 and case 4. It can be seen that the temperature difference between the two cases is small when compared to its daily variation.

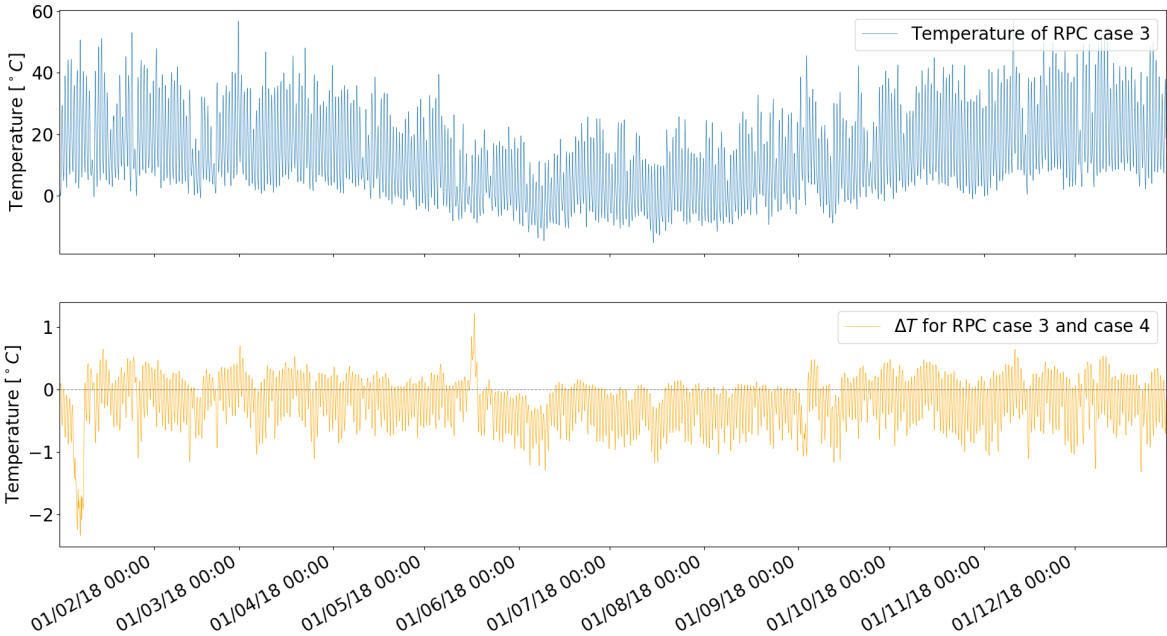


Figure 4.7: One-dimensional Temperature of RPC, Cases 3 and 4.

Now, the same four cases are presented where the only difference is the existence of an insulation layer. These last four cases are identified in Table 4.2. This layer, in the one-dimensional case, is placed on the top of the Module only. It is 5 [cm] thick. Figure 4.8 shows all the eight cases under analysis.

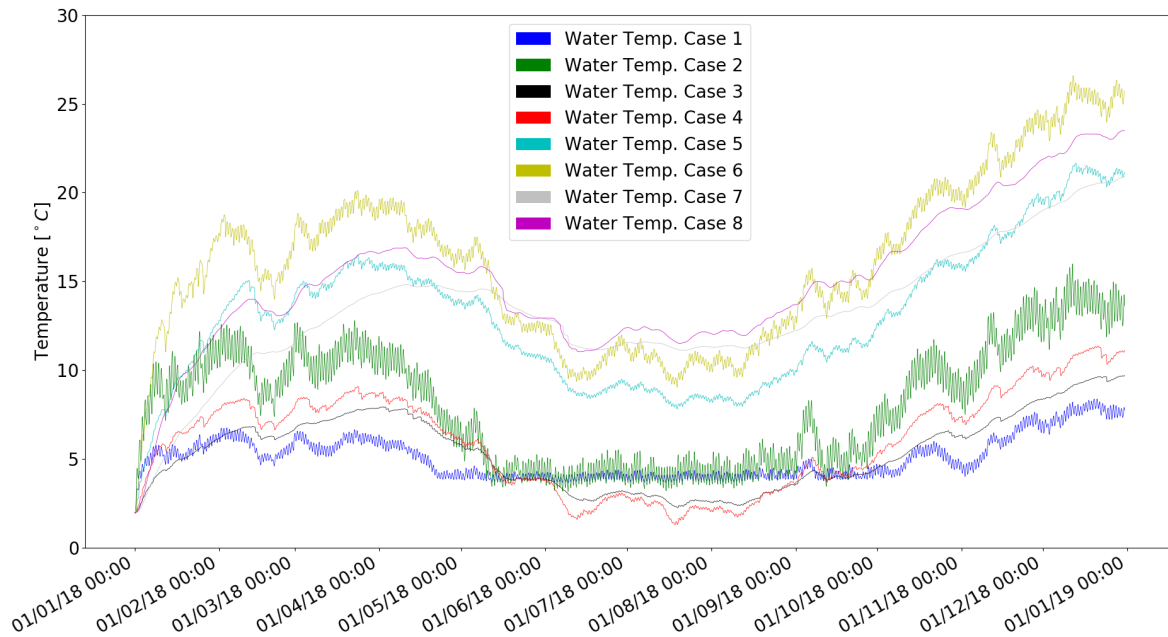


Figure 4.8: One-dimensional Water Temperature, Cases 1, 2, 3, 4, 5, 6, 7 and 8.

First, it should be noted, that the insulation has only two CV's, meaning each CV has a  $dx = 2.5[cm]$  which is not a very refined discretisation for this part of the Module. This discretisation came out of necessity from the 1 minute time step that was too long in some cases creating an imbalance in the solar irradiation which is a known variable for the time step being calculated versus the convection that is a variable based on the previous solution of temperatures. This issue happens, for example, when convection is not particularly high for the time step in question and the solar irradiation for this time step is particularly high. Then, during 1 minute, the first CV increases its temperature according to the “high” solar irradiation without the compensation of the supposedly increasing convective heat transfer in the opposite direction, which yields an abnormal high temperature in the surface of the Module. Then, in the next time step, compensation arrives in the form of a higher convection that balances the temperature situation. If the time step is infinitely small this situation never occurs because convection is constantly updated. On the other hand if the time step is too long, this unbalance may become unstable and yield an amplifying oscillatory behaviour that crashes in a few time steps. One way to work around this issue, besides decreasing the time step, is to make the boundary CV's where the problem occurs less prone to temperature variation by increasing their thermal mass. This is accomplished by increasing its size which translates to reducing the number of CV's in this part of the Module. This is known as a stability issue [13].

### 4.3 Two-Dimensional Calculations

The two-dimensional case may be calculated in two manners regarding the convective heat transfer in the water domain. One uses correlations for convection as in the one-dimensional case. The other

calculates the convective flow in the water. The latter one is computationally heavy hence its results are incomplete. Nevertheless, the solution thus far is presented.

### 4.3.1 Results with Convection Correlation in the Water

The result for case 1 is shown in Figure 4.9. The temperature does not drop below  $4^{\circ}\text{C}$  keeping a positive coefficient of thermal expansion throughout the year.

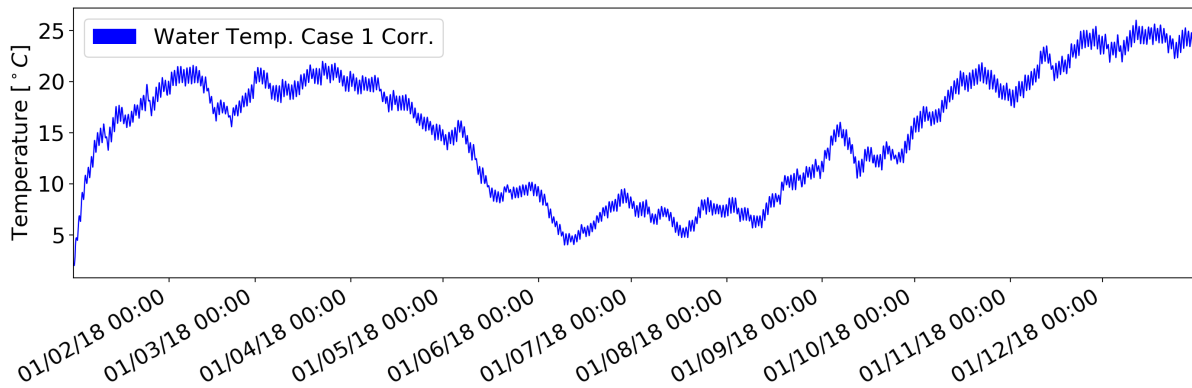


Figure 4.9: Two-dimensional Water Temperature using convection correlation, Case 1.

The temperature fluctuation within one day is higher when compared to the one dimensional analysis. It is so due to the two additional faces exchanging heat with the atmosphere. For a row of Modules as shown in Figure 3.15, this solution may be seen as a first approximation.

### 4.3.2 Results with Convective Flow in the Water

The results for the eight cases used for the one-dimensional analysis are presented up to the available solution. Figure 4.10 shows the results for the water temperature.

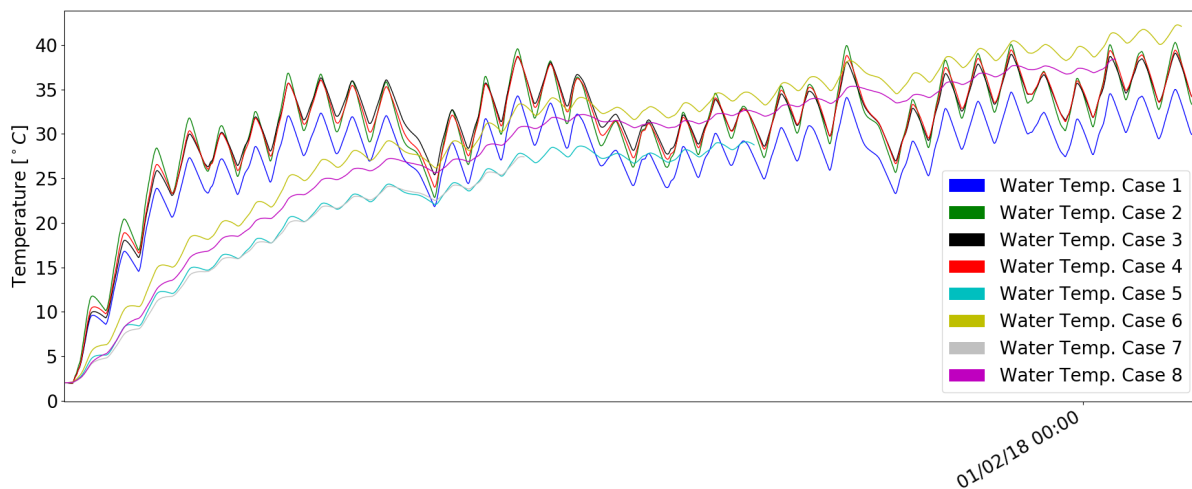


Figure 4.10: Two-dimensional Water Temperature with convective flow, Case 1 through 8.



The higher temperature of the water is noticeable when compared to the two-dimensional with correlation results. This is due to a higher heat exchange with the water which is due to the lower thermal resistance associated with convection in the side walls instead of conduction.

All cases use a mesh refinement in the water of  $8 \times 8$  CV's. A higher mesh refinement would be demanding computationally. It should be noted that although the temperatures in the water are obtained with the convective flow, the walls surrounding the water volume are still made of one single CV, meaning that the temperature at each face surrounding the water volume is constant throughout the area of the surface. This implementation of the geometry was originally made because the use of a correlation for the water convective heat flux imposes a single discrete temperature at each face and also in order to minimize the total number of CV's hence minimizing the computational cost, Section 3.4.3. Nevertheless, when a convective flow is computed in the water with its associated mesh, the side walls now could and should also bear a mesh to allow for different temperatures at each wall. This is not tested, but the implementation as is, accounts for this mesh refinement at each block of the geometry as explained in Section 3.2.3.

## 4.4 Three-Dimensional Calculations

These are the most interesting results since they use all the implemented material for obtaining a solution.

### 4.4.1 Results with Convection Correlation in the Water

The only results available for the three-dimensional case with convection correlation in the water are during the first 20 days. This incomplete solution is shown in Figure 4.11.

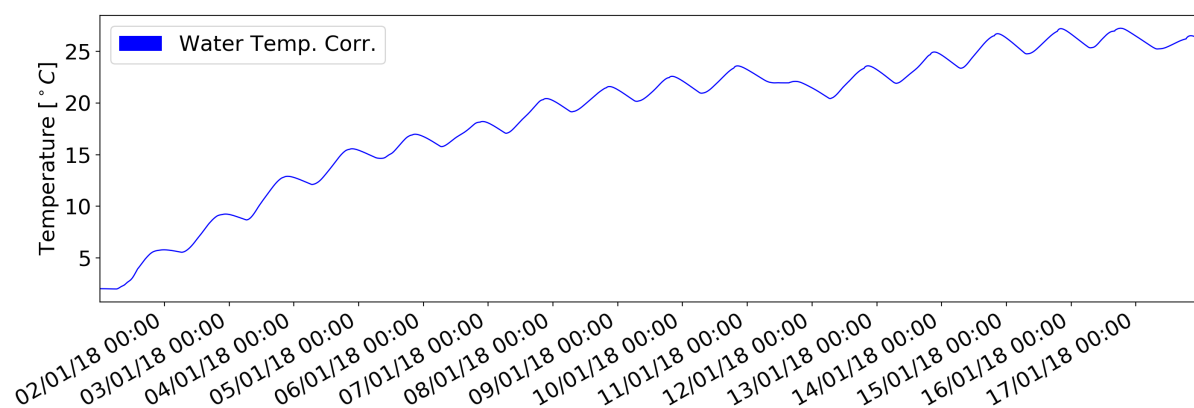


Figure 4.11: Three-dimensional, correlated convection, water temperature.

The behaviour is similar to the two dimensional case, but the temperatures are higher.

### 4.4.2 Results with Convective Flow in the Water

The results for this situation, three dimensional with convective flow in the water, have the least availability. The first day is computed thus far. This incomplete solution is shown in Figure 4.12.

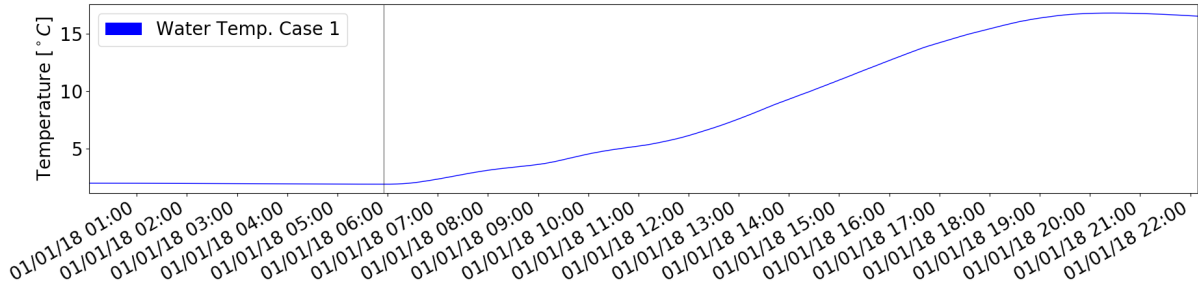


Figure 4.12: Three-dimensional, water temperature.

The three-dimensional analysis has the highest variation in the water temperature which reaches  $\approx 15^{\circ}C$  in the first day, due to the additional faces. This behaviour is present in the cooling phase during night time and heating after sunrise. Figure 4.13 shows a close up of the water temperature during night time. The vertical line in both Figures represents sun rise.

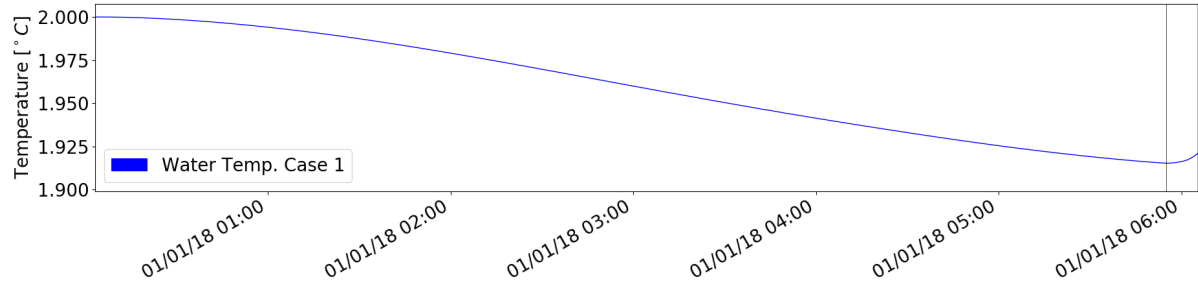


Figure 4.13: Three-dimensional, water temperature, cooling.

Besides the additional lateral walls, many factors influence this temperature evolution, for example, convection is different in the three-dimensional case, the sun's irradiation is slightly higher because of the declination of the sun, etc.. Hence the entire yearly solution would have to be obtained in order to draw conclusions regarding temperatures in the water.

# Chapter 5

## Discussion

In this Chapter an in depth view of how and why the temperatures in the Module change in each CV in each time step is made. To accomplish this, a short period of time is scrutinised regarding the thermal behaviour in the Module. Mostly this period is during the first 24 hours after the initial condition.

The default case that is going to be used is case 1 from Section 4.2. This is the simplest case, hence the more appropriate for this discussion.

Mostly, what is going to be said and shown may be inferred from what has been said in Chapters 2 and 3. This Chapter may be viewed as a type of validation of the results, since the fundamental aspects of heat transfer must be reflected in the results.

### 5.1 One Dimensional

First, it must be acknowledged that there are two distinct mechanisms regarding sources affecting the Module's surfaces. These are irradiation which imposes a heat flux at the surface, and heat exchange with surroundings which depends on the atmospheric conditions and surface temperature.

The first is due to the sun and depends only on the surface properties of the Module. This means that regardless of the temperatures involved, the sun's direct and diffuse irradiation from the climate data file together with the surface properties yield the heat flux which is always positive (the surface gains heat (which will be the convention adopted from now on)),  $q \geq 0$ , and a known variable a priori throughout the year.

The second, heat exchange that depends on the atmospheric conditions and surface temperature, is unknown and has to be calculated at each time step.

#### 5.1.1 Sources

Figure 5.1 shows the initial condition up to sunrise, which is represented by the vertical line at 05:54.

First, the air temperature is higher than the surface temperature, hence convective heat flux is positive. Second the heat exchanged with the sky is negative since the used approximation for the sky temperature,  $T_{sky} = 0.0552 T_{amb}^{1.5}$ , Section 3.5.2, yields for a ambient temperature of  $\approx 5^\circ C$ ,  $T_{sky} = -17^\circ C$

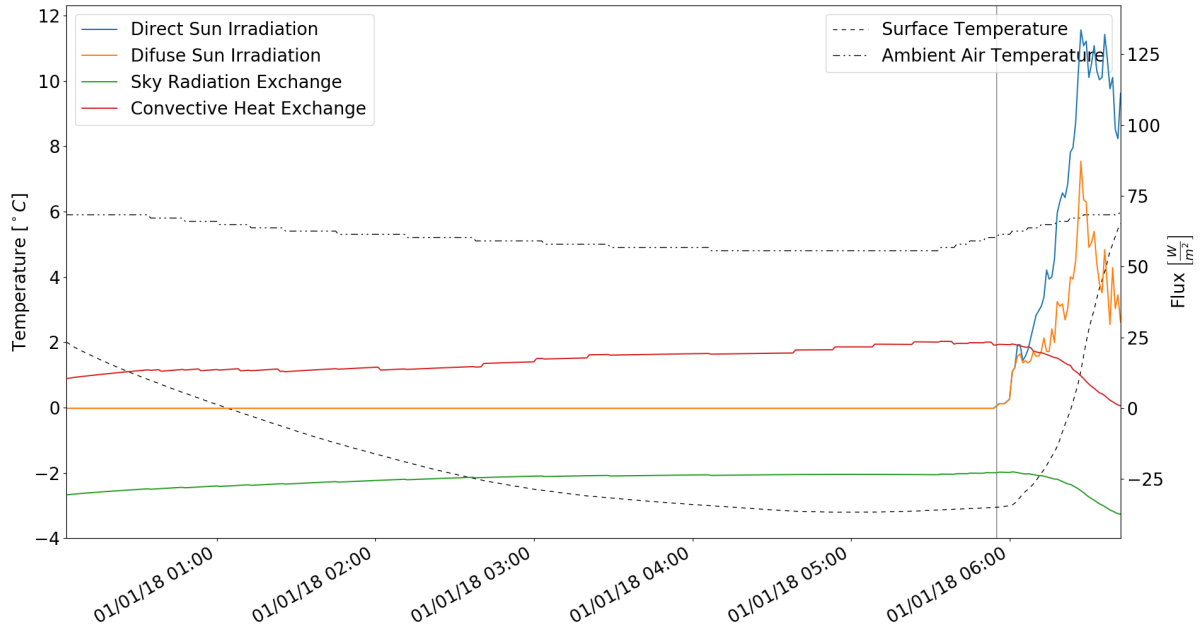


Figure 5.1: One-dimensional initial condition, Case 1.

which means that for radiative heat exchange with the sky to be zero, the Module's surface would have to be at  $-17^{\circ}\text{C}$  based on equation 3.24 that approximates the resulting heat flux. The main information present in this plot is therefore, that, initially, convection  $\approx 1 [\text{W}/\text{m}^2]$  is not capable in this situation to overcome the loss of energy due to radiative heat exchange with the sky  $\approx -3 [\text{W}/\text{m}^2]$ . Hence the Module's surface will lower its energy, or decrease its temperature. The consequences of this decreasing temperature are that the temperature difference between the ambient air and the surface of the Module increases resulting in an increase of convective heat transfer and the radiative heat exchange with the sky decreases due to the decreasing surface temperature. These conclusions assume a constant ambient air temperature which is a reasonable approximation for the considered time period.

Right before sunrise, the magnitude of these two fluxes, convective and radiative, are nearly equal. This may be interpreted as an equilibrium situation. At this time, the surface temperature is nearly constant.

This equilibrium temperature is approximately  $-3^{\circ}\text{C}$ . This temperature may seem low, but it is intrinsically borne out of the correlations used for convection and radiative heat exchange, and also the material of the surface of the Module and to a lesser extent of the materials underneath, namely their thermal diffusivity  $\alpha$ . Still, the only heat flux lowering the surface temperature of the Module is the sky radiative heat exchange which depends on the effective sky temperature. This parameter is not only difficult to measure but is highly dependent on geographical location and local weather. The many propositions to correlate this temperature yield different results, some include other variables as input like dew point temperature or vapour pressure, some methods approximate the sky emissivity, and finally there are methods for clear and cloudy sky, [8], [9]. Summing it up, this parameter does not have a reliable representation as is, since it depends on weather conditions, hence, accurate effective sky

temperature values would need to be measured at each time step like, e.g. air temperature, and also, this type of measurement is not trivial.

Wind speed is also a relevant aspect for the convective heat transfer, as may be seen in Figure 5.2. When wind velocity decreases, convective heat transfer also decreases and vice versa. Since the wind speed during this period is always relatively high or, more meaningfully, the dimensionless group  $(Gr_L/Re_L^2)$  is always small or,  $\ll 1$ , the heat transfer correlation is for forced convection. Figure 5.3 shows these variables. It must be said that this wind speed is from the data file and not corrected according to the logarithmic wind profile Section 3.5.1.

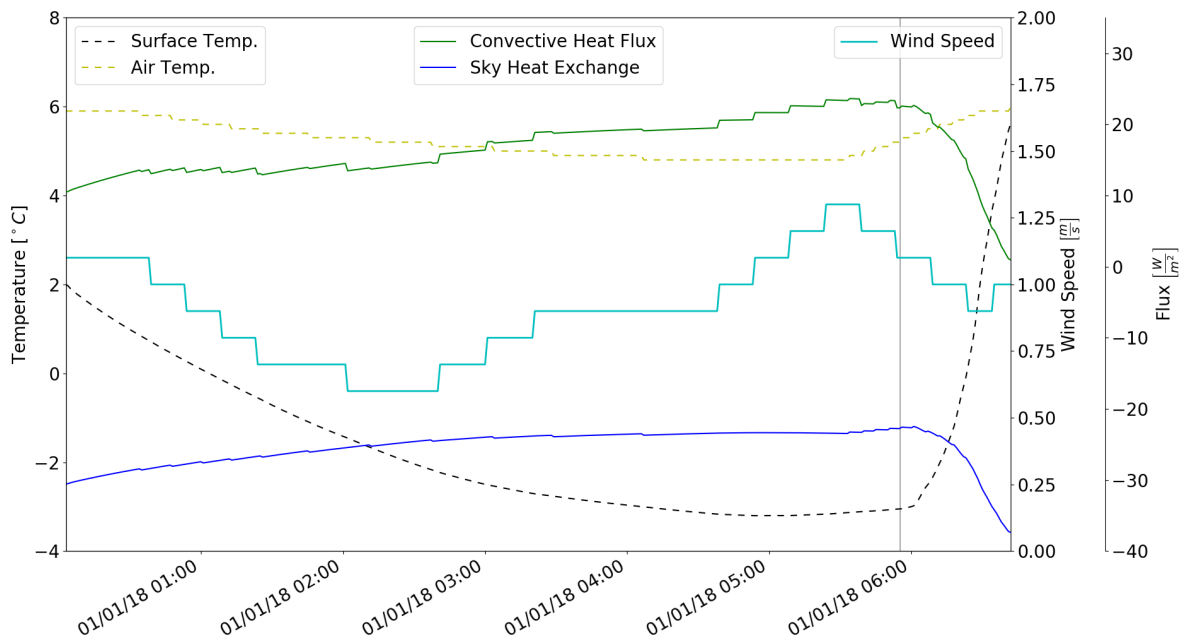


Figure 5.2: One-dimensional initial condition influence of wind speed in convection, Case 1.

If there is no velocity of the air,  $(Gr_L/Re_L^2) = \infty$ , and the corresponding correlation is for natural convection. This situation occurs for the first time in the third day at 00:00 as Figure 5.4 shows. In this plot, the  $(Gr_L/Re_L^2)$  is limited to 120. It should be noted that the correlations used for convection depend on the dimensionless number  $(Gr_L/Re_L^2)$  and the used threshold for natural, mixed and forced convection are,  $(Gr_L/Re_L^2) < 0.01$  for forced convection,  $0.01 \leq (Gr_L/Re_L^2) \leq 100$  for mixed convection and  $(Gr_L/Re_L^2) > 100$  for natural convection. The step in the convective heat flux in between transition from one type of convection to another is small and is considered to be reasonable.

### 5.1.2 Temperature

The temperatures involved in the Module during the initial condition are shown in Figure 5.5.

The Lid of the reservoir is comprised of four CV's that are set to be equally spaced. The thickness of all the reservoir walls is 1.5 cm. The four CV's of this wall have an initial temperature of 2°C and until sunrise they decrease their temperature according to the sources in the CV in contact with the exterior.

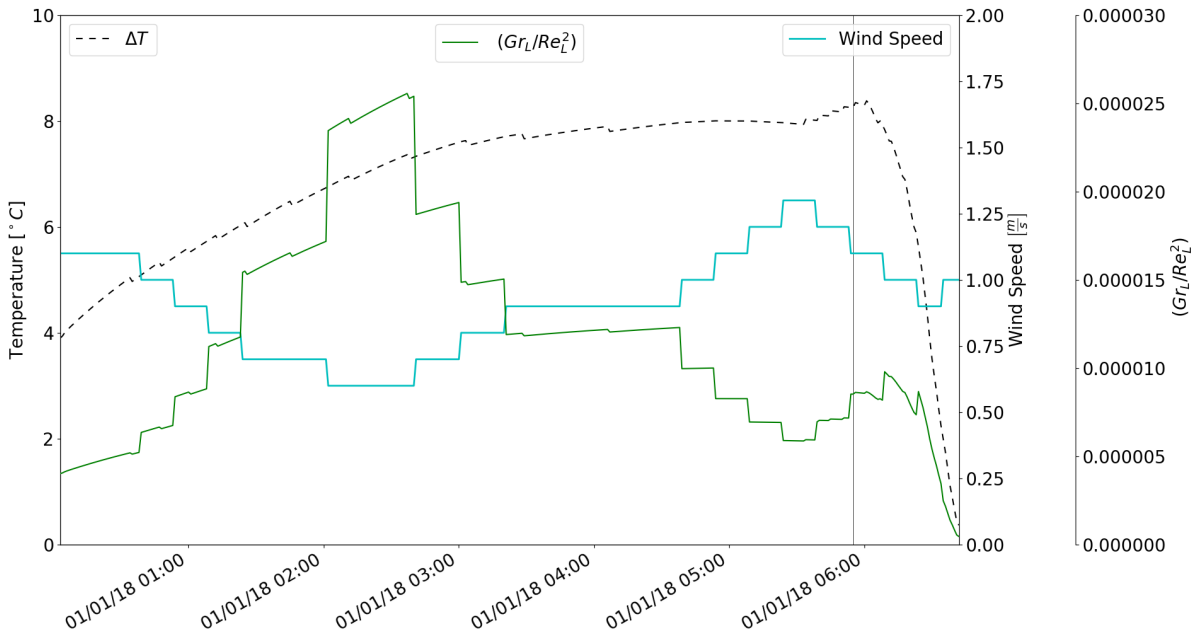


Figure 5.3: One-dimensional initial condition, Grashof number, Case 1.

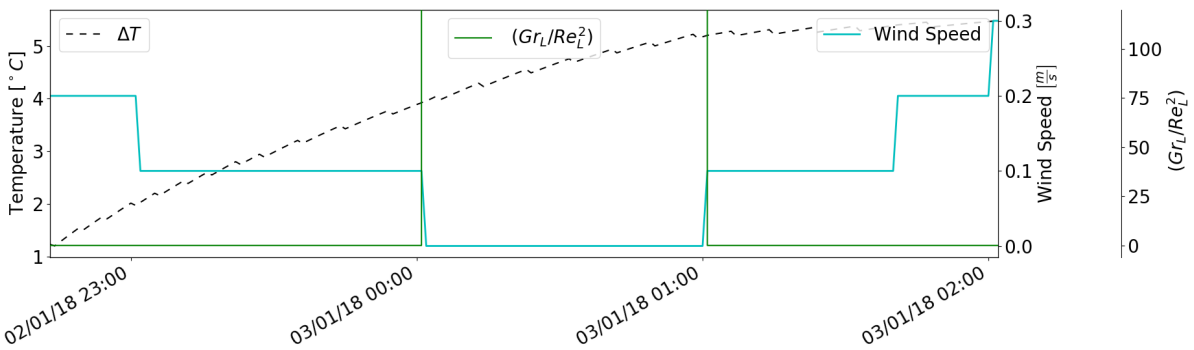


Figure 5.4: One-dimensional initial condition, zero air velocity, Case 1.

The other CV's alter their temperature according to their adjacent CV's. The temperature variation of the water is not noticeable. Figure 5.6 shows only the water temperature.

The first CV of the reservoir, CV 1, where the sources are applied, has the steeper temperature gradients. Hence, after sunrise the order of the temperatures in the four CV's of the reservoir turns around and the first CV that had the lowest temperature while the heat sources were negative (lowering Module's energy) has now the highest temperature followed by CV 2, 3 and 4. This behaviour is obvious, but is presented for clarity. Figure 5.7 shows what has just been described.

The air, CV5, beneath CV4, also behaves in the same manner qualitatively. Since the properties are different the temperature response is according to them. The behaviour of the air may be seen in Figure 5.5. The air temperature, CV5 is closer to the temperature of CV 4 above it than to CV 6 beneath it. After sunrise, the temperature of CV5 is now more or less between both its adjacent CV's. This situation is better visualised in Figure 5.8 which has the same data as Figure 5.5 but is extended until

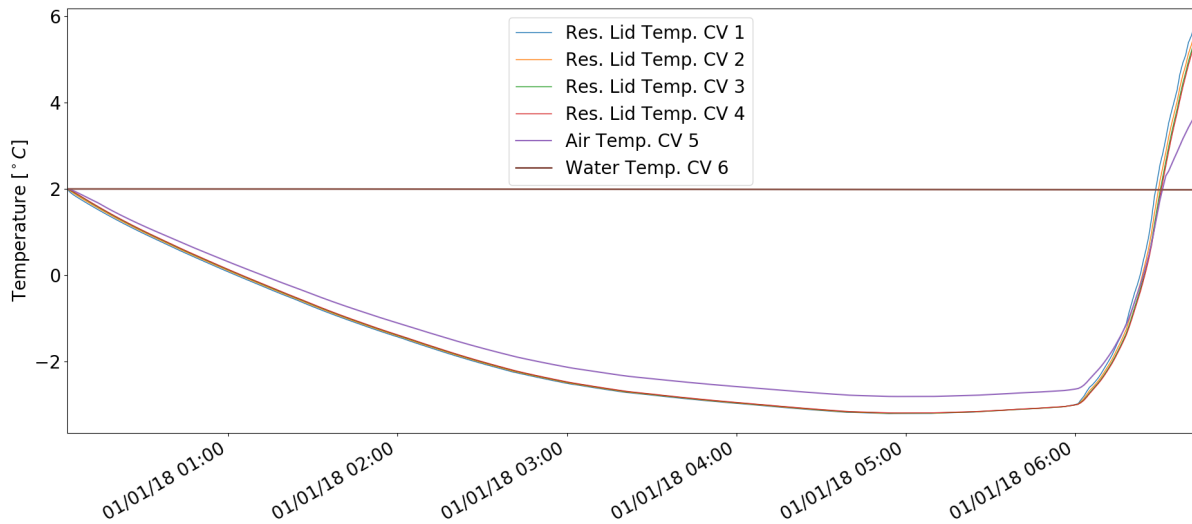


Figure 5.5: One-dimensional initial condition, temperatures, Case 1.

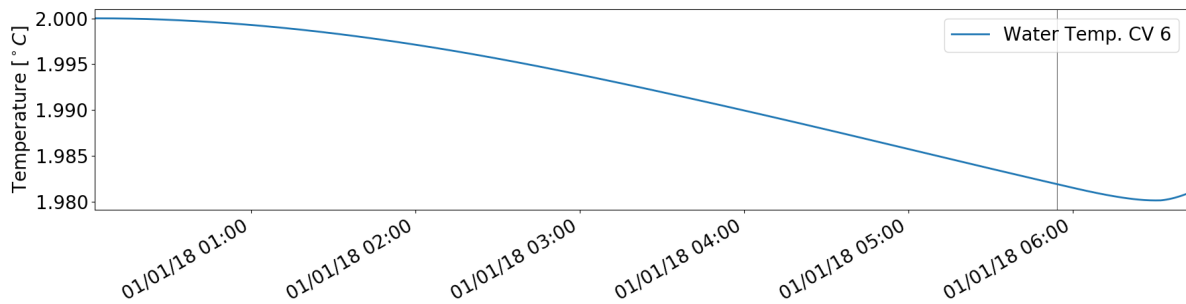


Figure 5.6: One-dimensional initial condition, Water temperature, Case 1.

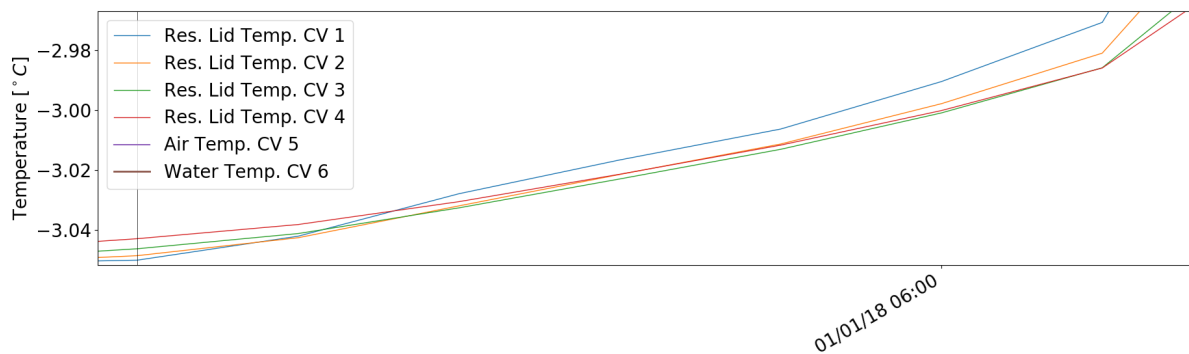


Figure 5.7: One-dimensional sun rise, temperatures, Case 1.

approximately 10:00.

The reason for the shift in the relative position of the air temperature is due to the fact that it is a fluid, hence undergoes convection in certain situations. In the one-dimensional analysis, convection is calculated through a correlation. This correlation is used only if convection conditions apply, which until sunrise they do since the upper surface of the air is being cooled, yielding convective heat transfer in this

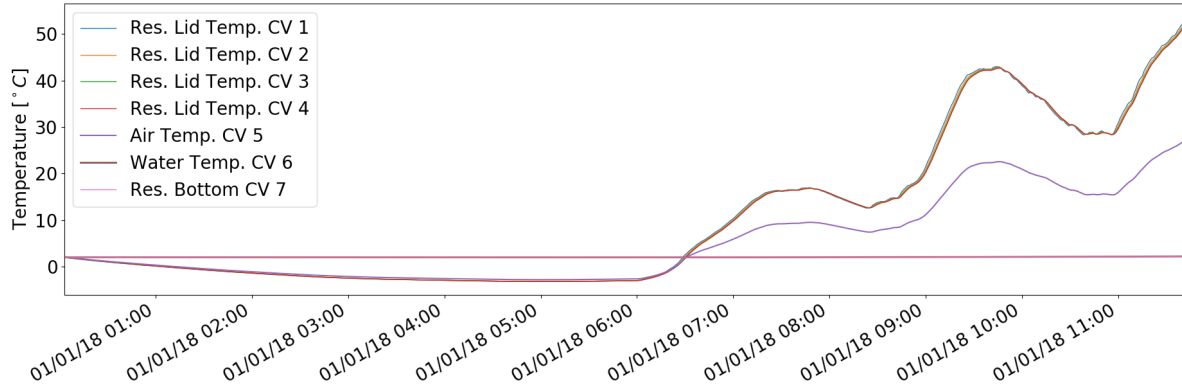


Figure 5.8: One-dimensional, Air temperature, Case 1.

enclosure, and after sunrise they do not since the upper surface of the air is being heated. When the situation is the latter, heat transfer is through conduction and the air temperature tends to an average value of the temperatures above and below it. This is because the equivalent thermal resistance between CV's 4 and 5 and between CV's 5 and 6 are approximately the same after sun rise. When the situation is convective (before sun rise), the temperature of the air is closer to the reservoir temperature because the thermal resistance between the air and the reservoir is lower than the thermal resistance between the air and the water, which is also a fluid and is in a conductive situation until sunrise and convective after sunrise.

### 5.1.3 Thermal Resistance

Each CV has a diffusion coefficient. For a fluid this may be its conductivity or the equivalent conduction coefficient if undergoing convection. The diffusion equation applied to one CV uses a diffusion coefficient for each side of the CV. Each one of these two  $\Gamma$  is the diffusion coefficient between the CV under calculation and the adjacent CV, one  $\Gamma$  for each side. The two diffusion coefficients  $\Gamma$  on each side of the CV is what is being addressed. For clarity the diffusion term corresponding to one CV face of the diffusion equation is shown in equation 5.1.

$$\Gamma A \frac{\partial \phi}{\partial x} = \Gamma A \frac{\phi_{CV5} - \phi_{CV4}}{\delta x_{CV4-5}} = \Gamma A \frac{\Delta \phi}{\frac{\delta x_{CV5}}{2} + \frac{\delta x_{CV4}}{2}} \quad (5.1)$$

This equation considers that the nodes at each CV are placed at the centroid and also, allows for different sized CV's, which is the case being addressed. This situation may be visualised in Figure 5.9

By inspection of this Figure and equation 5.1, the diffusion term may be further developed. Equation 5.2 show the end result for what is being explained. The area term is dropped for simplification since it appears in every term and is the same for an orthogonal mesh.

$$\Gamma \frac{\Delta \phi}{\frac{\delta x_{CV5}}{2} + \frac{\delta x_{CV4}}{2}} = \frac{1}{\frac{\delta_P}{2 \cdot \Gamma_P} + \frac{\delta_W}{2 \cdot \Gamma_W}} \Delta \phi \quad (5.2)$$



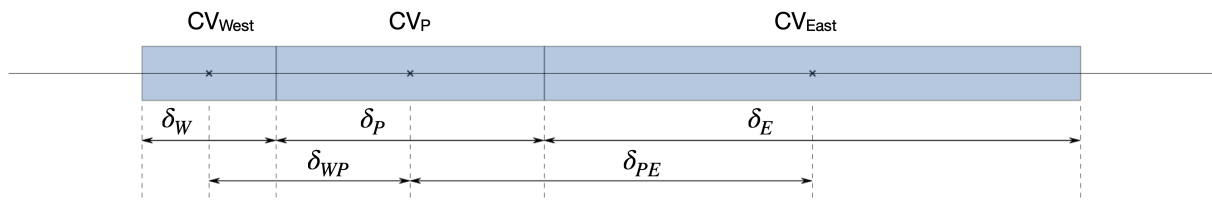


Figure 5.9: One-dimensional, characteristic dimensions.

What has just been made in equation 5.2 is simply to approximate the diffusion coefficient between two adjoining CV's by the inverse of the sum of the corresponding resistances for each of the two CV's. This method allows for different sized CV's. If the CV's are equally spaced, there is no need to transform the diffusion coefficients into resistances and a simple average may be used. In this case the diffusion coefficient is the inverse of the sum of the thermal resistance of half the length of each CV in one direction. This represents the total thermal resistance between the node in the centroid of  $CV_{West}$  and  $CV_P$  or, CV4 and CV5. Now, all there is to do is to use the conduction coefficient in place of  $\Gamma$ , and if the CV in question is a fluid under convection state, use the equivalent conduction coefficient. Of course, if the fluid is under a conduction, its conduction coefficient should be used.

E.g. the thermal resistance between CV5 and CV4, according to equation 5.2 is the sum of the thermal resistance between node 5 and the face in between node 4 and 5 plus the thermal resistance between this face and node 4, Figure 5.9 shows a representation of these nodes, faces and distances. The thermal resistance from CV4 is constant since this CV represents a solid material, hence its thermal resistance is always the same and is a function of its dimensions and conductivity. On the other hand, CV5, where the material is air, may undergo a convective heat transfer or a conductive heat transfer, and when in convection, its equivalent coefficient of conduction must be calculated at each time step, hence its thermal resistance is not constant. Hence the total thermal resistance between CV5 and CV4 is not constant.

In order to make this idea clear, Figure 5.10 shows the two thermal resistances of CV5. One is between CV5 and CV4, and the other between CV5 and CV6.

Initially the air cavity exchanges heat through conduction only since thermal resistance is constant during this period. Although the actual reason is that the *Rayleigh* number does not overcome its threshold value due to a low temperature difference during the initial condition, a constant thermal resistance is considered a good enough symptom for a conduction condition for this discussion. Then, approximately at 00:45 convective heat exchange starts and consequently the thermal resistance decreases due to a  $Nusselt > 1$ . This situation holds approximately until sun rise. In the water a conduction state exists during the whole night time since the air above it is cooler and the water is below  $\approx 4^\circ C$  or rather has a negative thermal expansion coefficient at this temperature. When the sun starts to heat the upper surface of the reservoir, the air switches to a conductive state at about 06:28. At this time the thermal resistance between the air and the water, CV's 5 and 6 respectively, is exactly the same as in the initial condition. This may be seen in the orange line at the upper region of Figure 5.10. This situation holds for a mere 3 minutes since by the time the air temperature crosses the water temperature, the

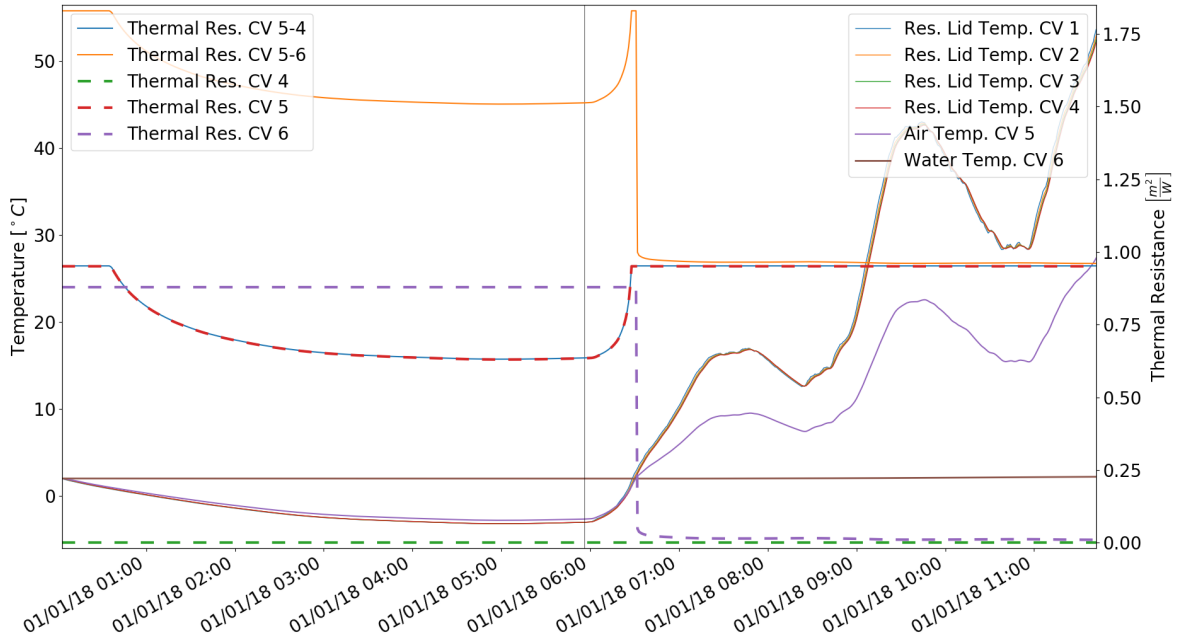


Figure 5.10: One-dimensional, Thermal Resistance for the Air enclosure.

water, that has been so far in a conduction state, switches to a convection state that affects the thermal resistance between CV's 5 and 6. Therefore the thermal resistance between these CV's drops at about 06:31 due only to convection in the water since the air keeps its conductive state.

As stated earlier, regarding Figure 5.8, the air temperature is close to the temperature of its upper surface during night time and during day time the relative position of the air temperature shifts to approximately half way between the temperature of its upper surface (reservoir lid) and its lower surface (water). This behaviour is now fully justified based on the thermal resistances of CV5 to CV4 and CV5 to CV6. The reason for the temperature of the air being closer to temperature of its upper surface is a consequence of the thermal resistance to this upper surface being lower than the thermal resistance to its lower surface. After sun rise, these two thermal resistances are approximately the same, therefore the temperature of the air is approximately half way between the two (given its low thermal mass). Figure 5.10 shows exactly what has just been said.

### 5.1.4 Energy

The first CV in the domain receives the heat flux imposed by the boundary condition, changes its temperature and exchanges energy with its adjoining CV by means of a heat flux at the corresponding CV wall. This second CV undergoes the same treatment and so on and so forth with all CV's in the domain. The energy variation at each CV is calculated according to equation 5.3. Figure 5.11 shows the change in energy in each CV.

$$\dot{E}_{stored} = \rho V c_p \frac{\partial T}{\partial t} = \frac{\partial}{\partial x} \left( k \frac{\partial T}{\partial x} \right) \quad (5.3)$$

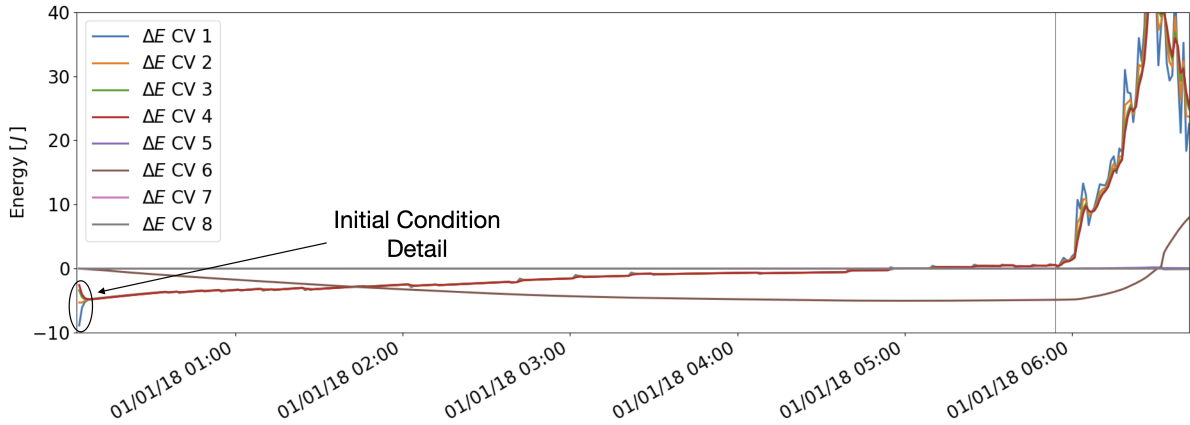


Figure 5.11: One-dimensional, Energy change at each CV.

It can be seen that initially, the four CV's of the reservoir lid represent the greatest energy decrease. Naturally, CV1 is the first CV to decrease its energy followed by CV2 and so on. After a short time, depending on the thermal diffusivity of the material, the subsequent CV's also decrease their temperature. Figure 5.12 shows a detailed view of this initial condition.

During this initial condition the energy change of CV1 is the greatest and decreases to a situation where its temperature variation is minimal and all the heat flux from the boundary condition at the surface, is mostly passed onto the adjoining CV2, and CV1 retains a relatively small portion of this flux to alter its energy. The other CV's have the same behaviour, hence after about 8 minutes, the energy variation of each CV changes its order, meaning CV1 as the least energy variation at each time step and CV4 as the greatest. This behaviour is imposed by the transient energy equation 3.10.

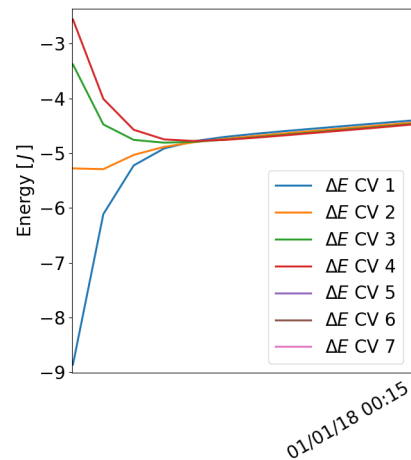


Figure 5.12: One-dimensional, Energy change in the first four CV's.

Regarding  $\Delta E$  in the air, CV5, and water, CV6, as expected, the energy change in the air is relatively small due to a low  $\rho V c_p$  and in the water, the energy change may be high if the heat flux is also high due to a high  $\rho V c_p$ . These two CV's are presented in Figure 5.13 for the first two hours.

A detailed view of CV's 5, 6 and 7 during the first 8 minutes is shown in Figure 5.14. As expected the air CV is the first to reduce its energy followed by the water CV.

Also, regarding Figure 5.11 a close up of the temperatures at approximately 06:30 where the change from conduction to convection in the water occurs, shows a sudden decrease in the temperature of CV 7, the base of the reservoir. Once again due to the lower thermal resistance between CV 6 and CV 7. CV 7 alters its temperature in the direction of the water temperature. Figure 5.15 shows a close up of

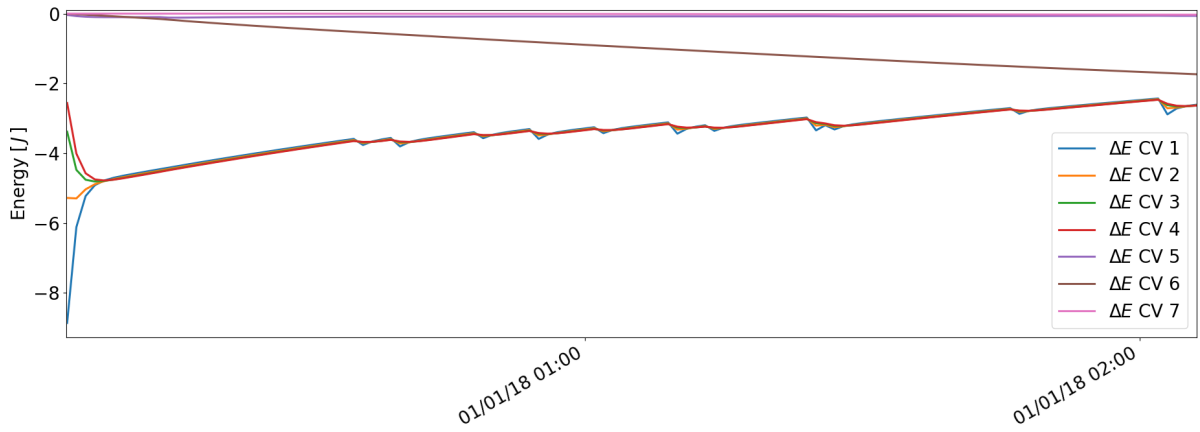


Figure 5.13: One-dimensional, Energy change in air and water.

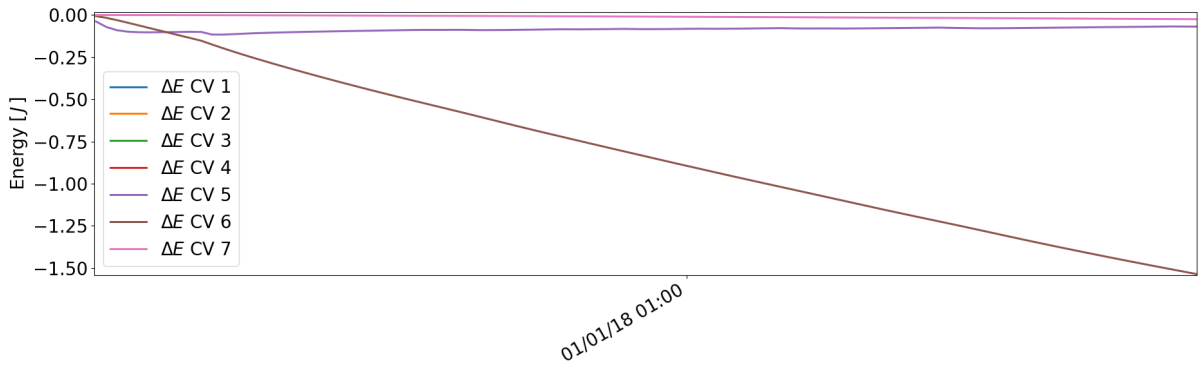


Figure 5.14: One-dimensional, Energy change in air and water, detail.

this particular moment.

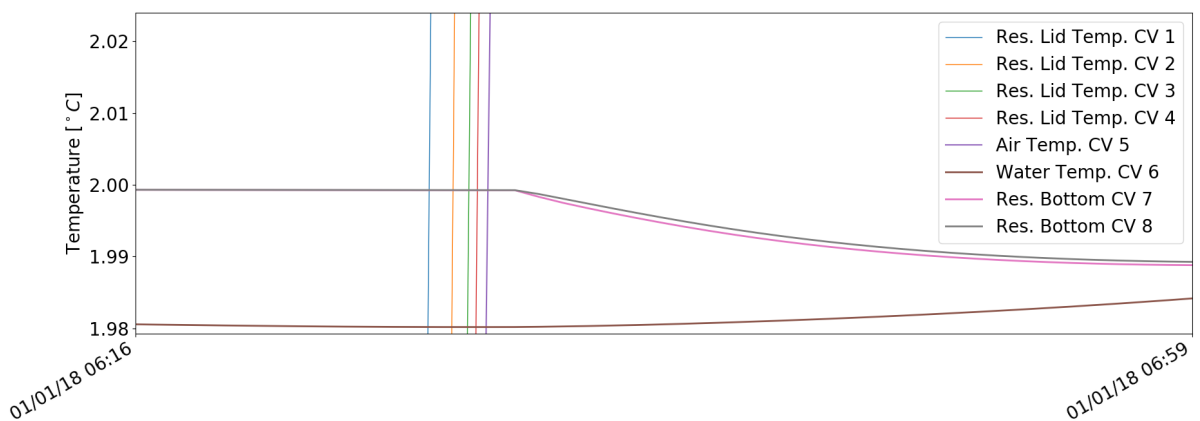


Figure 5.15: One-dimensional, Energy change at each CV, detail.

The same information presented for  $\Delta E$  may be seen through the heat fluxes at each adjoining face between CV's. Figure 5.16 shows these fluxes.

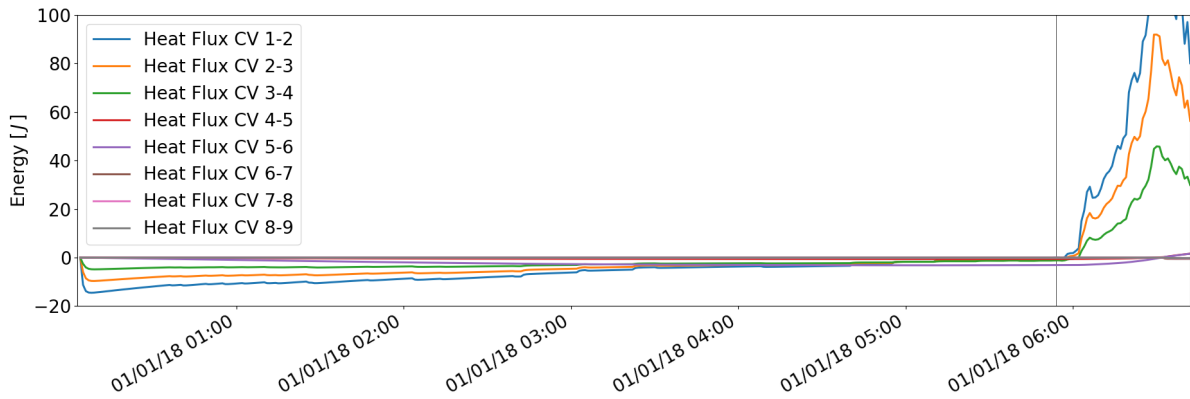


Figure 5.16: One-dimensional, Heat Flux between CV's.

### 5.1.5 Rayleigh number

Finally, one more interesting parameter to acknowledge here is the Rayleigh number. Figure 5.17 shows this number together with the temperatures of the water and CV's above and below it. The threshold value for convection to exist is  $Ra > 1708$ . This value is set by the correlation, equation 3.27.

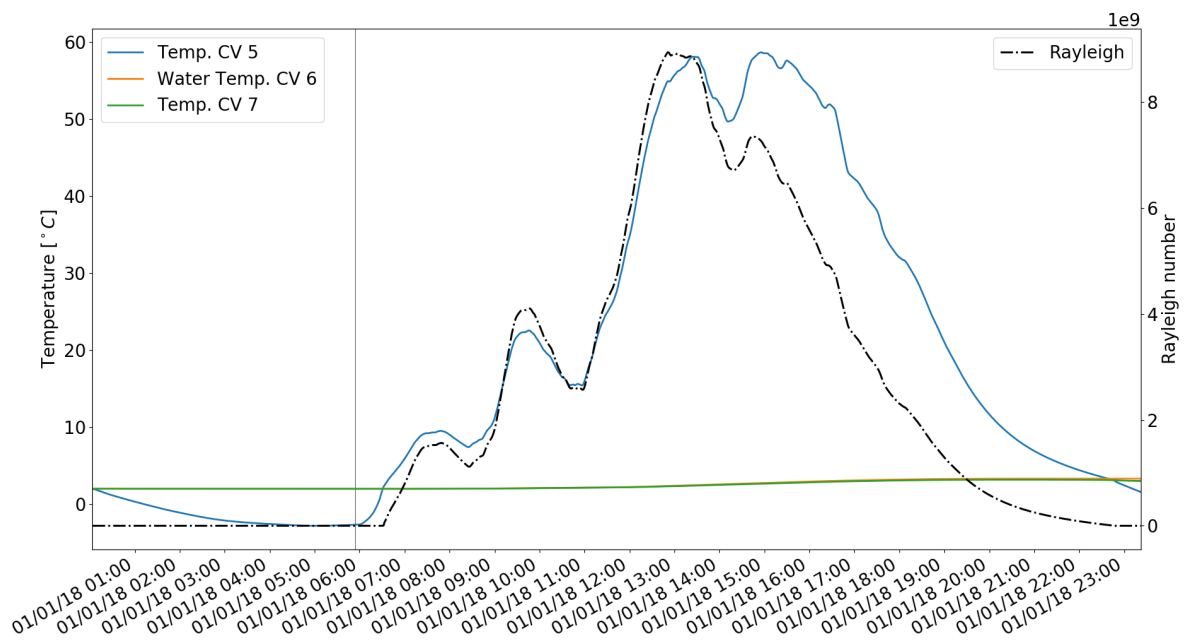


Figure 5.17: One-dimensional, Rayleigh number in Water domain.

The value of the Rayleigh number shown in Figure 5.17 may be considered high. A value of  $Ra \approx 10^9$  is referenced as the transition from laminar to turbulent [1]. This reference value is for free convection in a vertical flat plate. For an enclosure or any other distinct geometry, this limit would ideally be measured. Most correlations for free convection for any specific geometry, possess a range of applicability regarding the Rayleigh number.

The high  $Ra$  value is due to the initial condition where the temperature difference and thermal ex-

pansion coefficient make up for a Rayleigh number of  $\approx 10^{10}$ . Figure 5.18 shows the Rayleigh number for the whole year. Nevertheless, a  $Ra > 10^9$  is relatively common throughout the year for this case.

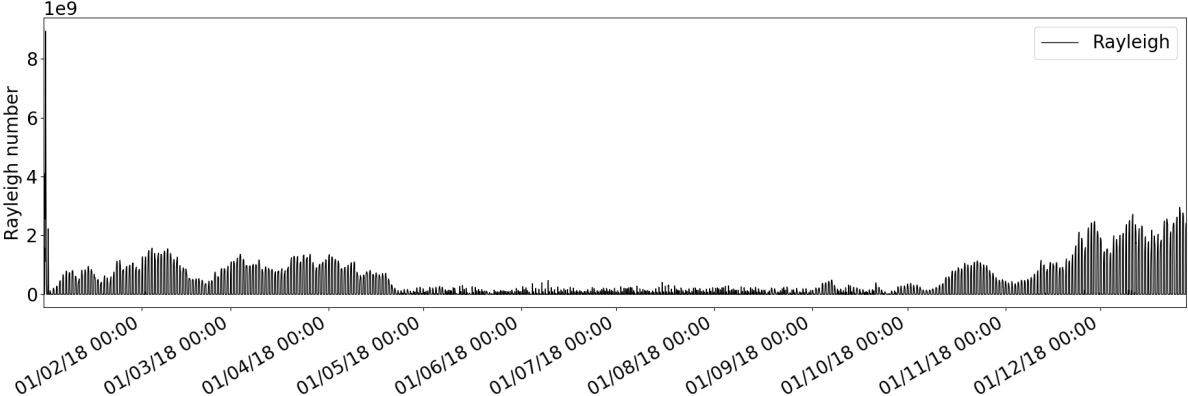


Figure 5.18: One-dimensional, Rayleigh number in Water domain, one year.

### 5.2 Two Dimensional

For the two dimensional case, a comparison between correlated convection and convective flow is made. Figure 5.19 shows this comparison for cases 1.

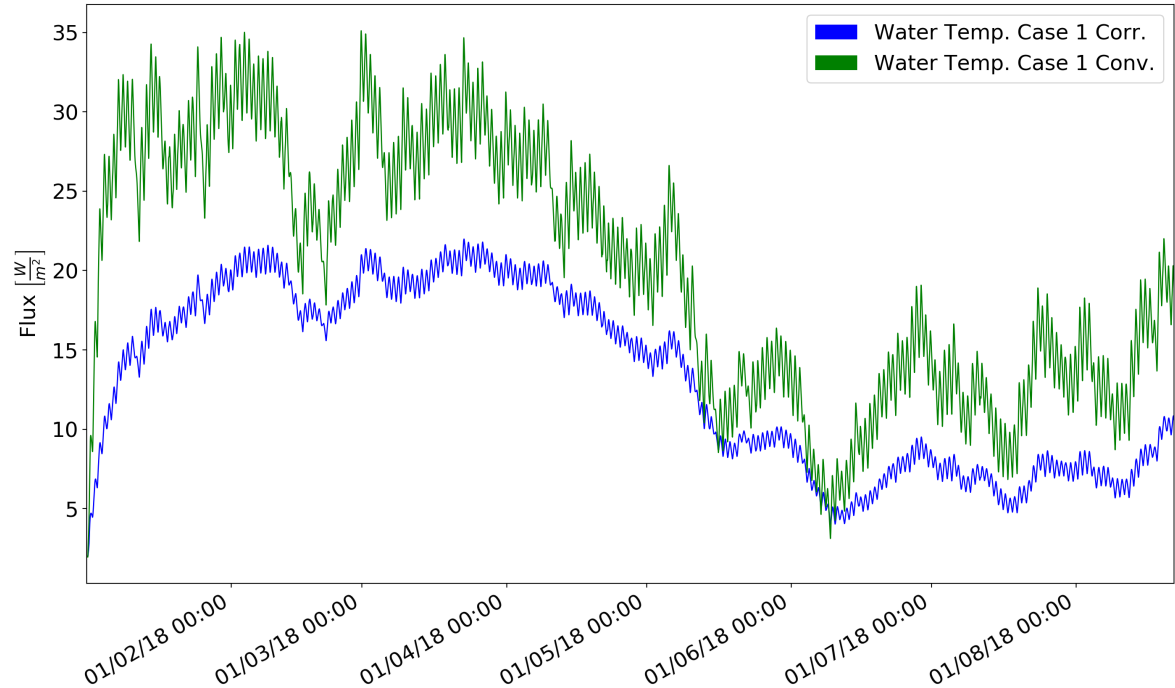


Figure 5.19: Two-dimensional, Correlation Vs. Convection.

First it may be seen that the flow case as a higher average temperature than the correlated case. This is justified by a higher absorption of heat by the water in the flow case. The reason is, as previously

mentioned, that a temperature difference between a lateral wall and the water imposes a convective heat transfer in the side walls. Therefore, comparing the side wall heat transfer, in the flow case there is always convection and in the correlated case always conduction. Another consequence of this aspect is that in the flow case, as long as there is convection in any of the surfaces, the resulting convective flow is transported to every other wall due to the viscosity of the fluid making for a  $\overline{Nu} > 1$  in every wall. These flows may be seen in Appendix C.

The higher heat exchange with the water in the convective flow analysis lowers the temperature gradients between the water and the walls hence the temperature of the surface of the walls does not fluctuate as much. For instance, during day time, when irradiation is heating the surfaces of the Module, the temperature of the surface is regulated by this higher heat transfer with the water lowering convection heat loss to the exterior. Figure 5.20 shows for the first 24 hours convection heat transfer in the east and west walls for convective correlation and convective flow.

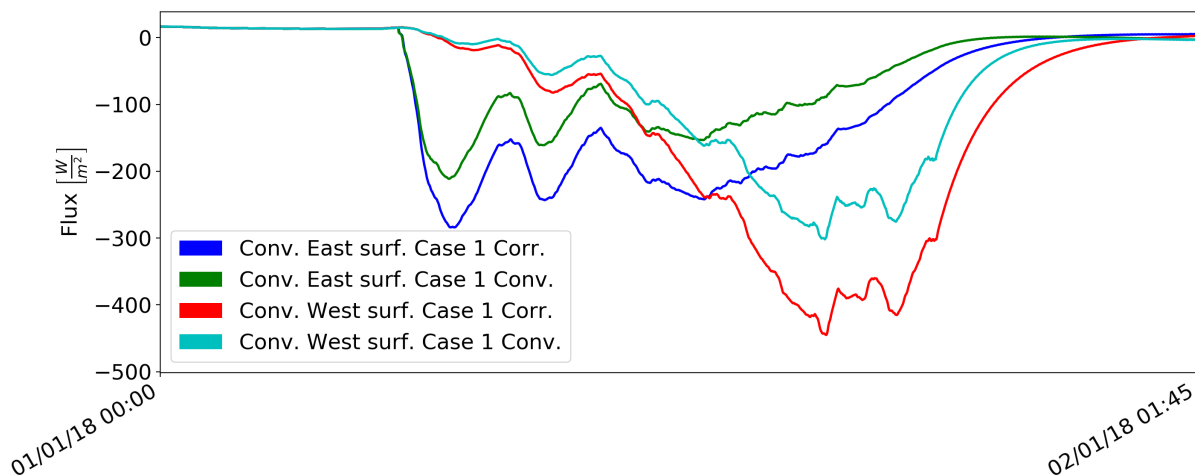


Figure 5.20: Two-dimensional, Convection heat flux in East and West walls.

A detailed view of Figure 5.19 during the first day is shown in Figure 5.21. The correlated case presents convection in a on / off manner.

The energy graph, which is simply the first derivative of the previous plots multiplied by  $\rho V c_p$ , may be seen in Figure 5.22. As expected, the energy variation for the correlated case during the convection period is much higher than for the convective flow case where the energy change in the water is continuous through the whole period. Also when in conduction, the energy variation is lower in magnitude than the convective flow case.

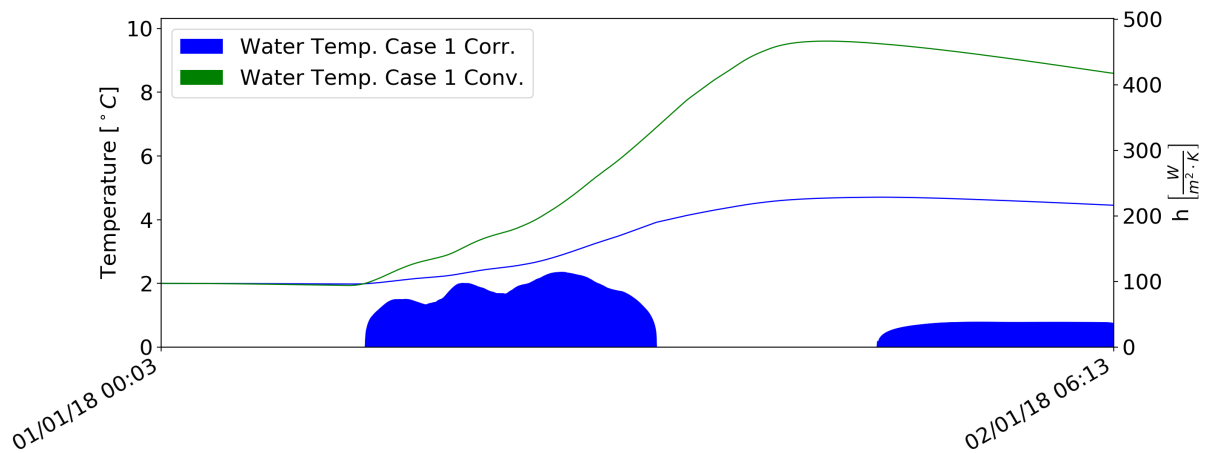


Figure 5.21: Two-dimensional, Correlation Vs. Convection, detail.

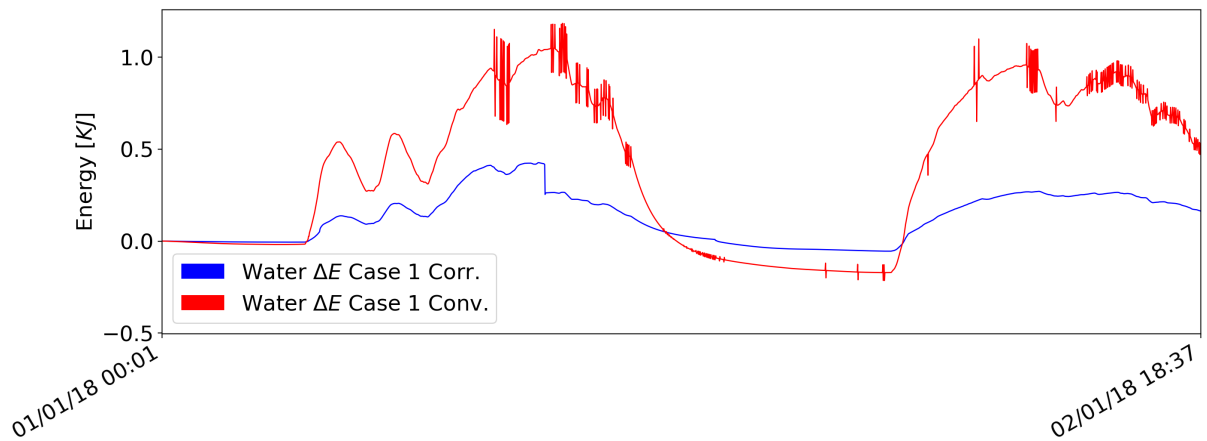


Figure 5.22: Two-dimensional, Correlation Vs. Convection, Energy variation.

### 5.3 Three Dimensional

Figure 5.23 compares the correlated and convective flow for the three dimensional analysis. Only the first 20 hours are available.

Comparing these temperature values with the two dimensional in Figure 5.19, the maximum temperature reached during the first day is higher in the three dimensional analysis.

With the same interpretation and justification as in the two dimensional case, but applied to the three dimensional case, convection with the exterior for the four lateral faces is shown in Figure 5.24. Due to the quantity of information in this graph, the night period is left out.

The declination of the sun's trajectory yields an extra irradiation component in the north facing surface of the Module. Hence, convection in this wall is slightly higher than the south facing surface since this wall gains more energy than the south.



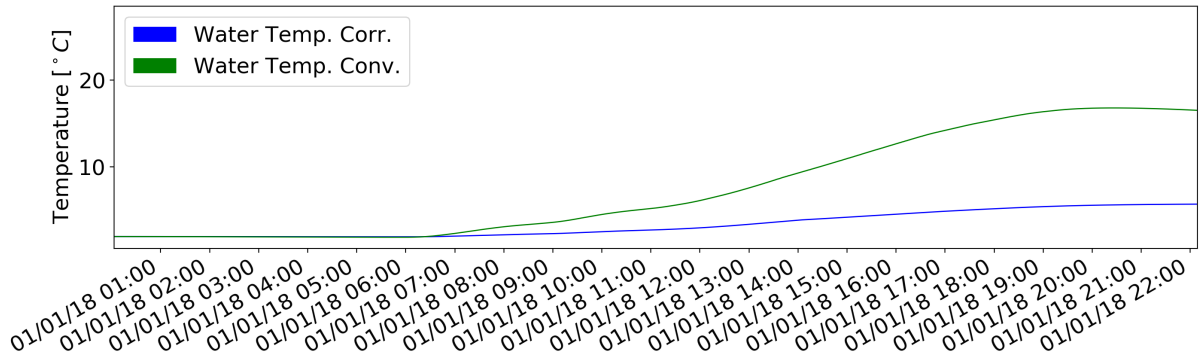


Figure 5.23: Three-dimensional, Correlation Vs. Convection.

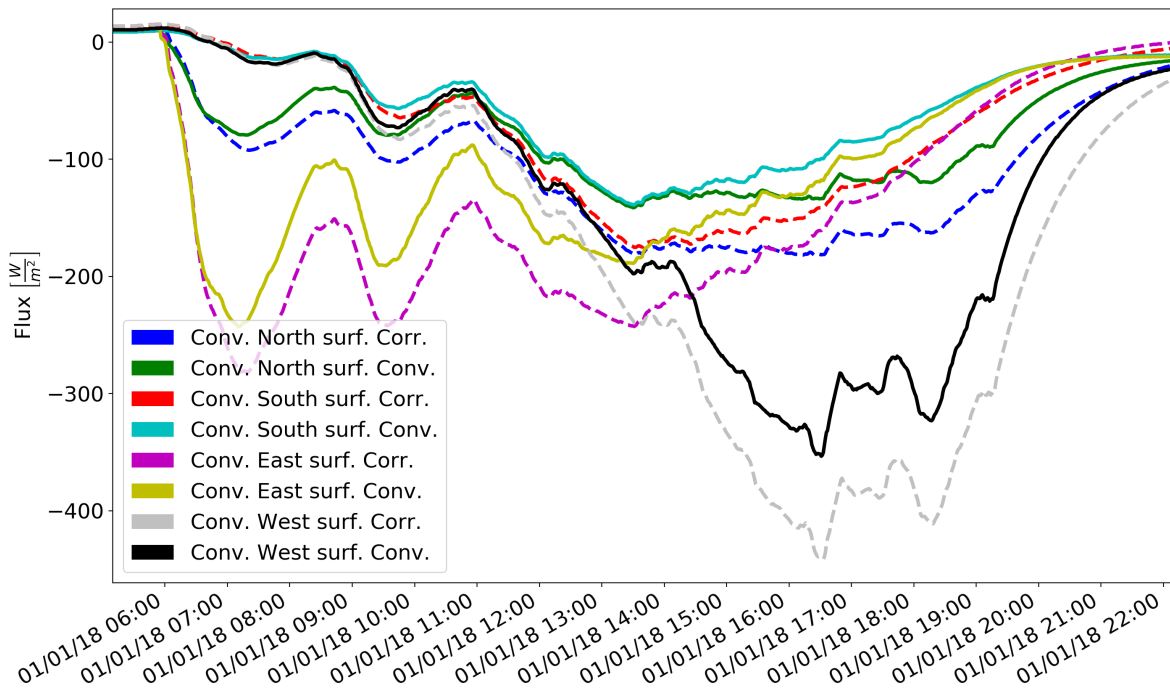


Figure 5.24: Three-dimensional, Convection heat flux in North South East and West walls.

Again, convection in the correlated analysis is similar to the two dimensional case as may be seen in Figure 5.25.

Also  $\Delta E$  is qualitatively similar to the two dimensional analysis, although the magnitude of the energy is slightly higher in the three dimensional case, Figure 5.26.

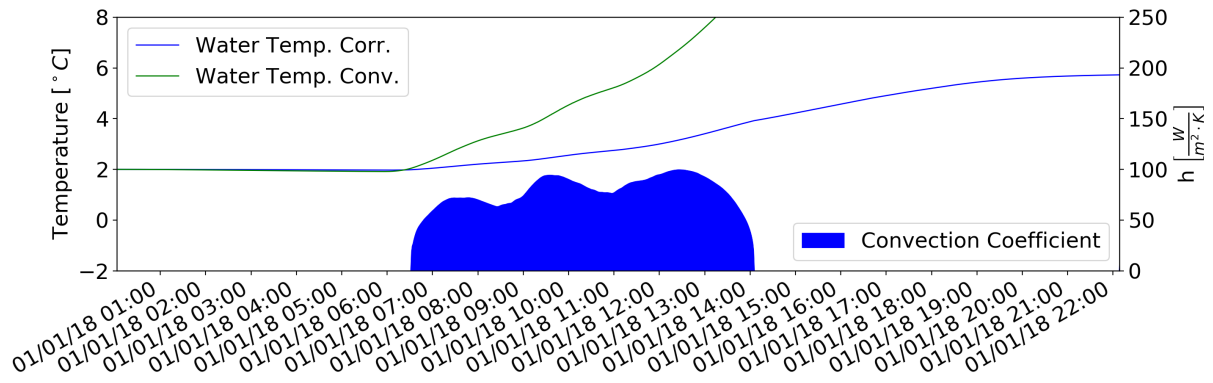


Figure 5.25: Three-dimensional, Correlation Vs. Convection, detail.

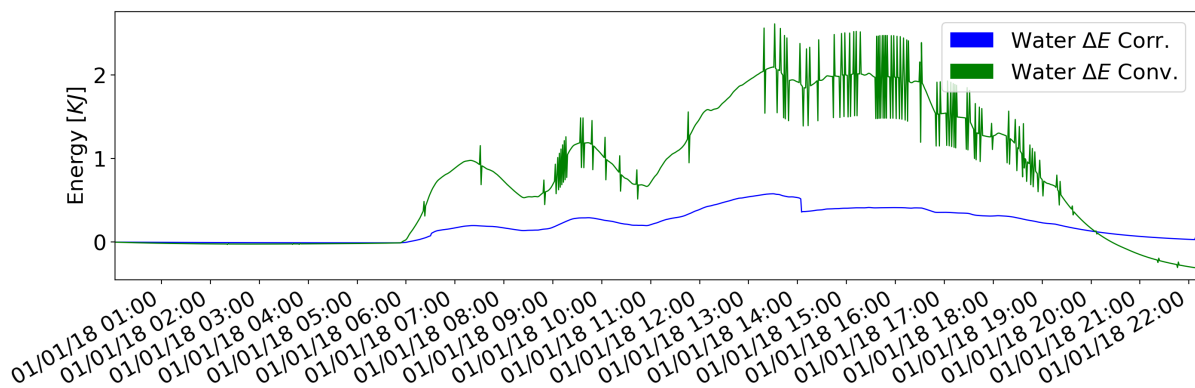


Figure 5.26: Three-dimensional, Correlation Vs. Convection, Energy variation.

# Chapter 6

## Conclusions

### 6.1 General Conclusions

In general, regarding the unwanted freezing of the water in the Module, it may be said that the minimum temperature of the water is a function of several variables. Some of these variables are not susceptible of being changed like the climate data at the site location, e.g. air temperature, irradiation, underground temperature. It is what it is. Other variables on the other hand are susceptible of being changed. These are the materials surrounding the water, their surface properties, the volume of water, etc.. Hence it could be said that the minimum temperature reached by the water relative to the unpredictable variables is a function of the variables that may be changed.

For example, regarding the volume variable, indeed an increase in volume has a linear relation to the amount of energy needed to alter the temperature of the water through its specific heat  $c_p$ , which is considered to be high. But the surface area of the Module also increases and consequently its heat exchange. Surface area to volume ratio for a cube decreases with increasing volume, Figure 6.1, hence the bigger the reservoir the less the temperature of the water changes, assuming the heat flux remains the same, which does not. Nevertheless, assuming it is a similar heat flux regardless of the size of the Module, a bigger Module would indeed alter its temperature

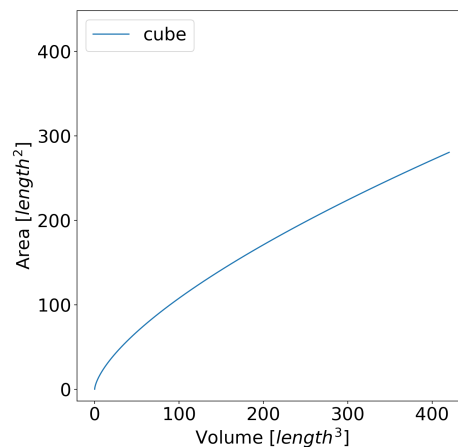


Figure 6.1: Surface area to volume ratio for a cube.

slower. But the time scale must not be forgotten. Whatever the size of the Module if the atmospheric conditions are prone to freezing, then, its only a matter of time for the water to freeze as well. Even if the water reservoir was big enough to cycle its temperature with a period of one year (with only one change in concavity during this period), it would still be unknown if the water would freeze or not (given

the climate data) without calculating each time step. What is known is that having a big reservoir will not make any difference if the heat exchange with the water throughout the year is conducive to freezing. Therefore the size of the reservoir should be designed with the intent of alleviating its extreme temperatures, reducing its amplitude, if the lower end of these temperatures is below freezing and the average is not.

The heat flux through the surfaces of the Module is the relevant aspect that can be to some extent manipulated. Maximizing the energy intake of the Module is in a way to make it as close as possible to solar collector. The objective is to maximize the incoming energy from the sun through a high absorptance coefficient at the surface and minimize losses from convection and emissivity.

There is however one more aspect that is not predictable in a linear way. The thermal diffusivity of the materials between the water and the exterior faces of the Module have an unclear influence on the water temperature. Of course, a material with a higher thermal diffusivity promotes a higher temperature variation in the water for the day / night temperature cycle (assuming a reasonable thickness between the water surfaces and the exterior), on the other hand a lower thermal diffusivity insulates the water. The question is, which thermal diffusivity yields the highest minimum temperature in the water over the entire year. There is also the thickness of this material which of course has its own bearing in the answer together with the thermal diffusivity.

The difficulty in the matter addressed by this Thesis, is that it is a transient analysis. The effect of the climate data on a particular set of Module's characteristics is not susceptible of being estimated in a comprehensive way. The solution of the next time step depends on the solution of the previous time step together with the climate data for the next time step.

What could be done is to develop correlations that approximate results in a statistically meaningful way. These results could be numerically calculated, experimental, or both.

## 6.2 Numerical Conclusions

Conclusions regarding the actual water temperature should be based at least in the two-dimensional if not in the three-dimensional case.

For the one dimensional case the increase in insulation to the water whether from the RPC or from the 5[cm] of insulation material added or both, results in a general temperature increase in the water throughout the year. The decrease of this insulation on top of the water will on the other hand increase, not its general temperature, but rather its minimum temperature, since the increase of temperature in the water is faster than its decrease below  $\approx 3.9^{\circ}C$  hence, at this temperature, the temporary high solar radiation during day time provides a sufficient increase to the water temperature in order to compensate for the losses during night time.

The two dimensional case using convection correlation in the water shows a similar behaviour but with a higher daily temperature range in the water due to the two additional faces exposed to the atmospheric conditions. The two-dimensional case with convective flow in the water shows a higher temperature of the water in general. This is due to a higher heat transfer between the water and the

side walls. In other words, the heat gain from the sun in a side wall is relatively more absorbed by the water in comparison to the correlated case where heat transfer to the water is through conduction. The shedded heat due to convection in the outside surface of the wall is naturally less in the convective flow analysis because the water absorbs more energy hence lowers the outside surface temperature.

The three dimensional results present a too short time period to draw meaningful conclusions. Nevertheless the maximum temperature reached in the first day is the highest of all results. Hence it foresees a higher daily temperature range and also, although less predictable, yearly temperature range. The shown behaviour so far is similar to the two dimensional qualitatively.

## 6.3 Achievements

The main concern motivating the proposition of this Thesis, is the freezing of the water in the reservoir. Based on the gathered results there is no tendency for the water temperature to drop to  $0^{\circ}C$  for the one dimensional case. This scenario is, of course, based on the used input and type of analysis, and must be interpreted accordingly. For example, if a colder climate data set were to be used, naturally the water temperature would be lower as well. Or if the surface is not painted black, that is assumed in all cases, the radiative heat gains would be lower, hence the water temperature be lower.

The differentiating factors that were compared in Chapter 4 show a more or less predictable result. As long as the climacteric conditions are known and the domain is well defined regarding properties of materials, boundary conditions etc., the qualitative aspects of the results are foreseeable with regard to the influence of each differentiating factor. Nevertheless, since, for example, freezing of water happens at a discrete temperature, calculation of the temperatures in the Module is always necessary.

One of the main achievements of this Thesis is the tool developed for temperature analysis. This tool is presented in Appendix A.2 and may be downloaded through the following [link](https://drive.google.com/drive/folders/1IU98jXzmq2qHkeqdw3LT16SKiuMZbvK?usp=sharing):

<https://drive.google.com/drive/folders/1IU98jXzmq2qHkeqdw3LT16SKiuMZbvK?usp=sharing> where an application to be run in Mac OS plus a climate data file are available. The available climate data set is not the used one for liability reasons. Instead a climate data constructed with freely available data is offered. This file was used throughout this Thesis except for the final results shown in this document. Through this application, the most important input variables may be defined and set in the pre processor phase, and the results may be clearly viewed.

The actual conditions for freezing not to occur would better be drawn from a three-dimensional analysis, but for the tested cases in Chapter 4 with the corresponding assumptions, freezing never occurs. This result though, since there is no three-dimensional result for the whole year yet, should not be interpreted as accurate due to its limitations. Of course a modern computer with higher CPU and RAM specifications would improve the duration of a solution.

## 6.4 Future Work

There are many areas where improvements could and should be made.

The one-dimensional case is not one to pursue due to its limitations. The purpose of this study is better suited to a three-dimensional analysis.

A correlation for non circular cylinders in cross flow, for a square shape should have been implemented and used for greater accuracy. This correlation is only applicable to the three dimensional analysis. The only short come of the use of this correlation is that it imposes an equal heat flux in every lateral wall which is not accurate, but the used correlation also has its flaws which are relative to the velocity of the air at each face.

Although the calculations being made are intrinsically a series computation due to the transient nature of the problem, some parts of the solver may, to some degree and with yet unknown benefit, be parallelized. The advantage, if so, increases with the total grid size, hence, even if only a marginal gain is achieved, the scaling of the grid size becomes viable. Also, this type of implementation (parallelization) requires a substancial rework of the structure of the source code since it was not implemented with this in mind from the beginning. Moreover, several approaches to parallelization can be made regarding the splitting of the calculation work and subsequent assembly of the results. Hence this task may be laborious.

The model used for phase change, although perfectly adequate for a first approach, may be improved with the expense of assuming a significant part of the computational work. Although this extra computational work appears only when freezing occurs. This implementation was intended, but had to be paused due to time constraints, hence the simpler approach is the currently used.

In a generic way, all correlations should, if possible be avoided. Since it is, theoretically, possible to obtain the actual energy flow at every CV based only on the governing equations for fluid flow and heat transfer assuming enough computational availability, no correlations are needed. Also, a solution obtained in this way would be the most reliable (although other factors may influence). This would imply a bigger domain. The domain would have the Module inside it and a space of air around it. At the boundaries of the domain, a constant temperature uniform flow of air together with radiation data would be the only boundary conditions in the domain, without the process of correlating them to a energy flux at each surface of the Module as is presently the case.

The existing source code should be profiled and analysed for possible improvements in the time spent to solve each time step. This has been a continuous work but is only partially dealt with so far.

Regarding the climate data, the use of a TMY is the best solution so far. Nevertheless the weather station at the APEX site shows a lower air temperature which raises the question of the reliability of the used statistical climate data. If a solar irradiance measuring device (pyranometer) were available at the site there would be direct climate measurement of all the climate variables and if nothing else, results could be compared. Also, the underground temperature at the site could be measured so a reliable value could be used.

# References

- [1] Frank P. Incropera and David P. Dewitt. *Fundamentals of Heat and Mass Transfer*. John Wiley & Sons, fifth edition edition, 2002. ISBN:0-471-38650-2.
- [2] Sadik Kakaç, Ramesh K. Shah, and Win Aung. *Handbook of Single-Phase Convective Heat Transfer*. John Wiley & Sons, 1987. ISBN:0-471-81702-3.
- [3] Rolf H. Sabersky, Allan J. Acosta, Edward G. Hauptmann, and E.M. Gates. *Fluid Flow: a first course in fluid mechanics*. Prentice Hall, 4rd edition edition, 1999.
- [4] Greg F. Naterer. *356 Heat Transfer in Single and Multiphase Systems*. CRC Press, 2002.
- [5] H. K. Versteeg and W. Malalasekera. *An Introduction to Computational Fluid Dynamics*. Pearson Education Limited, second edition edition, 2007.
- [6] H.S. Carslaw and J. C. Jaeger. *Conduction of Heat in Solids*. Oxford University Press, second edition edition, 1959.
- [7] John A. Duffie and William A. Beckman. *Solar Engineering of Thermal Processes*. John Wiley & Sons, 1980. ISBN:0-471-05066-0.
- [8] Salem Algarni and Darin Nutter. Survey of sky effective temperature models applicable to building envelope radiant heat transfer. -, 07 2015.
- [9] Omemah Glliah, Boguslaw Kruczek, Seyed Gh Etemad, and Jules Thibault. The effective sky temperature: An enigmatic concept. *Heat and Mass Transfer*, 47:1171–1180, 09 2011.
- [10] Tomasz Michałek and Tomasz Kowalewski. Simulations of the water freezing process - numerical benchmarks. *Task Q.*, 7, 01 2003.
- [11] Kong Ling and Wen-Quan Tao. A sharp-interface model coupling voset and ibm for simulations on melting and solidification. *Computers and Fluids*, 178, 09 2018.
- [12] David R. Lide. *CRC Handbook of Chemistry and Physics*. CRC Press, 74th edition, 1993 - 1994.
- [13] M. Peric and J. H. Ferziger. *Computational Methods for Fluid Dynamics*. Springer, 3rd edition edition, 2002.
- [14] August 2019.

# Appendix A

## Source Code

In Python there are Libraries available to facilitate the management of data where operations are performed. The most used package was Numpy from SciPy which is a free and open-source Python library used for scientific computing and technical computing. Also, from SciPy, Matplotlib and Pandas were used. The first is a plotting package, the second is a data management package. Apart from these packages other modules native to Python were used for several tasks.

It should be mentioned that the use of this Language was subject to a steep learning curve, that took its time and effort. The available online information about almost every possible aspect that concern at least this implementation is incredibly vast and helpful.

Hence the code implemented here, is not finished in any way, but rather an ongoing process. There are still many features that need to be added and the code needs to be improved in a general way from a coding standpoint. Still, as is, it performs exactly as intended.

### A.1 Code Structure

The Source Code created is mainly made by a series of functions or subroutines that interact with each other. Each one performs a specific task for the general purpose of the code.

For the computing of the temperatures there is a central loop that is fed at each time step with the necessary data obtained from auxiliary functions.

There is also a data management structure that stores the results and allows for the interruption of the run and continuation at a latter time.

The central part of code, disregarding its auxiliary but needed routines, is shown in the next Flowcharts. These are separated into a pre processing stage and a processing stage. Of course there is also a post processing stage for the compilation of the results which is made according to the desired representation of the results. This is not shown where since it is not a fixed code.



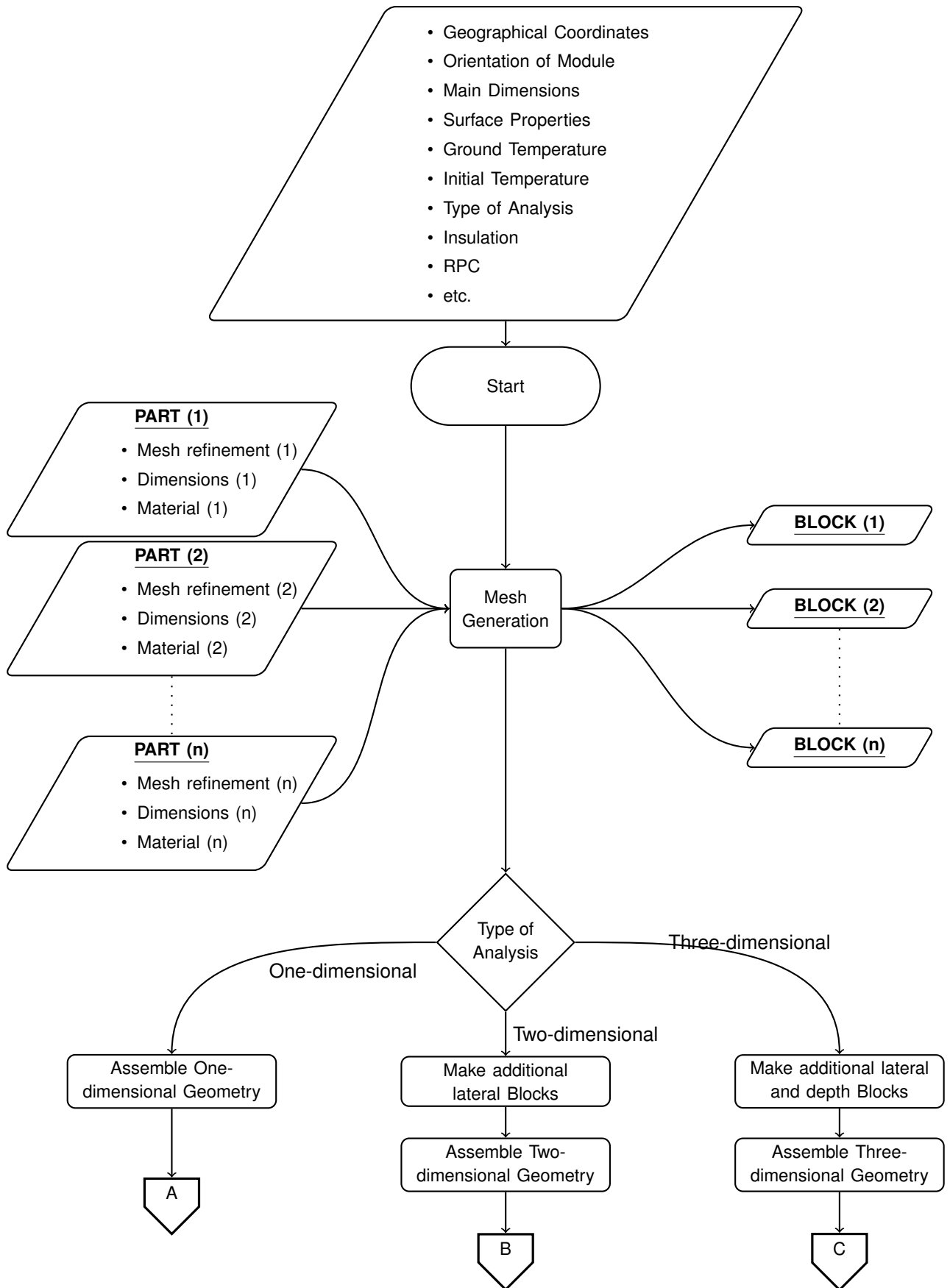


Figure A.1: Flowchart Pre Processor (1).

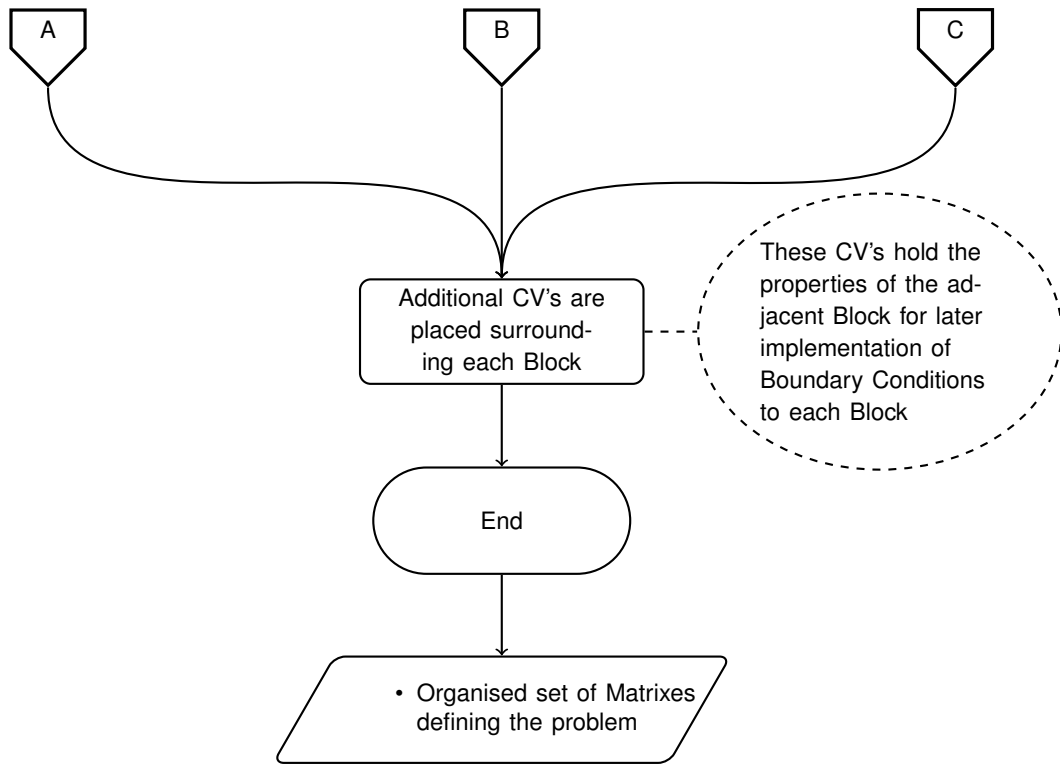


Figure A.2: Flowchart Pre Processor (2).

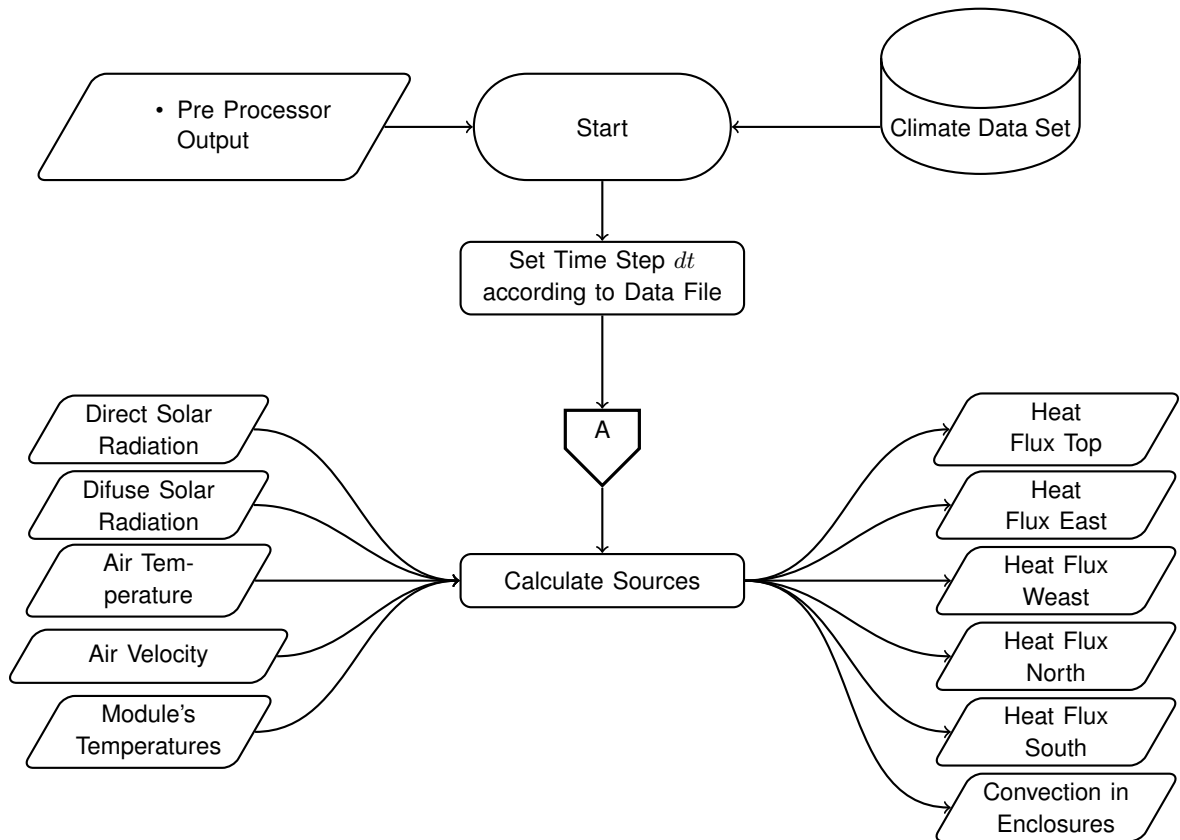


Figure A.3: Flowchart Processor (1).

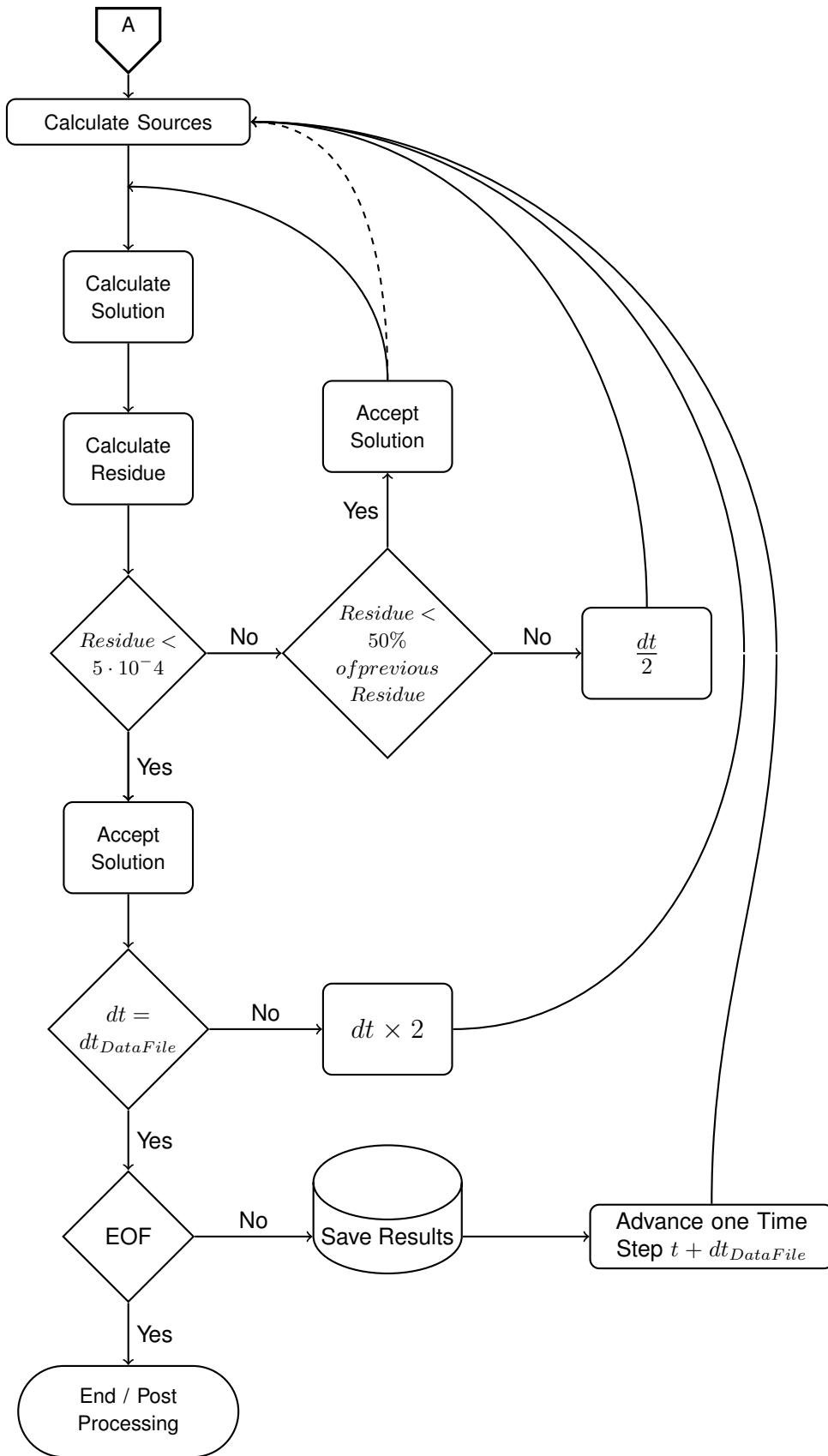


Figure A.4: Flowchart Processor (2).

## A.2 GUI

The code created is run in a console, where the input data is in a separate file or embedded in the code. At a latter stage in this Thesis appeared the motivation to implement a graphical user interface (GUI) so that the use of the source code could be simplified. To this end, another library was used, named Tkinter. “Tkinter is a Python binding to the Tk GUI toolkit. It is the standard Python interface to the Tk GUI toolkit, and is Python’s de facto standard GUI” [14].

This GUI code is object oriented which is a distinct approach from the one used in the numerical code for calculating the temperatures where there is no need for classes, or objects. It is based on a recursive object that is constantly updated to show the desired frames.

This independent part of the code, the GUI, uses the calculation code shown in the previous section. Its only function is to provide an interface to the user. It accomplishes this by launching a thread that runs the calculation source code and communicates with it through the use of a file.

This is in an early stage of development, but nevertheless this interface is working as is, and allows for the use of the calculation program to be interacted in a self explanatory way.

This is tried and tested with OSx operating system, executable files for Windows System may be also generated but haven’t so far. Hence, using another library named PyInstaller, an application “.app” is created which incorporates all the necessary modules, libraries etc. that allows this application to be run as a stand alone program in any computer running OSx. An “.exe” for Windows OS may also be created in the future.

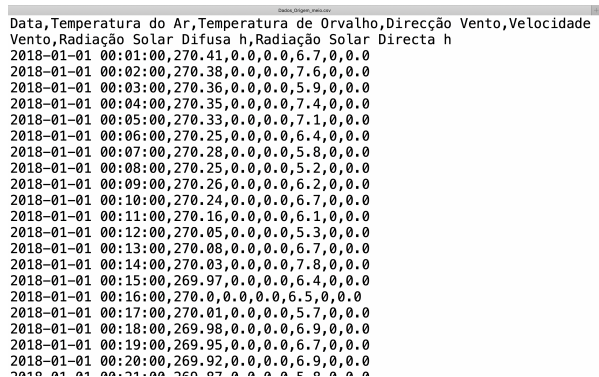
In order to run the application, first of all, there needs to be a Climate Data file in “.csv” format that must contain, for now, one line per time step, and in each line the first column is the timestamp, date and time of day, the second column, the air temperature that must be in  $Kelvin$ , the wind direction in  $[\circ]$ , the wind speed in  $[m/s]$ , the diffuse and the direct solar radiation in  $[W/m^2]$ .

This file, does not need to have equally spaced time steps since the calculations are according to the time step at each line. The columns do not need to be these in particular, but the code must be altered accordingly. In this implementation the wind direction is disregarded, the rest is all taken into account. A visualisation of the first few lines of a file is shown in Figure A.5.

The data file with the meteorological data should be placed in the Desktop. The application and climate data file are available in the following location:

<https://drive.google.com/drive/folders/1UUb98jXzMQ2qHkeqdw3LTl6SKiuMZbvK?usp=sharing>

When the application is launched, the first window appearing is shown in Figure A.6. It presents two options, creating a “New Analysis” or retrieving an existing one. In the first, the user should pick a name



```
Data, Temperatura do Ar, Temperatura de Orvalho, Direcção Vento, Velocidade Vento, Radiação Solar Difusa h, Radiação Solar Directa h
2018-01-01 00:01:00,270.41,0.0,0.0,6.7,0,0.0
2018-01-01 00:02:00,270.38,0.0,0.0,7.6,0,0.0
2018-01-01 00:03:00,270.36,0.0,0.0,5.9,0,0.0
2018-01-01 00:04:00,270.35,0.0,0.0,7.4,0,0.0
2018-01-01 00:05:00,270.33,0.0,0.0,7.1,0,0.0
2018-01-01 00:06:00,270.25,0.0,0.0,6.4,0,0.0
2018-01-01 00:07:00,270.28,0.0,0.0,5.8,0,0.0
2018-01-01 00:08:00,270.25,0.0,0.0,5.2,0,0.0
2018-01-01 00:09:00,270.26,0.0,0.0,6.2,0,0.0
2018-01-01 00:10:00,270.24,0.0,0.0,6.7,0,0.0
2018-01-01 00:11:00,270.16,0.0,0.0,6.1,0,0.0
2018-01-01 00:12:00,270.05,0.0,0.0,5.3,0,0.0
2018-01-01 00:13:00,270.08,0.0,0.0,6.7,0,0.0
2018-01-01 00:14:00,270.03,0.0,0.0,7.8,0,0.0
2018-01-01 00:15:00,269.97,0.0,0.0,6.4,0,0.0
2018-01-01 00:16:00,270.0,0.0,0.0,6.5,0,0.0
2018-01-01 00:17:00,270.01,0.0,0.0,5.7,0,0.0
2018-01-01 00:18:00,269.98,0.0,0.0,6.9,0,0.0
2018-01-01 00:19:00,269.95,0.0,0.0,6.7,0,0.0
2018-01-01 00:20:00,269.92,0.0,0.0,6.9,0,0.0
```

Figure A.5: Data File example.

for the directory that will be created in the Desktop which holds the results and auxiliary data, and fill it in the entry box. The second, “Existing Analysis”, loads a previously created analysis. Clicking it, a normal menu for choosing a directory pops-up and selecting the desired analysis the next two windows, which are seen next, are pre-filled with the saved options from the loaded analysis.

Assuming that a new analysis was chosen, the second and third windows is where the options for the analysis are selected. Figure A.7 and Figure A.8 show these windows. The fields are self explanatory. For example, the user should chose whether the analysis is one or two or three-dimensional, or wether the Module is to have an insulating layer, which if it doesn't, a value of zero should be filled, etc.. When all the fields from the second window are correctly filled, the button “Next” becomes available. Clicking it shows the third window which is similar to the second but with other options to be selected. When all fields in both these windows are filled the “Ok” button is enabled and the fourth window is shown upon pressing it.

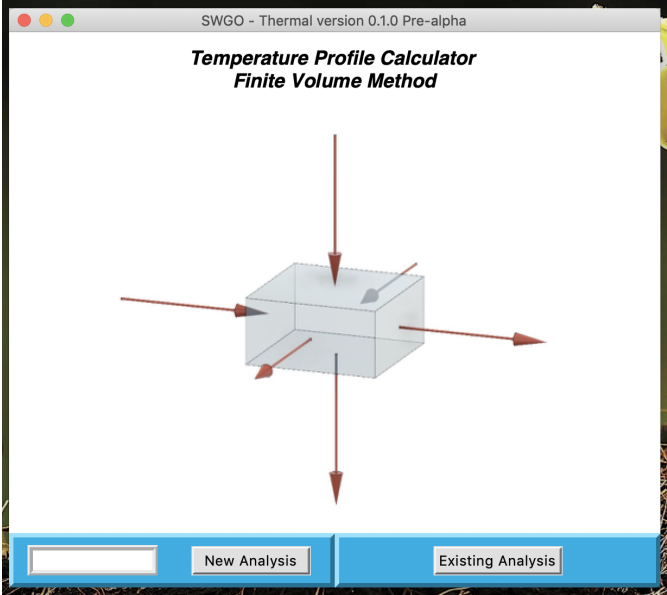


Figure A.6: First Window GUI.

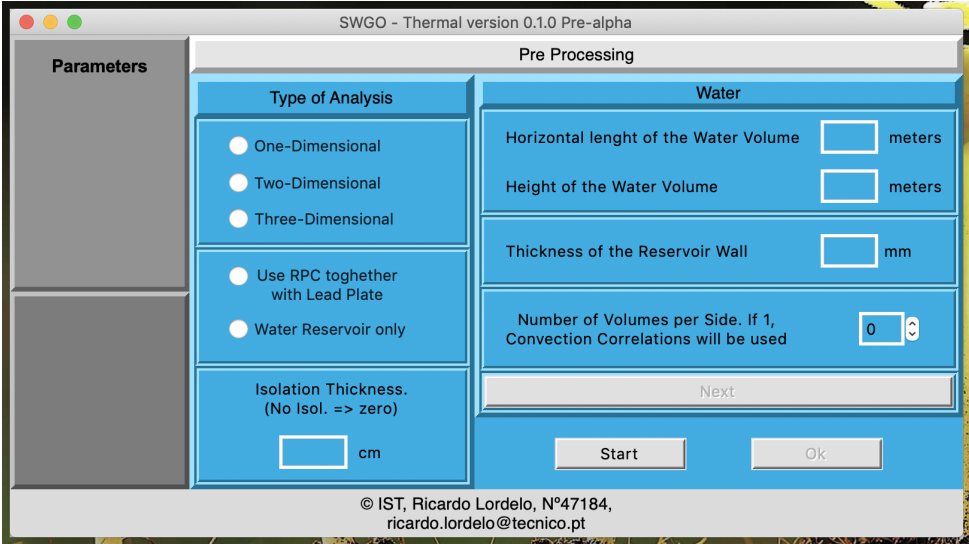


Figure A.7: Second Window GUI.

The fourth window resembles a console, the values of sources and mean temperature of the water are shown in real time. To start the run, the user should press “run”, to pause it press “pause”, etc.. The Parameters chosen appear in the left. In Figure A.9, a one-dimensional case was chosen, hence the

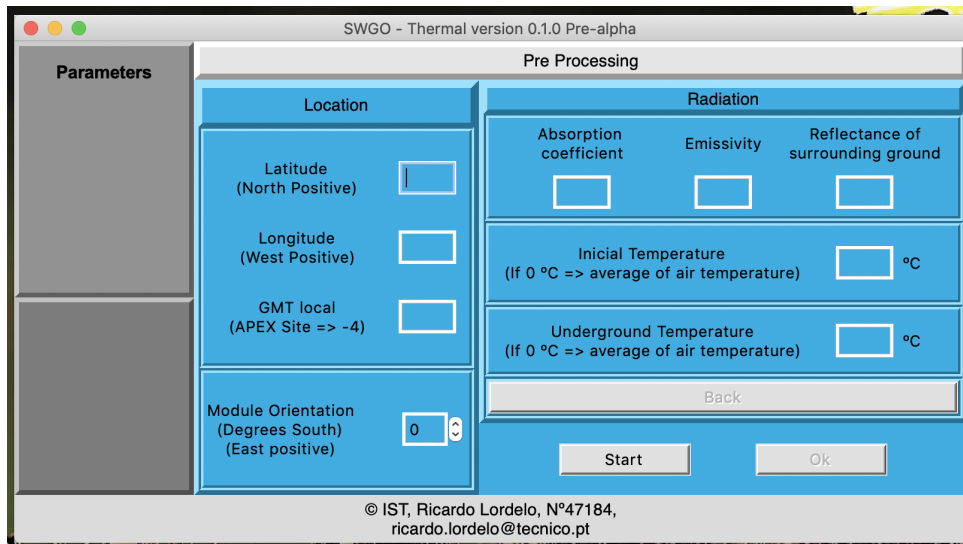


Figure A.8: Third Window GUI.

east, west, north and south values are zero.

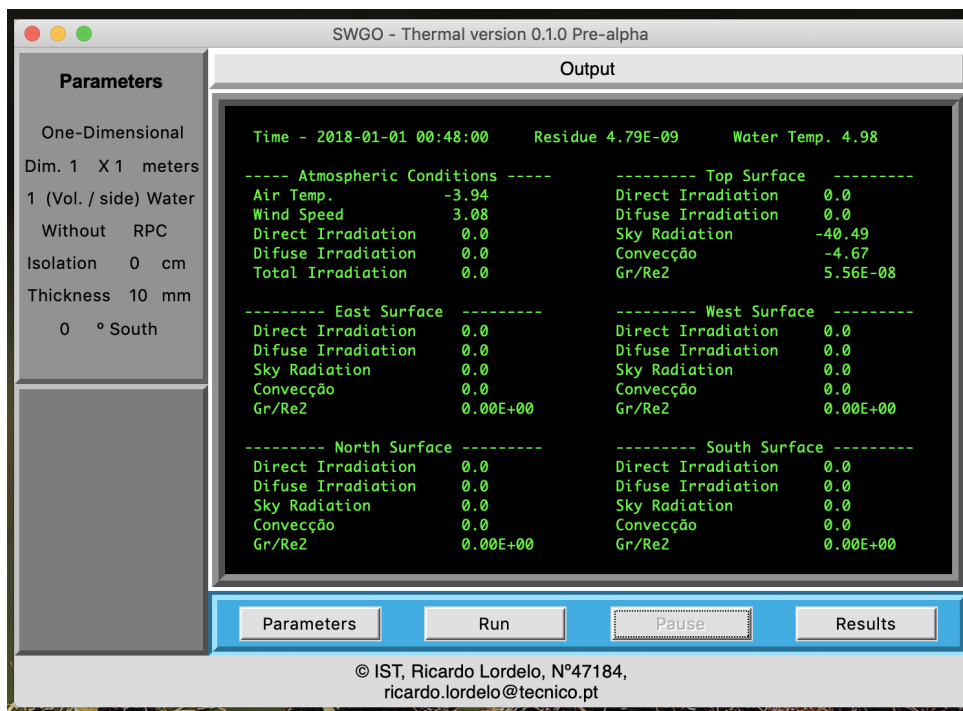


Figure A.9: Fourth Window GUI.

The fifth window is shown upon pressing “Results”. This window allow the visualisation of the generic variables of the solution. To see the plotted data, the user should select the desired variable and press “Show”. Two units may be seen simultaneously with as many variables as desired, as long as they are all represented by either one of these two units, for example, the user may check the variables, air temperature, water temperature, direct radiation, diffuse radiation, sky radiation, convection, etc., because all these have units of either temperature or heat flux.

After pressing “show” the graph is shown. Figure A.11 shows a plot for wind speed as an example.

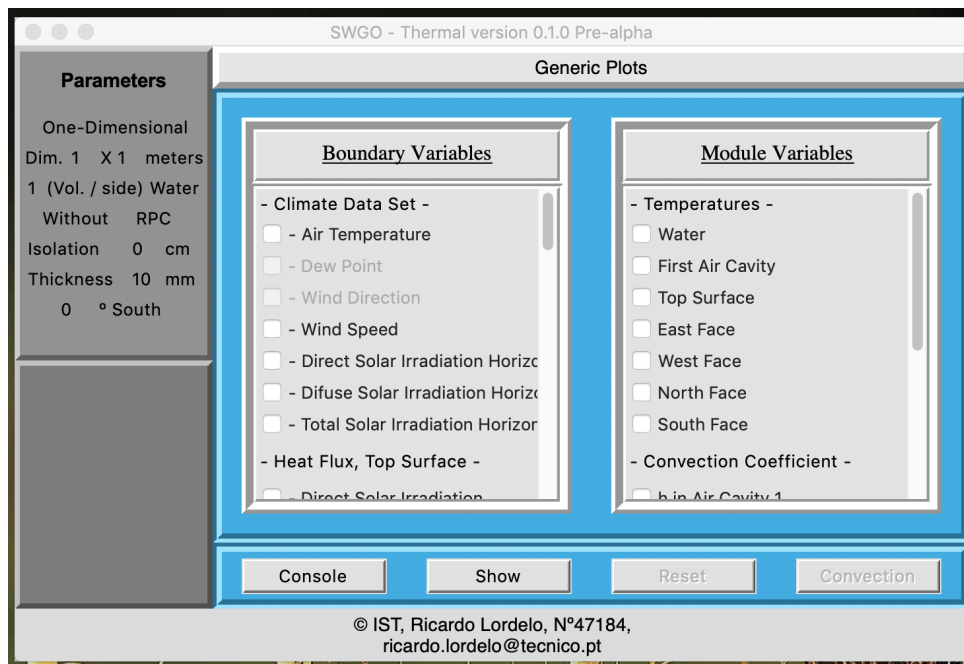


Figure A.10: Fifth Window GUI.

In this window the icons in the lower left corner of the graph, may not appear to the user. This is a known issue. It can easily be fixed by slightly resizing the window. Even so, when the mouse pointer goes through the area of these icons, their actions are displayed. This issue is mentioned because through these icons the user can zoom, pan, save the plot to a file etc., so it may be convenient.

To exit this plot view, the user should press “Reset” which returns to the fifth window where, it is possible to chose other plots, or go back to the console window, etc..

As can be seen in Figure A.10 the button “Convection” is not enabled. This is due to the test case having convection obtained through correlations. If a convective flow were to be calculated (by choosing the corresponding options in the pre-processor stage), the button would be enabled allowing the view of the sixth window. This window is shown in Figure A.12.

In this window, if a two dimensional analysis was considered, animated plots of the velocity field during the selected time period with a colour correspondence at each position may be visualised. An example is shown in Figure A.13. There is a colour bar with the corresponding temperature and a scale to the velocity field. If on the other hand a three-dimensional analysis was considered, only the velocity field is represented as may be seen in Figure A.14. In this case, by clicking on the plot and moving the mouse pointer, the plot will rotate in the direction according to the movement of the mouse.

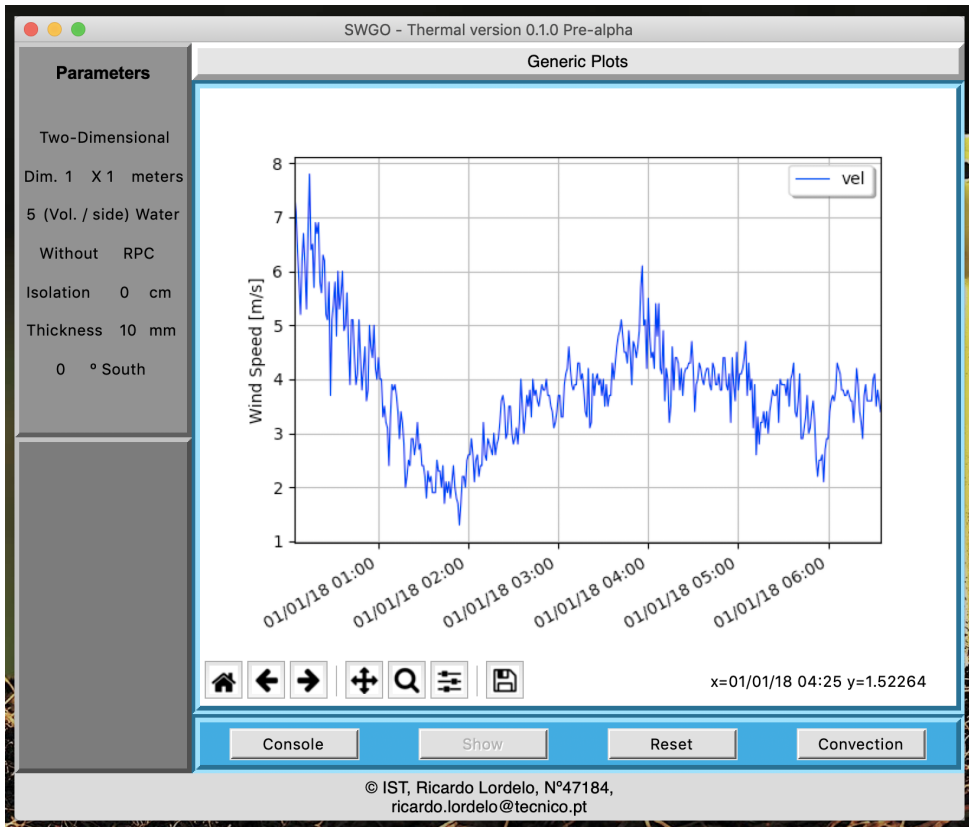


Figure A.11: Simple Plot GUI.



Figure A.12: Sixth Window GUI.



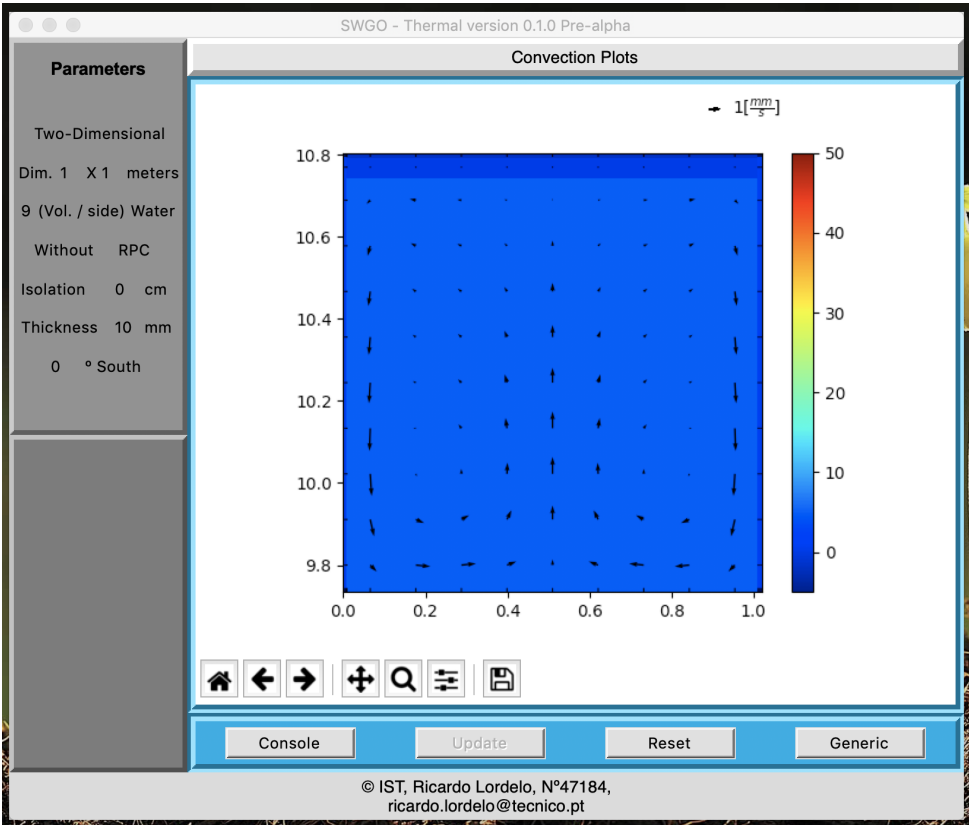


Figure A.13: Two-Dimensional plot of Convective Flow.

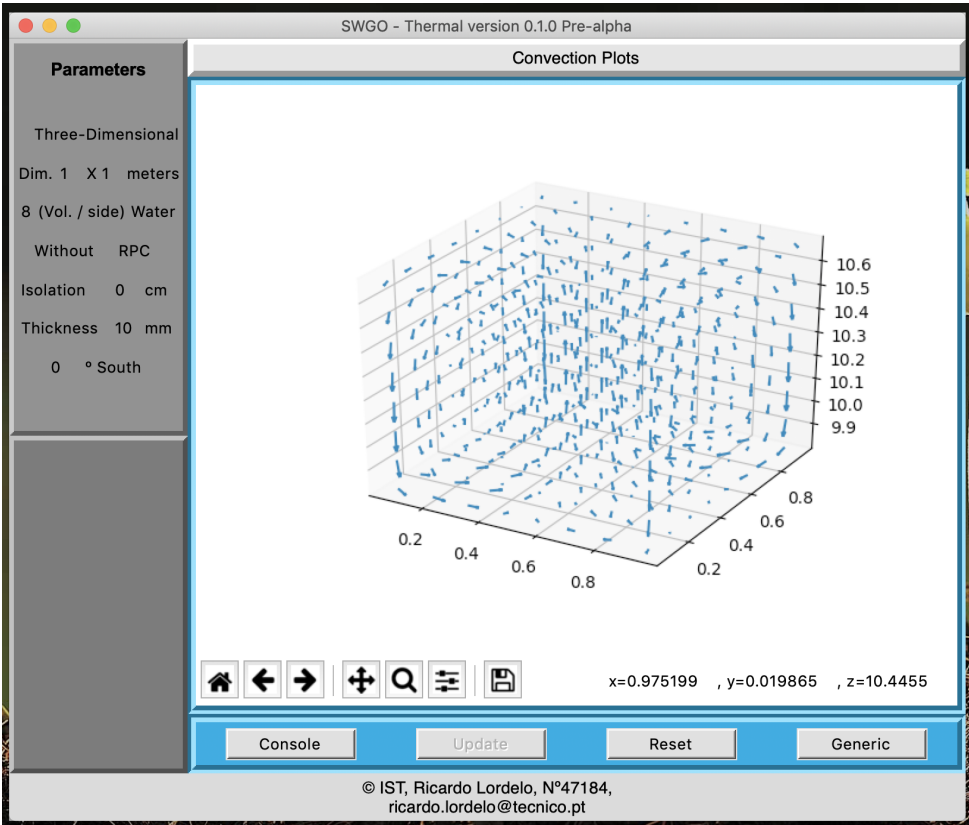


Figure A.14: Three-Dimensional plot of Convective Flow.



# Appendix B

## Selected Subroutines

Next, some of the most relevant functions and modules of the source code are presented. Apart from these modules and functions that perform specific tasks regarding the calculation process, there are several more that are needed in order for the code to work, like data and file management, that are outside the scope of this implementation and are left out.

### B.1 Sources

The Sources module, first obtains all the variables needed for its calculations. This process consists only of obtaining the needed data and performing the corresponding operation to yield the temperatures, dimensionless groups, etc.. This is not shown here. Then it calculates the convective heat transfer and the radiative heat transfer based on the temperatures of the previous time step and the climate data set.

#### B.1.1 Convection

For each surface, there is a conditional operator for evaluating which correlation to use according to the respective dimensionless groups and the corresponding flux [ $W/m^2$ ] is obtained. This flux is stored in a generic purpose list called “datos”.

Hence the if statements corresponding to the condition of forced mixed or natural convection are stated in the code shown next exactly as they are implemented.

It may be noted that the threshold values of ( $Gr_L/Re_L^2$ ) to distinguish between free mixed and forced convection are a rough estimate from Figure 2.2. These were taken as 0.01 and 100.

```
if ((Gra_top_for / (Rey_top ** 2)) < 0.01):
    dados[1,10] = Forced_Convection(Rey_top,Pr_top,
    ↪ k.film_top,Lx,T_ar,T_top)
elif (Gra_top_for / (Rey_top ** 2)) > 100:
    dados[1,10] = Natural_Convection(Rey_top_nat,k.film_top
    ↪ ,Ln,T_ar,T_top)
else:
```

```
datos[1,10] = Mixed_Convection(Rey_top,Gra_top_for,
    ↪ Pr_top,k.film_top,Lm,T_ar,T_top)
if (Gra_side_e / (Rey_side_e ** 2)) < 100:
    dados[1,15] = Side_Mixed_Convection(Rey_side_e,
    ↪ Gra_side_e,k.ar,Lz,Ly,T_side_e,T_ar)
else:
```

```

dados[1,15] = Side.Natural.Convection(Ray_side_e,
    ↪ Pr_side_e,k.film_side_e,Ly,T_side_e,T_ar)

if (Gra_side_w / (Rey_side_w ** 2)) < 100:
    dados[1,20] = Side.Mixed.Convection(Rey_side_w,
    ↪ Gra_side_w,k.ar,Lz,Ly,T_side_w,T_ar)
else:
    dados[1,20] = Side.Natural.Convection(Ray_side_w,
    ↪ Pr_side_w,k.film_side_w,Ly,T_side_w,T_ar)

if (Gra_side_f / (Rey_side_f ** 2)) < 100:
    dados[1,25] = Side.Mixed.Convection(Rey_side_f,

```

```

    ↪ Gra_side_f,k.ar,Lx,Ly,T_side_f,T_ar)
else:
    dados[1,25] = Side.Natural.Convection(Ray_side_f,
    ↪ Pr_side_f,k.film_side_f,Ly,T_side_f,T_ar)

if (Gra_side_t / (Rey_side_t ** 2)) < 100:
    dados[1,30] = Side.Mixed.Convection(Rey_side_t,
    ↪ Gra_side_t,k.ar,Lx,Ly,T_side_t,T_ar)
else:
    dados[1,30] = Side.Natural.Convection(Ray_side_t,
    ↪ Pr_side_t,k.film_side_t,Ly,T_side_t,T_ar)

```

After acknowledging the type of convection, it calculates the respective heat flux with the needed variables.

```

def Side.Natural.Convection(Ra,Pr,k,Ly,Ts,T_ar):
    Nu = 0
    if (abs(Ra) > 1e9):
        Nu = (0.825 + ((0.387 * (abs(Ra) ** (1 / 6))) / ((1 +
            ↪ ((0.492 / Pr) ** (9/16))) ** (8 / 27)))) ** 2
    else:
        Nu = 0.68 + ((0.67 * (abs(Ra) ** 0.25)) / ((1 +
            ↪ ((0.492 / Pr) ** (9 / 16))) ** (4 / 9)))
    flux = (k / Ly) * Nu * (T_ar - Ts)
    return(flux)

def Side.Mixed.Convection(Rey,Gra,k,L,Ly,Ts,T_ar):
    if Gra > 1e9: Gra = 1e9
    if Rey > 1e5: Rey = 1e5
    Nu = (Rey ** 0.5) * 0.804 * ((1 + (((0.752 * L / Ly) * ((Gra
        ↪ / ((Rey) ** (5 / 2))) ** (1 / 5))) ** 3.2)) ** (1 /
        ↪ 3.2))
    flux = (k / L) * Nu * (T_ar - Ts)
    return(flux)

def Natural.Convection(Ray,k,Ln,T_ar,Ts):
    Nu = 0
    if Ts > T_ar:
        if Ray < 1e4:
            print (...)
        elif Ray < 1e7:
            Nu = 0.54 * (Ray ** (1 / 4))
        elif Ray < 1e11:
            Nu = 0.15 * (Ray ** (1 / 3))
        else:
            print (...)
    else:

```

```

        if Ray < 1e5:
            print (...)
        elif Ray < 1e10:
            Nu = 0.27 * (Ray ** (1 / 4))
        else:
            print (...)
    flux = (k / Ln) * Nu * (T_ar - Ts)
    return(flux)

def Forced.Convection(Rey,Pr,k,L,T_ar,Ts):
    if Rey < 5e5:
        Nu = 0.664 * (Rey ** (1 / 2)) * (Pr ** (1 / 3))
    elif Rey < 1e8:
        Nu = ((0.037 * (Rey ** (4 / 5))) - 871) * (Pr ** (1 / 3))
    else:
        print (...)
    flux = (k / L) * Nu * (T_ar - Ts)
    return(flux)

def Mixed.Convection(Rey,Gra,Pr,k,Lm,T_ar,Ts):
    Nu = 0
    if (1e3 < Rey < 1e5) and (Gra < 1e7):
        F1 = 0.339 * (Pr ** (1 / 3)) * ((1 + ((0.0648 / Pr) ** (2
            ↪ / 3))) ** (-1 / 4))
        F3 = ((Pr / 5) ** (1 / 5)) * math.sqrt(Pr) * (1 / (0.25 +
            ↪ (1.6 * math.sqrt(Pr))))
        A = 2 * F1
        B = 5 * F3 / 3
        Xi = Gra / (Rey ** (5 / 2))
        m = 1 / 5
        n = 3
        Nu = A * math.sqrt(Rey) * ((1 + ((B * (Xi ** m) / A) **
            ↪ n)) ** (1 / n))

```

```

else: print (...)
flux=(k / Lm) * Nu * (T_ar - Ts)
return(flux)

def cavidades(T,H_cav,L_cav,dx,dy,dT_y,mat):
    if mat == 1:
        k = getattr(mat,f"k.t.1")(T)
        ro = getattr(mat,f"ro.t.1")(T)
        Cp = getattr(mat,f"Cp.t.1")(T)
        Beta = getattr(mat,f"B.t.1")(T)
        visc = getattr(mat,f"mu.t.1")(T)
        Ray_y = g * Beta * ((L_cav) ** 3) * (ro ** 2) * Cp *
            ↪ dT_y / (visc * k)
        if (Ray_y >= 1708) and (Ray_y <= 5830):
            h_y = (k / (L_cav)) * (1+(1.44*(1-(1708/Ray_y))))
        elif (Ray_y > 5830):
            h_y = (k / (L_cav)) * (1+(1.44*(1-(1708/Ray_y))))
            ↪ +(((Ray_y/5830)**(1/3))-1)

```

```

else:
    h_y = 0
else:
    k = getattr(mat,f"k.t.2")(T)
    ro = getattr(mat,f"ro.t.2")(T)
    Cp = getattr(mat,f"Cp.t.2")(T)
    Beta = 1 / (T)
    visc = getattr(mat,f"mu.t.2")(T)
    Ray_y = g * Beta * ((L_cav) ** 3) * (ro ** 2) * Cp *
        ↪ dT_y / (visc * k)
    if (Ray_y >= 1708) and (Ray_y <= 5830):
        h_y = (k / (L_cav)) * (1+(1.44*(1-(1708/Ray_y))))
    elif (Ray_y > 5830):
        h_y = (k / (L_cav)) * (1+(1.44*(1-(1708/Ray_y))))
            ↪ +(((Ray_y/5830)**(1/3))-1)
    else: h_y = 0
k_eq_y = h_y * dy
return(k_eq_y,h_y)

```

## B.1.2 Radiation

The radiation function does as stated in Section 3.5.2. For each surface of the Module three separate heat flux variables are stored, corresponding to direct solar irradiation, diffuse solar irradiation and radiative heat exchange with the sky.

```

def radiacao(dados,StefanBoltzmann,alpha,epsilon,ref,
    ↪ meridiano,Long,Lat,azim,T_ar,T_top,T_side_w,
    ↪ T_side_e,T_side_f,T_side.t):
    dir = dados[1,6]
    dif = dados[1,5]
    tot = dados[1,5] + dados[1,5]
    B = (pd.to_datetime(dados[1,0]).dayofyear - 1) * 360 /
        ↪ 365
    E = pd.Timedelta(minutes = (229.2 * (0.000075 +
        ↪ (0.001868 * cos(B)) - (0.032077 * sen(B)) -
        ↪ (0.014615 * cos(2 * B)) - (0.04089 * sen(2 * B)
        ↪ ))))
    ST = pd.Timestamp(dados[1,0]) + pd.Timedelta(minutes
        ↪ = (4 * (meridiano - Long))) + E
    w = ((ST.hour - 12) * 15)+(ST.minute) * 15 / 60
    decl = (180 / np.pi) * (0.006918 - (0.399912 * cos(B)) +
        ↪ (0.07257 * sen(B)) - (0.006758 * cos(2 * B)) +
        ↪ (0.000907 * sen(2 * B)) - (0.002697 * cos(3 *
        ↪ B)) + (0.00148 * sen(3 * B)))
    inc = [0,90,90,90,90]
    azi = [0, -azim - 90, -azim + 90, -azim + 180, -azim]
    x = [0,0,0,0,0] #[n,e,w,f,t]

```

```

x[0] = (sen(decl) * sen(Lat) * cos(inc[0])) - \
    (sen(decl) * cos(Lat) * sen(inc[0]) * cos(azi[0])) + \
    (cos(decl) * cos(Lat) * cos(inc[0]) * cos(w)) + \
    (cos(decl) * sen(Lat) * sen(inc[0]) * cos(azi[0]) * cos(
        ↪ w)) + \
    (cos(decl) * sen(inc[0]) * sen(azi[0]) * sen(w))
theta = acos(x[0])
p = np.poly1d([-6.9937e-13,1.7734e-10,-1.8e
    ↪ -8.9.0244e-7,-2.3026e-5,2.7314e
    ↪ -4,-1.5879e-3,1])
if theta < 90:
    for i in range(1,len(x)):
        x[i] = (sen(decl) * sen(Lat) * cos(inc[i])) - \
            (sen(decl) * cos(Lat) * sen(inc[i]) * cos(
                ↪ azi[i])) + \
            (cos(decl) * cos(Lat) * cos(inc[i]) * cos(w)
                ↪ )) + \
            (cos(decl) * sen(Lat) * sen(inc[i]) * cos(
                ↪ azi[i]) * cos(w)) + \
            (cos(decl) * sen(inc[i]) * sen(azi[i]) * sen
                ↪ (w))
        # ----- Direct
        ↪ -----

```

```

dados[1,7] = max((dir * x[0] / x[0]) * alpha * p(x[0]),
    ↪ 0)
dados[1,12] = max((dir * x[1] / x[0]) * alpha * p(x[1]),
    ↪ 0)
dados[1,17] = max((dir * x[2] / x[0]) * alpha * p(x[2]),
    ↪ 0)
dados[1,22] = max((dir * x[3] / x[0]) * alpha * p(x[3]),
    ↪ 0)
dados[1,27] = max((dir * x[4] / x[0]) * alpha * p(x[4]),
    ↪ 0)
# ----- Difuse
    ↪ -----
dados[1,8] = ((dif * ((1 + cos(inc[0])) / 2)) + (tot * ref *
    ↪ ((1 - cos(inc[0])) / 2))) * alpha
dados[1,13] = ((dif * ((1 + cos(inc[1])) / 2)) + (tot * ref
    ↪ * ((1 - cos(inc[1])) / 2))) * alpha
dados[1,18] = ((dif * ((1 + cos(inc[2])) / 2)) + (tot * ref
    ↪ * ((1 - cos(inc[2])) / 2))) * alpha
dados[1,23] = ((dif * ((1 + cos(inc[3])) / 2)) + (tot * ref
    ↪ * ((1 - cos(inc[3])) / 2))) * alpha

```

```

    dados[1,28] = ((dif * ((1 + cos(inc[4])) / 2)) + (tot * ref
    ↪ * ((1 - cos(inc[4])) / 2))) * alpha
# ----- Sky -----
dados[1,9] = ((1 + cos(inc[0])) / 2) * epsilon *
    ↪ StefanBoltzmann * (((0.0552 * (T_ar ** 1.5)) **
    ↪ 4) - (T_top ** 4))
dados[1,14] = ((1 + cos(inc[1])) / 2) * epsilon *
    ↪ StefanBoltzmann * (((0.0552 * (T_ar ** 1.5)) **
    ↪ 4) - (T_side_e ** 4))
dados[1,19] = ((1 + cos(inc[2])) / 2) * epsilon *
    ↪ StefanBoltzmann * (((0.0552 * (T_ar ** 1.5)) **
    ↪ 4) - (T_side_w ** 4))
dados[1,24] = ((1 + cos(inc[3])) / 2) * epsilon *
    ↪ StefanBoltzmann * (((0.0552 * (T_ar ** 1.5)) **
    ↪ 4) - (T_side_f ** 4))
dados[1,29] = ((1 + cos(inc[4])) / 2) * epsilon *
    ↪ StefanBoltzmann * (((0.0552 * (T_ar ** 1.5)) **
    ↪ 4) - (T_side_t ** 4))
return(dados)

```

## B.2 Iteration Function

The iteration function performs what is described in flowchart A.4. Every time step this loop is performed, when the convective flow is present, and the flow is not constant, meaning when velocity field is changing, the time step is more prone to its subdivision in order to get an acceptable residue through the one minute time step.

It should be noted that the one-dimensional analysis does not iterate because its temperature solution is fixed, or its governing equation is elliptic within each time step and the residue originates only from floating point roundoff errors.

```

def iterator(M,dt,dados,resi):
    lado = 0
    #####
    dados = ft.fluxos(dados,M)#
    #####
    M,a = solve(M,dt,dados,a)
    if a == 1:
        res = 1
    else:
        res = residue(M,dt,dados)
    if dados[1,-2] == 0:
        lado = 3
    elif resi[dados[1,-2]][0] == np.inf:
        lado = 0

```

```

elif resi[dados[1,-2]][1] == np.inf:
    lado = 1
else:
    print (...)
if dados[1,-2] == 0:
    resi[dados[1,-2]] = res
elif resi[dados[1,-2]][0] == np.inf:
    resi[dados[1,-2]][0] = res
elif resi[dados[1,-2]][1] == np.inf:
    resi[dados[1,-2]][1] = res
else:
    print (...)
while res > 0.0005:
    #####
    dados = ft.fluxos(dados,M)#

```

```
#####
M,a = solve(M,dt,dados,a)
res_ = residue(M,dt,dados)
if res_ < (res * 0.5):
    if dados[1,-2] == 0:
        resi[dados[1,-2]] = res_
    elif resi[dados[1,-2]][1] == np.inf:
        resi[dados[1,-2]][0] = res_
    else:
        resi[dados[1,-2]][1] = res_
    res = res_
else:
    dt /= 2
    dados[1,-2] += 1
    resi.append([np.inf,np.inf])
M,..,dados,.. = iterator(M,dt,dados,resi)
```

```
M,..,dados,res = iterator(M,dt,dados,resi)
if lado == 3:
    resi[0] = res
else:
    resi[dados[1,-2] - 1][lado] = res
del resi[dados[1,-2]]
dados[1,-2] -= 1
dt *= 2
if dados[1,-2] == 0:
    dados[1,-1] = resi[dados[1,-2]]
else:
    dados[1,-1] = sum(resi[dados[1,-2]])/2
res = dados[1,-1]
M = save(M)
return(M,a,dados,res)
```

### B.3 Calculator

This function fills the matrix to be solved afterwards with each coefficient at the appropriate locations. All the values that are feed to this function need to be calculated prior to its call. The functions that calculate these values at each time step are according to the unknown property  $\phi$ , one function for each property. One obtains these values for the energy property, and three other for the velocity in each direction. It should be noted that the velocity variables are staggered, hence their values must take into account the relative position of these CV's. Also, when the velocity field is calculated, there is going to be an additional equation for continuity that must also be implemented (which is not represented in Figure B.1 since it fills the matrix with its values by its own when called).

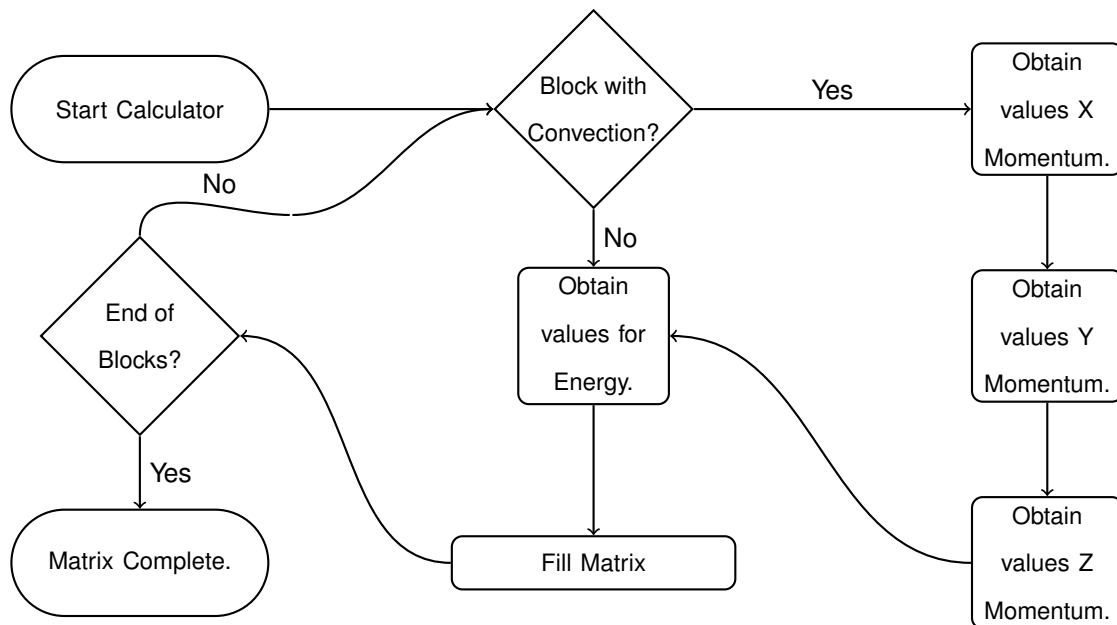


Figure B.1: Calculator Scheme.

```

def fill_matrix(ro,ro_east,ro_west,ro_north,ro_south,ro_front,
    ↪ ro_back,v_x_aft,v_x_bef,v_y_aft,v_y_bef,v_z_aft,
    ↪ v_z_bef,Dife,Difw,Difn,Difs,Diff,Dift,A_east,A_west,
    ↪ A_north,A_south,A_front,A_back,dx_aft,dx_bef,dy_aft
    ↪ ,dy_bef,dz_aft,dz_bef,dV,phi0,n,di,dj,dk,dt,gaus,dep
    ↪ ,swich_pres,p,Su,Sp,SBu,SBp):

Adv_east = ro_east * v_x_aft * A_east
Adv_west = ro_west * v_x_bef * A_west
Adv_north = ro_north * v_y_aft * A_north
Adv_south = ro_south * v_y_bef * A_south
Adv_front = ro_front * v_z_aft * A_front
Adv_back = ro_back * v_z_bef * A_back

Dif_east = Dife * A_east / dx_aft
Dif_west = Difw * A_west / dx_bef
Dif_north = Difn * A_north / dy_aft
Dif_south = Difs * A_south / dy_bef
Dif_front = Diff * A_front / dz_aft
Dif_back = Dift * A_back / dz_bef

Pec_x_aft = Adv_east / Dif_east
Pec_x_bef = Adv_west / Dif_west
Pec_y_aft = Adv_north / Dif_north
Pec_y_bef = Adv_south / Dif_south
Pec_z_aft = Adv_front / Dif_front
Pec_z_bef = Adv_back / Dif_back

# TIME
gaus[n,n] += ro * dV / dt
dep[n] += ro * dV * phi0 / dt

# PRESSURE
gaus[n,n+p+di] += swich_pres * A_east
gaus[n,n+p] -= swich_pres * A_west

# SOURCES
gaus[n,n] -= Sp * dV
dep[n] -= Su * dV

# BOUSSINESQ
gaus[n,n+3] -= SBp * dV / 2
gaus[n,n+3+di] -= SBp * dV / 2
dep[n] -= SBu * dV

# X

```

```

if Pec_x_bef >= 2:
    gaus[n,n-dj] -= Adv_west
elif Pec_x_bef <= -2:
    gaus[n,n] -= Adv_west
else:
    gaus[n,n-dj] -= (Adv_west * 0.5) + Dif_west
    gaus[n,n] -= (Adv_west * 0.5) - Dif_west
if Pec_x_aft >= 2:
    gaus[n,n] += Adv_east
elif Pec_x_aft <= -2:
    gaus[n,n+dj] += Adv_east
else:
    gaus[n,n+dj] += (Adv_east * 0.5) - Dif_east
    gaus[n,n] += (Adv_east * 0.5) + Dif_east

# Y
if Pec_y_bef >= 2:
    gaus[n,n-dj] -= Adv_south
elif Pec_y_bef <= -2:
    gaus[n,n] -= Adv_south
else:
    gaus[n,n-dj] -= (Adv_south * 0.5) + Dif_south
    gaus[n,n] -= (Adv_south * 0.5) - Dif_south
if Pec_y_aft >= 2:
    gaus[n,n] += Adv_north
elif Pec_y_aft <= -2:
    gaus[n,n+dj] += Adv_north
else:
    gaus[n,n+dj] += (Adv_north * 0.5) - Dif_north
    gaus[n,n] += (Adv_north * 0.5) + Dif_north

# Z
if Pec_z_bef >= 2:
    gaus[n,n-dk] -= Adv_back
elif Pec_z_bef <= -2:
    gaus[n,n] -= Adv_back
else:
    gaus[n,n-dk] -= (Adv_back * 0.5) + Dif_back
    gaus[n,n] -= (Adv_back * 0.5) - Dif_back
if Pec_z_aft >= 2:
    gaus[n,n] += Adv_front
elif Pec_z_aft <= -2:
    gaus[n,n+dk] += Adv_front
else:
    gaus[n,n+dk] += (Adv_front * 0.5) - Dif_front
    gaus[n,n] += (Adv_front * 0.5) + Dif_front
return(gaus,dep)

```



# Appendix C

## Convective Flow

Some plots of the convective flow are shown next as a complement to the Thesis. Although the flow itself is not relevant in this Thesis, its characteristics dictate the Nusselt number at each surface.

### C.1 Two Dimensional

Figure ?? shows case 1 200min. after the initial condition, meaning January 01, 03:20. At this time the water, initially at 2°C is being cooled through the side walls of the Module. The thickness of the lines in the Figure are proportional to the flow velocity. Figure ?? show the same case, the same day, at minute 420 or at 7 a.m. after sun rise. The east wall of the reservoir is being heated. Figure C.2 shows the flow at noon, or 12:00 at the same day.

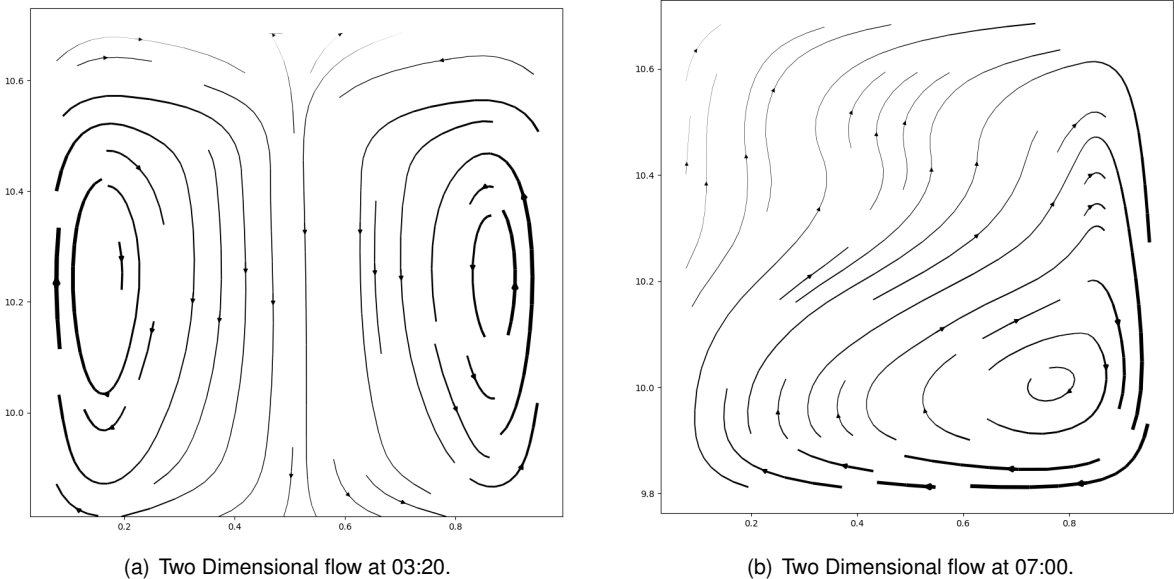


Figure C.1: Two Dimensional flow at 03:20 and at 07:00.

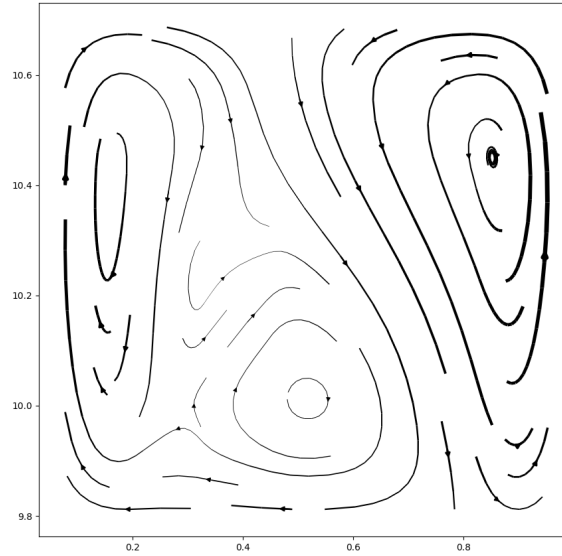
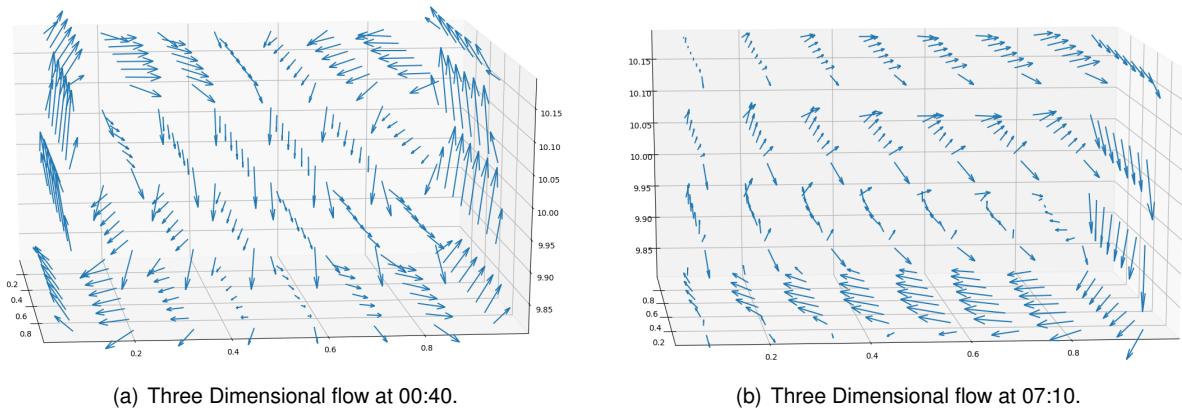


Figure C.2: Two Dimensional flow at 12:00.

## C.2 Three Dimensional

The three-dimensional case is more difficult to visualize in a drawing. Also, the heat flux is different in each wall regarding convection making for a lack of symmetry in the flow. Even so, Figure ?? shows a quiver plot of the same case 1,  $40min.$  after the initial condition. Figure ?? shows the same case  $430min.$  after the initial condition, or at 07:10 when the east wall starts to be affected by the sun's irradiation. In this Figure the velocity scale is reduced. Velocities are higher in general at this time than at 00:40.



(a) Three Dimensional flow at 00:40.

(b) Three Dimensional flow at 07:10.

Figure C.3: Three Dimensional flow at 00:40 and 07:10.

# Appendix D

## Sparsity of Matrix

The following shows the matrixes to be solved at each time step for the one dimensional case, two dimensional with correlation and without and for the three dimensional case to showcase their sparsity. All matrixes are for case 1. The Black areas are populated and the white area is zeros.

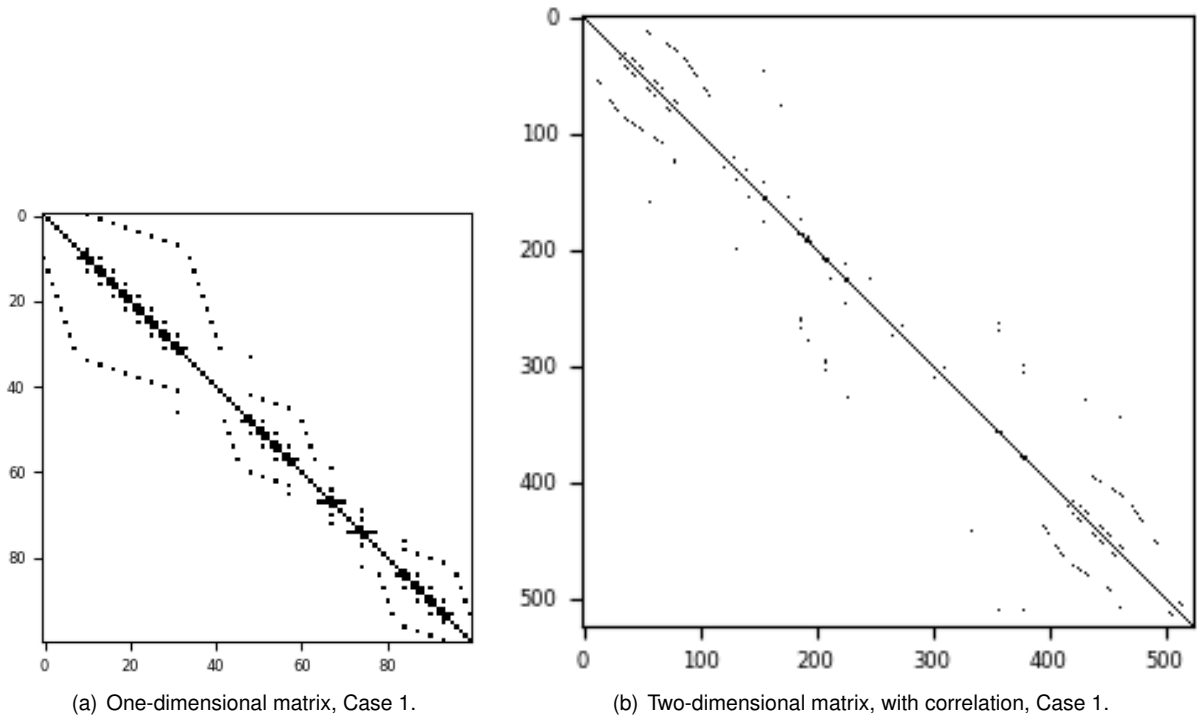


Figure D.1: One and Two Dimensional matrix with correlation, Case 1.

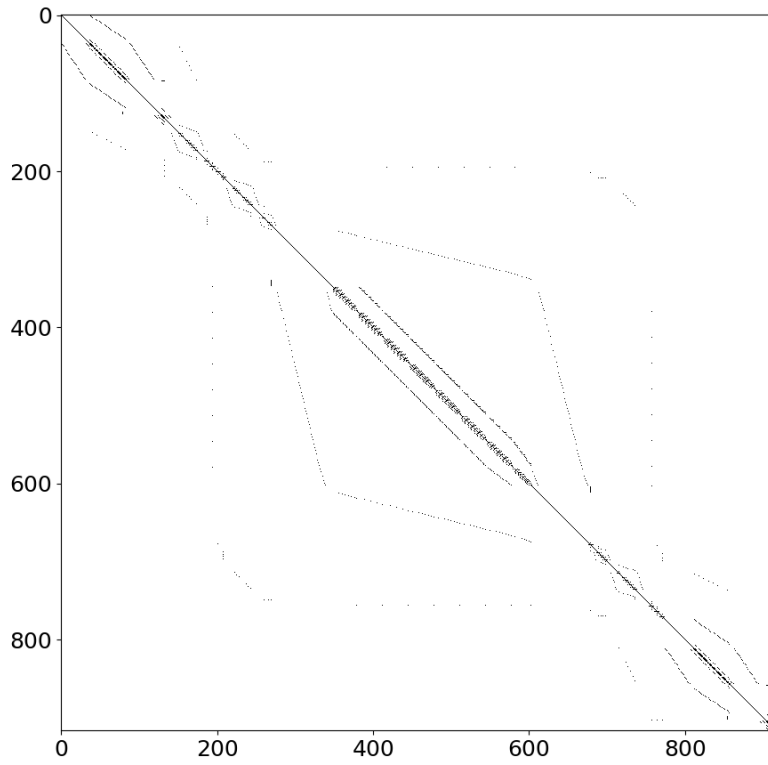


Figure D.2: Two-dimensional matrix, with flow, Case 1.

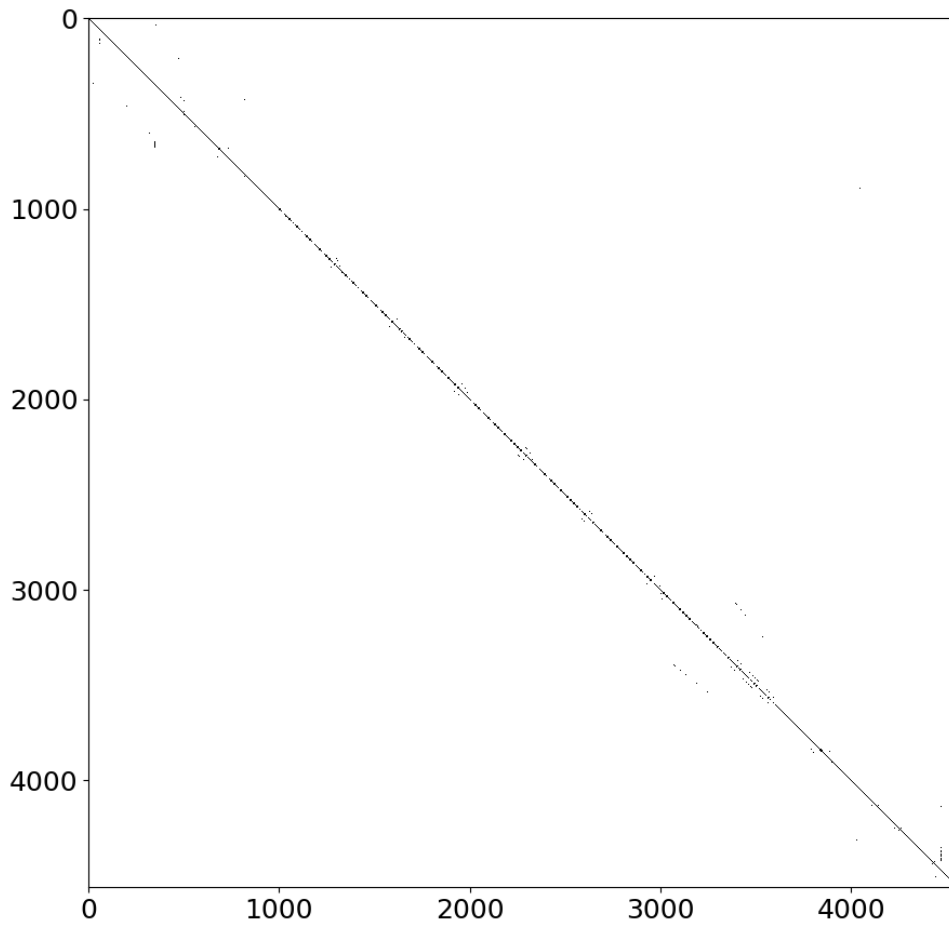


Figure D.3: Three-dimensional matrix, with flow, Case 1.